POWER SYSTEM IMPACTS OF PLUG-IN HYBRID ELECTRIC VEHICLES

A Thesis
Presented to
The Academic Faculty

by

Curtis Aaron Roe

In Partial Fulfillment
of the Requirements for the Degree
Master of Science in the
School of Electrical and Computer Engineering

Georgia Institute of Technology
August 2009

POWER SYSTEM IMPACTS OF PLUG-IN HYBRID ELECTRIC VEHICLES

Approved by:

Dr. A. P. Meliopoulos, Advisor
School of Electrical and Computer Engineering
Georgia Institute of Technology

Dr. David Taylor
School of Electrical and Computer Engineering
Georgia Institute of Technology

Dr. Shijie Deng
School of Industrial and Systems Engineering
Georgia Institute of Technology

Dr. Ronald Harley
School of Electrical and Computer Engineering
Georgia Institute of Technology

Date Approved: June 26, 2009

I dedicate this thesis to my wife, her love and encouragement has been and continues to be of marvelous importance in my life.

ACKNOWLEDGEMENTS

This MS thesis was initiated and partially supported by the Power System Engineering Research Center (PSERC) project T-34, "Power System Level Impacts of Plug-In Hybrid Vehicles". This support is gratefully acknowledged.

Significant contributions have been made by the following individuals Dr. A.P. Meliopoulos, Dr. Jerome Meisel, and Mr. Farantatos Evangelos. Each individual's contributions will be summarized next.

Dr. Meliopoulos lead this project, only with his extensive experience has this project gotten off the ground and come this far. Dr. Meisel conducted the Powertrain System Analysis Toolkit vehicle simulations and the results from these simulations provided critical support for this project. Mr. Farantatos conducted initial work on the impact that PHEV charging has on distribution transformers, from which probabilistic simulations were developed. These contributions are gratefully acknowledged.

Finally the MS Thesis reading committee members Dr. Shijie Deng, Dr. Ronald Harley, and Dr. David Taylor are greatly appreciated.

TABLE OF CONTENTS

LIST OF TABLES

LIST OF TABLES (2)

LIST OF FIGURES

LIST OF FIGURES (2)

LIST OF FIGURES (3)

LIST OF SYMBOLS

α_p	PHEV population variance coefficient
θ_u	Transformer insulation aging acceleration factor
$\vec{\mu}$	PHEV vehicle design parameters mean vector
μ_{BC}	PHEV usable battery capacity mean [kWh]
$\mu^{(c)}$	PHEV class-c population mean
$\mu_P^{(h)}$	Feeder real power demand mean in hour-h [W]
μ_m	Vehicle daily driving distance distribution mean [mi.]
$\mu_{\mathrm{T}}^{(\mathrm{p})}$	Vehicle timing distribution-p mean [h]
ρ	PHEV k_{PHEV} usable battery capacity correlation
$\boldsymbol{\Sigma}$	PHEV vehicle design parameters covariance matrix
σ_{BC}	PHEV usable battery capacity standard deviation [kWh]
$\sigma^{(c)}$	PHEV class-c population standard deviation
$\sigma_P^{(h)}$	Feeder real power demand standard deviation in hour-h [VA]
σ_{kPHEV}	PHEV k_{PHEV} standard deviation
σ_m	Vehicle daily driving distance distribution standard deviation [mi.]
$\sigma_T^{(p)}$	Vehicle timing distribution-p standard deviation [h]
$\boldsymbol{A}$	Linear least square known observation matrix
$A_{CO2}^{(c)}$	PHEV CO_2 rate function parameter [kg/mi.]
$A_E^{(c)}$	PHEV grid electric energy function parameter [kWh/mi.]
$A_{GPM}^{(c)}$	PHEV MPG function parameter [gal./mi.]
$A_{NOx}^{(c)}$	PHEV NO_x rate function parameter [kg/mi.]

LIST OF SYMBOLS (2)

a_h	Generator heat rate function parameter [kcal/h]
a_p	Generator emission rate function parameter [kg/h]
A_T^*	A particular value generated for the random daily arrival time [h]
$A_T^{(v,d)}$	RV representing the daily arrival time for vehicle-v on day-d [h]
$\boldsymbol{B}$	Lower triangle matrix computed using the Cholesky decomposition
B	LOL calculation aging rate constant [K]
BC	RV representing the useable battery capacity of PHEV [Wh]
$BC^{(c)}$	RV representing a PHEV in class-c usable battery capacity [kWh]
$BC_{\max}^{(c)}$	Maximum usable battery capacity for PHEV in class-c [kWh]
$BC_{\min}^{(c)}$	Minimum usable battery capacity for PHEV in class-c [kWh]
$B_{CO2}^{(c)}$	PHEV CO_2 rate function parameter
$B_E^{(c)}$	PHEV grid electric energy function parameter
$B_{GPM}^{(c)}$	PHEV MPG function parameter
$B_{NOx}^{(c)}$	PHEV NO_x rate function parameter
b_h	Generator heat rate function parameter [kcal/MWh]
b_p	Generator emission rate function parameter [kg/MWh]
c	Vehicle class-c, represents a group of vehicles of comparable sizes
$\boldsymbol{C}$	Electro-thermal transformer model thermal capacitance matrix [joules/˚C]
c_h	Generator heat rate function parameter [kcal/(MW)^{2}h]
$CO_2^{(c)}(0)$	PHEV charge sustaining CO_2 rate [kg/mi.]
$CO_2^{(c)}(k_{PHEV})$	PHEV performance metric CO_2 rate function [kg/mi.]
$C_A^{(q)}$	Hydro generator percent capacity available in quarter-q [%]

LIST OF SYMBOLS (3)

$C_T^{(v,d)}$	RV representing the daily recharge time for PHEV-v on day-d [h]
d	Day-d, a particular day in the simulation
D	Total number of days in the simulation
D_T^*	A particular value generated for the random daily depart time [h]
$D_E^{(v,d,c)}$	The daily recharge energy required by PHEV-v on day-d in class-v [kWh]
$D_{EAP}^{(v,d,c)}$	Daily EAP generated by PHEV-v on day-d in class-c [kg]
$D_G^{(v,d,c)}$	Daily gasoline consumed by PHEV-v on day-d in class-c [gal.]
$D_T^{(v,d)}$	RV representing the daily departure time for vehicle-v on day-d [h]
e	Iterative load flow error tolerance
EAP	Total EAP generated by N_T vehicles with P_{PHEV} penetration of PHEVs [kg]
$\overline{EAP_{IC}^{(c)}}$	Average EAP generated by IC vehicles in class-c [kg/veh.]
EAP_{IC}	Total EAP generated by N_T IC vehicles [kg]
EAP_{PHEV}	Total EAP generated by a fleet of $N_T \cdot P_{PHEV}$ PHEVs [kg]
$E^{(c)}(k_{PHEV})$	PHEV performance metric grid electric energy rate function [kWh/mi.]
E_L	Transformer insulation equivalent life [h]
$e(P)$	Generator emission rate as a function of demanded power level P [kg/h]
$E_A^{(q)}$	Hydro generator percent energy available in quarter-q [%]
G	Total gasoline consumed by N_T vehicles with P_{PHEV} penetration of PHEVs [gal.]
$\boldsymbol{G}$	Electro-thermal transformer model conductance matrix [W/˚C]
$\overline{G_{IC}^{(c)}}$	IC vehicle in class-c sample population average gasoline consumed [gal./veh.]
G_{IC}	Total gasoline consumed by a fleet of N_T IC vehicles [gal.]
G_{PHEV}	Total gasoline consumed by a fleet of $N_T \cdot P_{PHEV}$ PHEVs [gal.]

LIST OF SYMBOLS (4)

h_c	Hour when PHEV-v on day-d in class-c is charging [h]
H_E	Full energy available from hydro generators [MWh]
$h(P)$	Generator heat rate as a function of demanded power level P [kcal/h]
$H_P^{(q)}$	Hydro generator power available in quarter-q [MW]
I^*	Maximum current available from the charging circuit [A]
I_0	Transformer high voltage winding current [A]
I_1	Transformer 120 V winding line 1 current [A]
I_2	Transformer 120 V winding line 2 current [A]
$\overline{I_0}$	Transformer average high voltage winding current [A]
$\overline{I_1}$	Transformer average 120 V winding line 1 current [A]
$\overline{I_2}$	Transformer average 120 V winding line 2 current [A]
$IC_{CO2}^{(c)}$	Internal combustion vehicle CO_2 rate for class-c [kg/mi.]
$IC_{MPG}^{(c)}$	Internal combustion vehicle MPG for class-c [mi./gal.]
$IC_{NOx}^{(c)}$	Internal combustion vehicle NO_x rate for class-c [kg/mi.]
$\overline{I_{L1}}$	Transformer average 120 V load 1 current [A]
$\overline{I_{L2}}$	Transformer average 120 V load 2 current [A]
$\overline{I_{L3}}$	Transformer average 240 V load current [A]
$I^{(v,d,c)}$	The required recharge current for vehicle-v in class-c [A]
k_{PHEV}	PHEV amount of driving energy derived from electricity [%]
$k_{PHEV}^{(c)}$	RV representing the PHEV in class-c k_{PHEV} [%]
$k_{PHEV,\max}^{(c)}$	Maximum k_{PHEV} value for PHEV in class-c [%]
$k_{PHEV,\min}^{(c)}$	Minimum k_{PHEV} value for PHEV in class-c [%]

LIST OF SYMBOLS (5)

$LDC[h_c]$	Load demand array of the required power for all PHEVs in hour-h_c [MW]
$M_E^{(c)}$	PHEV charge depleting distance for PHEV in class-c [mi.]
M_E^*	Optimal trip length, i.e. X in PHEV-X [mi.]
$MPG^{(c)}(0)$	PHEV in class-c charge sustaining MPG performance [mi./gal.]
$MPG^{(c)}(k_{PHEV})$	PHEV performance metric MPG function [mi./gal.]
$M^{(v,d)}$	RV representing the daily distance driven by vehicle-v on day-d [mi.]
n	Sample size of the vehicles simulated
N	Standard normal distributed RV
$\vec{N}$	Vector of IID standard normal RVs
$N_{PHEV}^{(c)}$	Number of PHEVs in class-c
N_L	Transformer insulation normal life span [h]
$NO_x^{(c)}(0)$	PHEV charge sustaining NO_x rate [kg/mi.]
$NO_x^{(c)}(k_{PHEV})$	PHEV performance metric NO_x rate function [kg/mi.]
n_t	Center-tapped single phase transformer turns ratio
N_T	Total number of vehicle in the power system area
p	Distribution-p, the particular distribution from the daily timing distributions
P	Added real power demand due to PHEV [W]
$\bar{P}$	Average feeder real power demand [W]
$p^{(c)}$	Percentage of vehicles in class-c
$P^{(c)}(k_{PHEV})$	Generic term for $NO_x^{(c)}(k_{PHEV})$ or $CO_2^{(c)}(k_{PHEV})$ [kg/mi.]
$\overline{p.f.}$	Expected feeder power factor
$p.f.^{(h)}$	Discrete RV representing the feeder power factor in hour-h
$P^{(h)}$	RV representing the household electric load real power demand in hour-h [W]

LIST OF SYMBOLS (6)

P_L	Transformer insulation percent loss of life [%]
P_{PHEV}	Percentage penetration of PHEV into the light-duty vehicle fleet
p_v	PHEV power demand per hour [MW]
q	Quarter-q, calendar quarter
Q	Added reactive power due to PHEV [VAR]
$\bar{Q}$	Average feeder reactive power demand [VAR]
$\vec{Q}$	Electro-thermal transformer model heat input vector [W]
$Q^{(h)}$	Household electric load reactive power demand in hour-h [VA]
R_A	Transformer series resistance [p.u.]
S_{L1}	Center-tapped single phase transformer 120 V complex load 1 [VA]
S_{L2}	Center-tapped single phase transformer 120 V complex load 2 [VA]
S_{L3}	Center-tapped single phase transformer 240 V complex load [VA]
$\overline{S_{L1}}$	Average 120 V complex load 1 [VA]
$\overline{S_{L2}}$	Average 120 V complex load 2 [VA]
$\overline{S_{L3}}$	Average 240 V complex load [VA]
t	Trapezoidal integration method current time [sec]
$\vec{T}$	Electro-thermal transformer model temperature vector [˚C]
$\tilde{T}_h$	Transformer hot-spot temperature [˚C]
T^m	Total distance driven in the simulation period for vehicle-v [mi.]
u	Trapezoidal integration method time step length [sec]
U_1	Uniformly distributed (0,1] IID pseudo random number
U_2	Uniformly distributed (0,1] IID pseudo random number
v	Vehicle-v, a particular vehicle sampled from the total vehicle population

LIST OF SYMBOLS (7)

$\overline{V_1}$	Average 120 V load 1 voltage [V]
$\overline{V_2}$	Average 120 V load 2 voltage [V]
V_s	Center-tapped single phase transformer model source voltage [V]
$V^{(v,c)}$	RV representing the recharge voltage for vehicle-v in class-c [V]
$\vec{\mathrm{X}}$	Linear least square unknown vector
X_A	Transformer series reactance [p.u.]
$\vec{\mathrm{X}}_{VD}$	Vector of generated random vehicle design parameters
$\vec{Y}$	Linear least square known data vector
$\overline{Y_{EAP}^{(c)}}$	PHEV sample population average EAP generated per vehicle in class-c [kg/veh.]
$\overline{Y_G^{(c)}}$	PHEV sample population average gasoline consumed per vehicle in class-c [gal./veh.]
$Y_{EAP}^{(v,c)}$	Yearly EAP generated by PHEV-v in class-c [kg]
$Y_G^{(v,c)}$	Yearly gasoline usage consumed by PHEV-v in class-c [gal.]
Z_0	Center-tapped single phase transformer high voltage winding impedance [Ω]
Z_1	Center-tapped single phase transformer low voltage winding 1 impedance [Ω]
Z_2	Center-tapped single phase transformer low voltage winding 2 impedance [Ω]
$Z_{\text{base high voltage}}$	High voltage per-unit base impedance value [Ω]
$Z_{\text{base low voltage}}$	Low voltage per-unit base impedance value [Ω]
$Z_{\text{p.u.0}}$	Center-tapped single phase transformer high voltage winding impedance [p.u.]
$Z_{\text{p.u.1}}$	Center-tapped single phase transformer low voltage winding 1 impedance [p.u.]
$Z_{\text{p.u.2}}$	Center-tapped single phase transformer low voltage winding 2 impedance [p.u.]

LIST OF ACRONYMS AND INITIALISMS

ADVISOR	Advanced Vehicle Simulator
AEC	Average Electricity Cost
BEV	Battery Electric Vehicle
CC	Combined Cycle generation plant
CT	Combustion Turbine
EAP	Environmental Air Pollution
EIA	Energy Information Agency
EPRI	Electric Power Research Institute
FOR	Forced Outage Rate
GE	Total Generated Energy
GPS	Global Positioning Satellite
GUI	Graphical User Interface
HEV	Hybrid Electric Vehicle
HWFET	Highway Fuel Economy Test
IC	Internal Combustion
IID	Independent and Identically Distributed
LOL	Loss-of-Life
LOLP	Loss-of-Load Probability
MLE	Maximum Likelihood Estimator
MPG	Miles per Gallon
MTTF	Mean Time to Failure
MTTR	Mean Time to Repair
NEMS	National Energy Modeling System

LIST OF ACRONYMS AND INITIALISMS (2)

NERC	North American Electric Reliability Corporation
NESSIE	National Electric System Simulation Integrated Evaluator
NILDC	Normalized Inverted Load Duration Curve
ORCED	Oak Ridge Competitive Electricity Dispatch
PHEV	Plug-In Hybrid Electric Vehicle
PPC	Probabilistic Production Costing
PROSYM	Proprietary Hourly Power System Evaluation Model
PSAT	Powertrain System Analysis Toolkit
RTS	Reliability Test System
RV	Random Variable
ST	Steam Turbine
TFC	Total Fuel Cost
TVA	Tennessee Valley Authority
UDDS	Urban Dynamometer Driving Schedule
UE	Unserviced Energy
US06	Updated federal test driving cycle

SUMMARY

Two studies are presented quantifying the impact of plug-in hybrid vehicles (PHEVs) on power systems. The first study quantifies this impact in terms of (a) primary fuel utilization shifts, (b) pollution shifts, and (c) total cost for consumers. The second study quantifies this impact on distribution transformers.

In the first study vehicle fleet and power system simulations are used. The vehicle fleet simulations compute the amount of added electric load demand to charge the PHEV fleet, the amount of gasoline used by both internal combustion (IC) vehicles and PHEVs, and the amount of environmental air pollution (EAP) generated by both IC vehicles and PHEVs. The power system simulations simulate how much fuel usage and subsequent EAP are generated by a specific power system.

In the second study the impact on distribution transformers is quantified through a loss-of-life (LOL) calculation that is based on the transformers hot-spot temperature. This temperature is estimated using an electro-thermal transformer model and is a function of the transformer currents. These currents are computed using a center-tapped single phase transformer model.

The results from this research indicate that PHEVs offer cleaner transportation (depending on the generation mix used to charge the vehicles) with decreased gasoline utilization at a lower operating cost to consumers. The utility infrastructure impact to pay for these three advantages is added wear to distribution transformers.

CHAPTER 1

INTRODUCTION

Presently, the U.S. is importing crude oil at the rate of 10.0 Mb/day [1]. Additionally, approximately 5.1 Mb/day of crude oil are produced domestically [1]. Two-thirds (62.9%) of this oil is refined into gasoline and diesel fuel to power U.S. passenger vehicles and trucks [2]. Thus, the majority of U.S. passenger vehicles and trucks are fueled by imported oil. A number of options have been proposed to reduce the use of imported oil including: finding more oil, increasing vehicle fuel economy, using ethanol as a vehicle fuel, using conventional hybrid electric vehicles (HEVs), and using plug-in HEVs (PHEVs).

Aftermarket conversion of a currently available HEV into a PHEV is possible today [3], suggesting that PHEV technology is feasible for significant levels of market penetration in the near future. PHEVs represent a potentially lucrative new semi-dispatchable load for the electric utility industry.

The key potential benefit to the electric utility industry is the possible addition of a large controllable load. Just under 400 million gallons of gasoline a day are used in the U.S. [4]. If PHEV drivers were to charge off peak this additional load would be added with minimal increased need for added generation.

Displacing petroleum usage with electric energy would diversify the transportation sector energy usage. The energy mix used in transportation (Figure 1.1) is 96% petroleum [5]. Displacing a small portion of this energy distribution with the energy

mixture used in the electric power system (Figure 1.2) has the potential to add three new fuel types to the transportation sector energy mix.

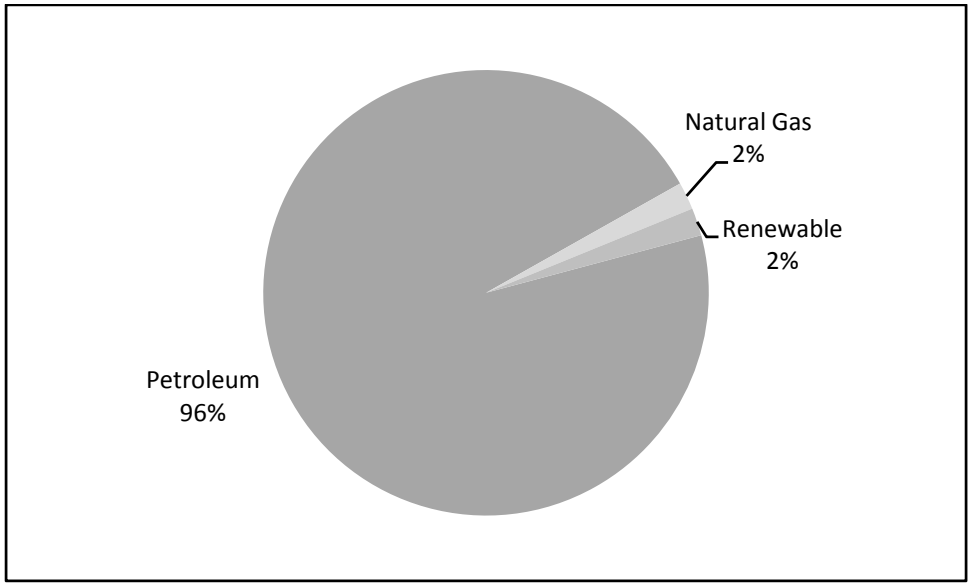

Figure 1.1. Energy mix used in transportation [5].

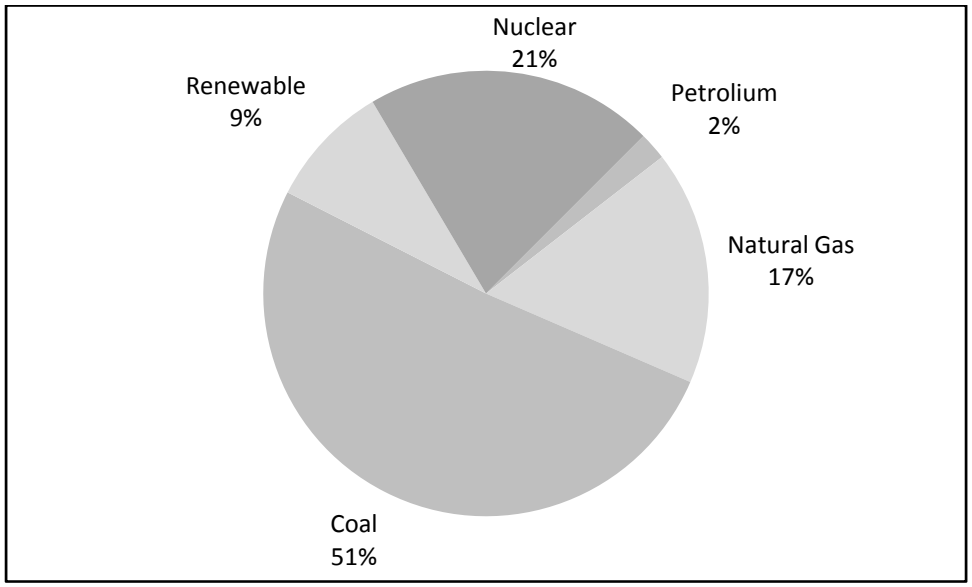

Figure 1.2. Energy mix used in the electric utility industry [5].

The remainder of this thesis is organized as follows:

- Related published literature is examined and the context which this thesis fits into the broader research is evaluative (Chapter 2).

- Research into the impact of diversifying the transportation energy mix is described in terms of primary energy source utilization, environmental air pollution (EAP), and gasoline consumption (Chapter 3).
- Research into the potential impact of increased loading on an aging infrastructure is described utilizing a loss-of-life indication on distribution transformers (Chapter 4).
- A summary of the results are included in the conclusion (Chapter 5).

CHAPTER 2

LITERATURE REVIEW

Two foci of this research are (1) which power system fuel types will be utilized to meet the added electric energy demand used to charge plug-in hybrid electric vehicles (PHEVs) and (2) what will be the impact of the increased electricity demand on pole top distribution transformers. The first focus includes two related considerations of (1) how many vehicles an existing power system can accommodate and (2) the total system environmental air pollution (EAP) which includes EAP from both the vehicle fleet and from the power system.

2.1 First Focus

The first focus of this research has received much attention in currently available literature. The second focus has received only minimal attention in currently available literature. First, a subset of the currently available literature related to focus number one is introduced. Second, a single document is introduced related to focus number two. Finally, the contribution provided by the present work is summarized.

What impact will charging PHEVs have on the electric power system? This question has been investigated by many research groups, in many different ways, focusing on a number of implications. The questions answered by others include:

- How many vehicles can a power system accommodate?
- Which fuel types will the added load utilize?
- What added EAP will be generated by this new load?
- Can the electric utility infrastructure withstand the potential additional load?

Two investigations which computed the number of vehicles that existing power systems could support found that the percentage of the U.S. light duty vehicle fleet that could be supported was 34% (charging the vehicle between 22:00 and 08:00) [6], 43% (charging between 18:00 and 06:00) and 73% (charging all day) [7]. The calculations in both reports are quite similar.

Key PHEV assumptions made in both investigations, including vehicle energy required per mile and total miles driven per year, shown in Table 2.1.

Table 2.1. Vehicle assumptions made in penetration level papers.

Report	Total Miles Driven [mi.]	Grid energy required per mile [kWh/mi.]
[6]	14,300	0.41
[7]	12,000	0.26 – Compact sedan
		0.30 – Mid-size sedan
		0.38 – Mid-size SUV
		0.46 – Full-size SUV

Clear reasons for the discrepancy between these results include more conservative charging time limits in [6] then [7], more miles driven per year in [6] then [7], and higher grid energy requirements in [6] over every vehicle size in [7] except the full size SUV. Each of these factors leads to a lower percentage penetration result in [6] then [7].

In [8] an optimal dispatch charging procedure is outlined and results conclude that 50% penetration of the light duty vehicle fleet, where vehicles derived 40% of their miles from electricity, could be met by existing generation capacity. In this report the vehicle assumptions include an average grid electric energy demand of 0.34 kWh per mile and different average daily driving distances depending on different U.S. regions, from 29.8 miles per day in the southwestern study region to 42.2 miles per day in the central study region. This level of penetration is clearly within the ranges indicated in the first two reports discussed ([6], and [7]).

Additional research has focused on the impact that charging PHEVs will have on primary energy source utilization, where primary energy source utilization refers to which power system fuel type/s will be utilized to meet the added demand due to PHEV charging. Specifically, investigations have been performed using the Xcel power system [9] and the 13 regions specified by the North American Electric Reliability Corporation (NERC) [10].

In [9], three vehicle types were modeled: conventional vehicles (CVs), HEVs, and PHEV-20s, where PHEV-X indicates a PHEV which is capable of driving X miles using the battery alone. Each vehicles equivalent miles per gallon (MPG) is shown in Table 2.2. The PHEV fuel efficiency was computed using Advanced Vehicle Simulator (ADVISOR) [11].

Table 2.2. Vehicle MPG [9].

	CV	HEV	PHEV-20
MPG [mi./gal.]	26	36	37

In [9] vehicle assumptions include an annual driving distance of 13,900 miles per year, a PHEV grid electric energy demand of 0.36 kWh per mile, and a PHEV battery capacity of 7.2 kWh. Further, in [9] four vehicle charging cases were defined:

Case 1. Uncontrolled charging, which meant each vehicle charged at a rate of 1.4 kW where charging started whenever the vehicle arrived home and charged only at home.

Case 2. Delayed charging, which meant all vehicles from case 1 are delayed until 10 pm to start charging.

Case 3. Off-peak charging, which meant utility control of vehicle charging times at a rate of 3.2 kW (providing a least cost scenario).

Case 4. Continuous charging, which meant each vehicle charged at a rate of 1.4 kW where mid-day charging is capable (providing a maximum amount of electric drive mileage and minimum gasoline case).

Finally, vehicle fleet daily driving performance was based on global positioning satellite (GPS) recorded vehicle data of 227 vehicles in St. Louis, Missouri [9]. Results

of electricity usage, gasoline consumed, and total fuel costs are shown in Table 2.3. In these results fuel cost is the cost of only gasoline purchasing for CVs and HEVs where as this cost includes both gasoline and electric energy purchasing for the PHEV cases.

Table 2.3. Vehicle performance results [9].

	CV	HEV	PHEV Cases 1-3 (Charging once per day)	PHEV Case 4 (Continuous charging)
Electricity Required [kWh] (Daily / Annual)	0	0	5.3 / 1,944	9.4 / 3,530
Annual Gasoline Use [gal.]	535	386	237	145
Annual Fuel Cost [$]	1,375	993	778	614

The annual fuel cost was computed using $2.57 per gallon of gasoline and 8.6 cents per kWh electricity rates [9]. From the results in Table 2.3, it is clear that total gasoline consumption and annual fuel cost are reduced in all PHEV cases over the CV and HEV operation. Regardless of charging method the annual reduction in gasoline utilization, driving PHEVs versus CV, would be at least 298 gallons of gasoline per vehicle and at least $597 saved in fuel costs per vehicle.

The primary energy source utilization results in [9] include the impact of PHEV charging on the total system load, the EAP emissions (vehicle and power system), and the marginal cost of electricity. This study considered a penetration level of 500,000 vehicles, or equivalently 30% of the light-duty vehicle fleet in the Xcel Energy, Inc. service territory. The power system simulations were computed using Proprietary Hourly Power System Evaluation Model (PROSYM). The PROSYM software computed generator dispatching, on an hourly basis, and generated EAP for each of the four charging cases [9].

The 2005 power system generating mix and energy generated for all of Colorado based on fuel type is shown in Figures 2.1 and 2.2. Xcel Energy, Inc. serves

approximately 55% of the total Colorado population and supports 55% of the total Colorado annual electricity demand.

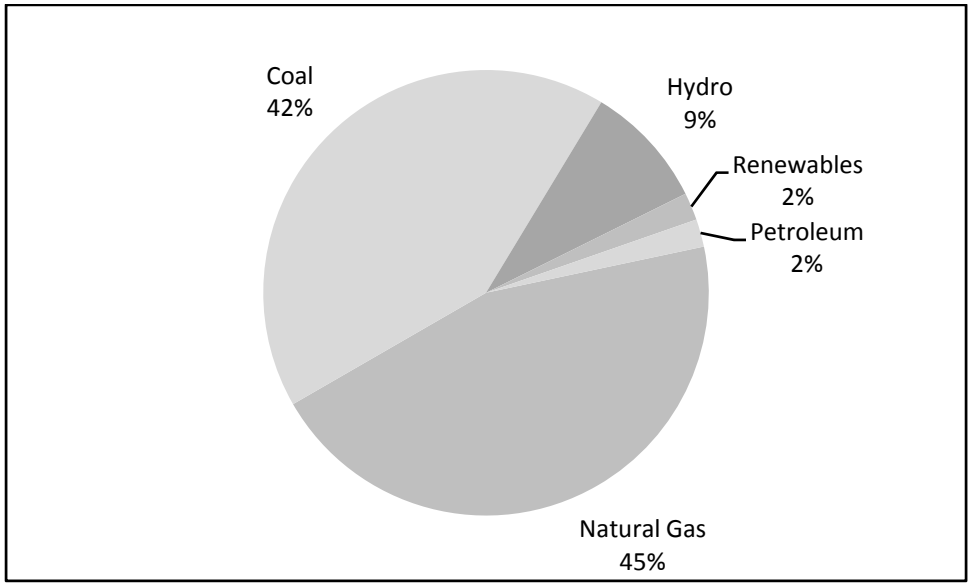

Figure 2.1. 2005 electric power system generation capacity by fuel type for Colorado [9].

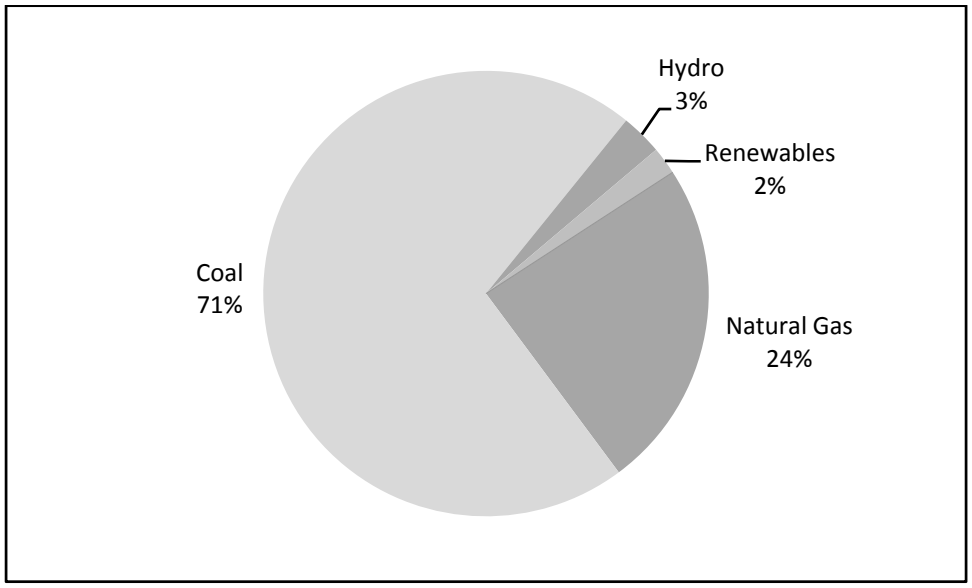

Figure 2.2. 2005 electric power system energy generation by fuel type for Colorado [9].

In [9] results showed the percent of energy from each generator type for the four charging cases. The three generator types considered were simple cycle and other gas

(reciprocating and steam units); combined cycle gas; and coal. The percentage of energy produced from each generator type for each charging scenario is shown in Figure 2.3.

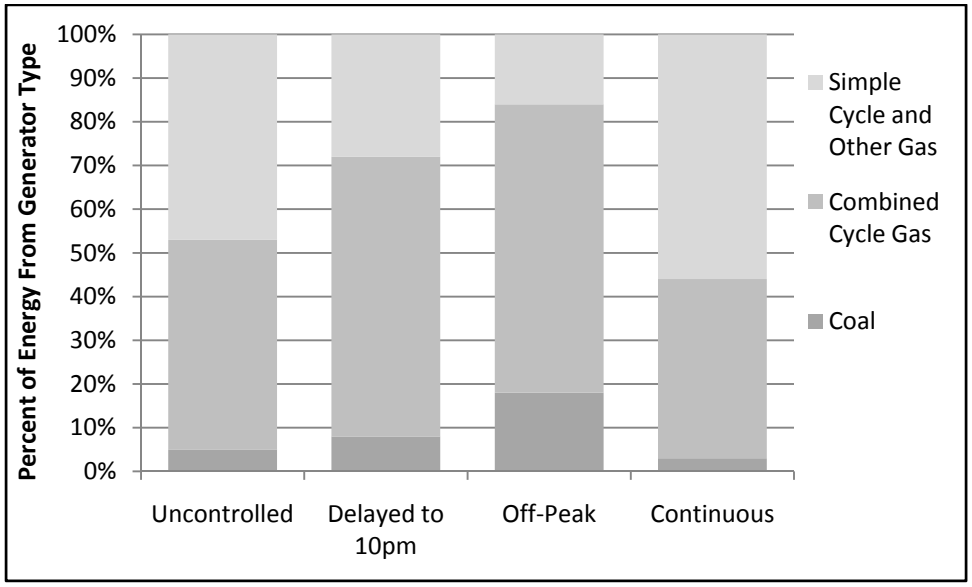

Figure 2.3. Generator type used to charge PHEV in the Xcel service area [9].

This analysis showed that natural gas is utilized to meet the majority of the PHEV charging load. Also, as the PHEV charging load is shifted later in the evening and off peak the coal utilization increased. Further results drawn in this work include a small decrease in total NO_x generated and a significant reduction in total CO_2. Next, the investigation of the 13 regions specified by the NERC in terms of PHEV primary energy source utilization [10] is described.

In [10] an analysis is provided of primary energy source utilization due to PHEV charging for each of the 13 NERC regions of the U.S. This analysis utilized the Oak Ridge Competitive Electricity Dispatch (ORCED) model to compute primary energy source utilization and power system EAP generated. This analysis included two different charging time considerations and three different charging rates. The first charging time was called "evening" and was defined by PHEV charging starting at 5 pm and the second

charging time scenario was called "night" and was defined by PHEV charging starting at 10 pm. The three charging rates were 120V/15A (1.4kW), 120V/20A (2kW), and 220V/30A (6kW). All PHEV charging included nine hours of charging. Two future time frames were simulated. The first time frame was in the year 2020 and the second in the year 2030. The projected level of PHEV penetration in 2020 was estimated to be 19.58% and in 2030 was estimated to be 50.39%.

This report [10] documented results for all 13 NERC regions. The results summarized here are the sum of the results for all 13 regions. The *power* generating capacity for the 13 regions projected to 2020 is shown in Figure 2.4. The base case *energy* generated for the 13 regions in 2020 is shown in Figure 2.5. Comparable figures for 2030 are Figures 2.6 and 2.7. In each of these figures ST, CT, and CC represent steam turbines, combustion turbines and combined cycle generation plants respectively.

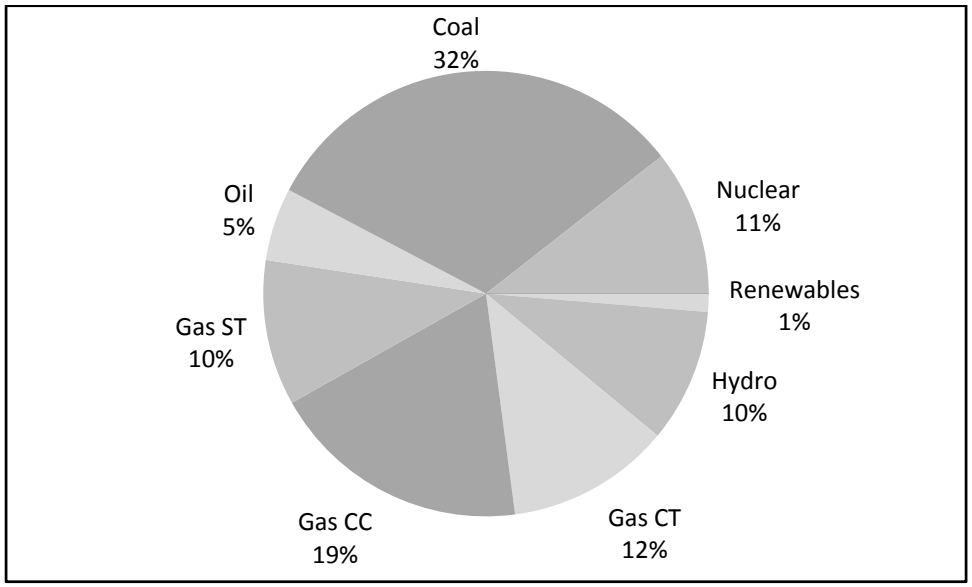

Figure 2.4. Projected power generating capacity in 2020 [10].

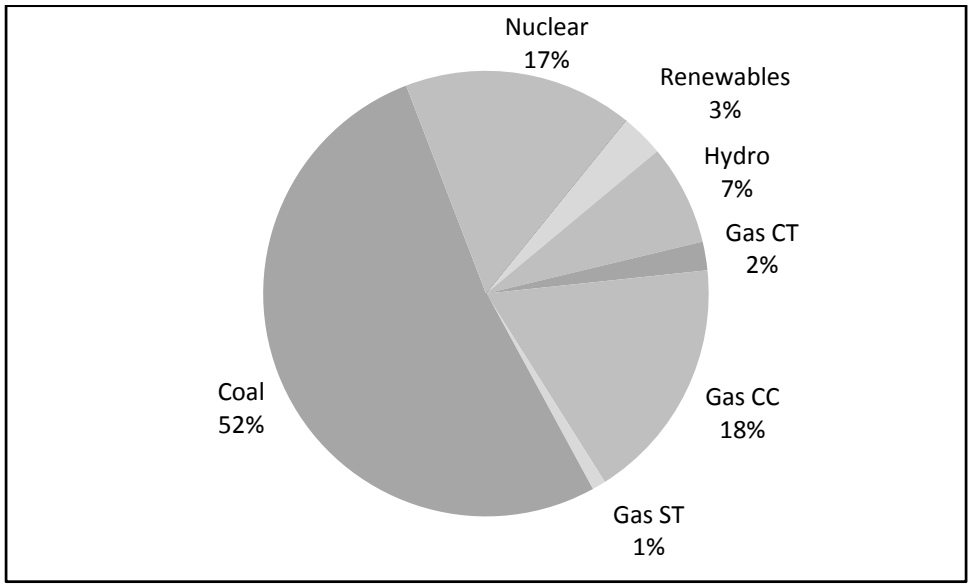

Figure 2.5. Computed base case energy generated in 2020 [10].

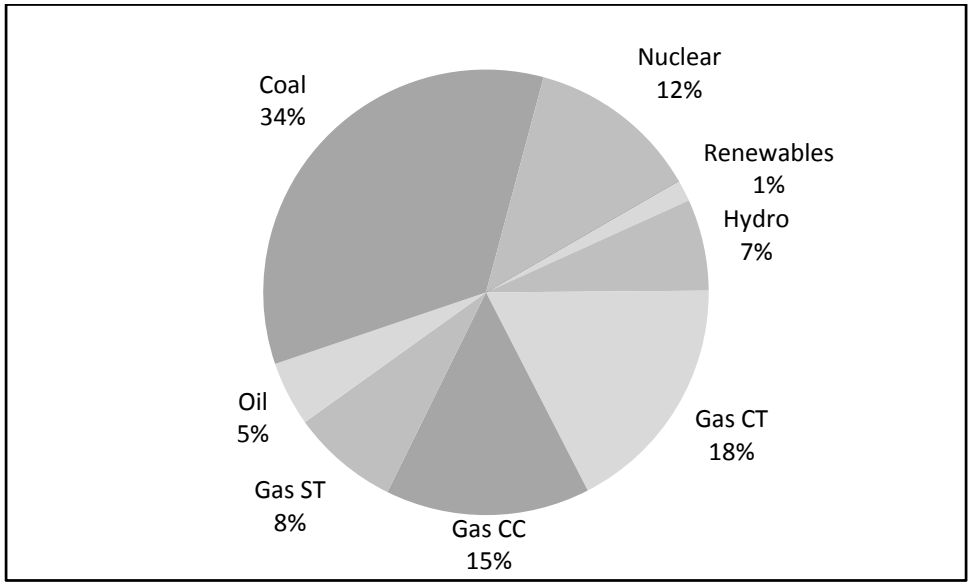

Figure 2.6. Projected power generating capacity in 2030 [10].

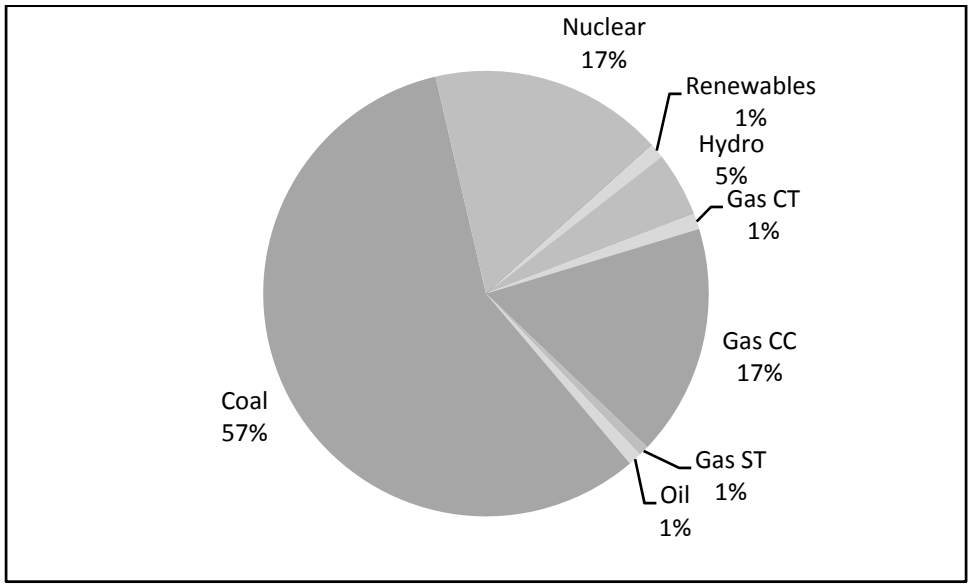

Figure 2.7. Computed base case energy generated in 2030 [10].

This investigation [10] compared the projected primary energy source utilization and EAP generated with and without PHEV penetration in the years 2020 and 2030 for each charging scenario. Vehicle assumptions included daily driving distance of 20 miles per day, PHEVs operated in an all electric driving mode, and a HEV fuel efficiency of 40 MPG. The primary energy source utilization results from this investigation for each charging scenario are summarized in Figures 2.8 and 2.9 for the 2020 and 2030 results respectively. In each of these figures the projected increase in energy generated for each fuel type is shown.

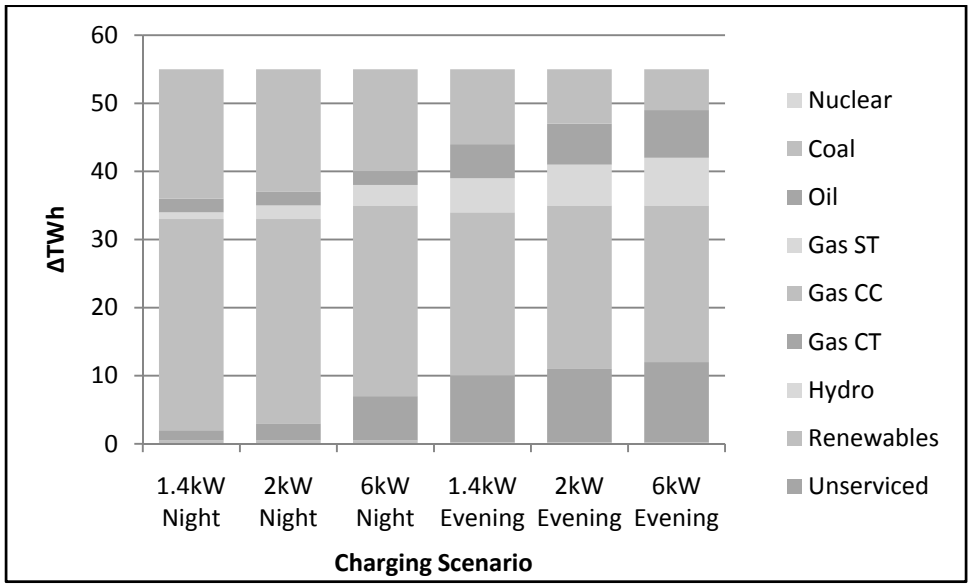

Figure 2.8. Computed increase in energy per fuel type for 2020 [10].

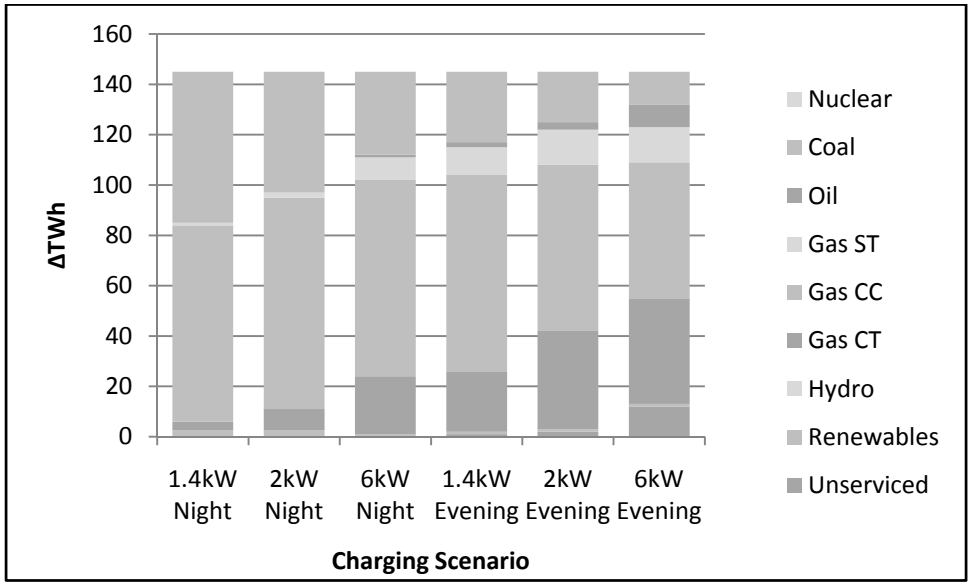

Figure 2.9. Computed increase in energy per fuel type for 2030 [10].

In both time frames 2020 and 2030 and all charging scenarios, the three most utilized fuel types were gas CC, gas CT and coal. Emission results showed CO_2 emissions slightly higher in most NERC regions, contradicting the CO_2 results in [9]. The generation of the other two pollutants considered, NO_x and SO_2, were limited by regulation caps. This limitation invalidates any comparison of emission results between

studies for NO_x and SO_2. Next, an additional study of EAP effects of PHEV use is summarized.

In [12] nine scenarios of annual CO_2 emission scenarios were simulated. The nine scenarios were all possible combinations of three levels of power system CO_2 emission intensity and three levels of PHEV penetration levels. From the nine scenarios the follow conclusions were drawn:

- CO_2 emissions decreased significantly in each of the nine scenarios.
- The maximum of CO_2 reduction was achieved with the combination of high PHEV penetration and the low power system CO_2 intensity.
- Cumulative CO_2 emission reductions were simulated in the range of 3.4 to 10.3 billion tons. The simulation operated in the time span of 2010 through 2050.
- Regionally each area of the country will have CO_2 reductions.

The common reduction in CO_2 for each regional area was contradicted in [10] where emission levels did not follow any consistent pattern.

The modeling in [12] simulated the evolution of the power system and transportation utilization over the 2010 to 2050 time span. The power system model was a combination of the Energy Information Agency's (EIA) National Energy Modeling System (NEMS) [13] and the Electric Power Research Institute (EPRI) National Electric System Simulation Integrated Evaluator (NESSIE). The transportation utilization modeled both vehicle emissions and market adoption of PHEVs.

Additional research literature which investigated the impact that PHEV operation will have on EAP production includes [14], [15], and [16]. These investigations lack an analysis of EAP produced from the electric power system, thus missing half of the picture when comparing the operation of PHEVs with the use of CVs. Next, literature documenting the impact of PHEV charging on the electric infrastructure is introduced.

2.2 Second Focus

Thus far, the mentioned research has focused on (1) the number of vehicles an existing power system idle generation capacity can accommodate, (2) the primary energy source utilization of PHEV charging, and (3) the EAP produced by PHEV utilization. The question remains what, if any, impact will PHEV charging have on the electric power infrastructure itself? The potential impact was quantified in [17].

An advantage of a higher utilization factor of the electric power utility, achievable with the use of PHEVs [6], [7], and [8], is "an efficiency gain, distributing average costs over a greater number of kilowatt-hours" [17]. However, oil-cooled transformers rely on common utilization patterns to avoid the detrimental effects of overheating. In [17] the transformers temperature and life expectancy were modeled using a Montsinger equation. Further, a sensitivity analysis of the modeled transformer temperature indicated that, "the current transformer designs may represent a significant constraint with respect to integration PHEVs into central-station power systems" [17].

In summary, a review of the literature shows that existing reserve capacity is capable of supporting a sizable portion of the light duty vehicle fleet replaced by PHEVs, the added electric energy will be met by primary energy sources depending on the generating mix, mixed EAP results, and oil-cooled transformers may represent a constraint on integrating PHEVs into the existing infrastructure.

This thesis adds to the existing body of research by (1) developing a probabilistic analysis of the well documented topic of PHEV primary energy source utilization, (2) quantifying the loss-of-life of pole top transformers using probabilistic simulations.

The impact of PHEV charging on primary energy source utilization is described next.

CHAPTER 3

IMPACT OF PHEV CHARGING ON PRIMARY ENERGY SOURCE UTILIZATION

To quantify where the electric energy used to charge plug-in hybrid electric vehicles (PHEVs) is generated, a probabilistic simulation program was developed. Two key steps of this simulation program include vehicle fleet simulations and power system simulations. The vehicle fleet simulations compute the amount of added electric load demand to charge the PHEV fleet, the amount of gasoline used by both internal combustion (IC) vehicles and PHEVs, and the amount of environmental air pollution (EAP) generated by both IC vehicles and PHEVs. The power system simulations simulate how much fuel usage and subsequent EAP are generated by a specific power system. The specific power system simulation is based on the Probabilistic Production Costing (PPC) [18] power system simulation procedure.

3.1 Probabilistic Simulation of an Integrated Power System with Distributed PHEVs Methodology

A top level block diagram of the probabilistic simulation program is shown in Figure 3.1.

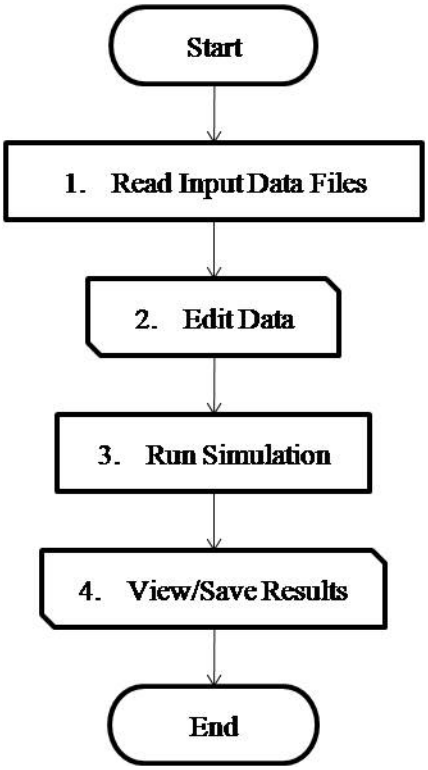

Figure3.1. Simulation overview block diagram.

In Figure 3.1 step 1 is initiated when an input file is opened, step 2 is an optional step where the program user may or may not edit the input data, step 3 is broken into four sub-steps shown in Figure 3.2, and step 4 is an optional step where the program user may or may not view or save the simulation results.

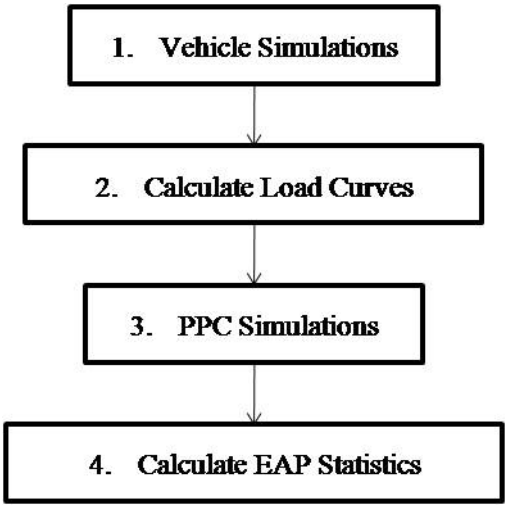

Figure 3.2. Simulation sub-steps block diagram.

Each sub-step in Figure 3.2 is used to perform the probabilistic simulation. Specifically, sub-step 1 initializes the vehicle fleet performance metrics, generates the vehicle operation distributions, and computes the gasoline usage statistics. Sub-step 2, computes the chronological load demand curves and the normalized inverted load duration curves (NILDCs). Sub-step 3, performs the PPC power system simulation procedure. Sub-step 4, computes the IC vehicle EAP and PHEV EAP statistics.

In the reminder of this section:

- The vehicle fleet simulations are fully described.
- The power system load curve calculation method is fully described.
- The power system simulations are fully described.

3.1.1 Vehicle Simulation

In the first sub step of Figure 3.2 the vehicle fleet parameters are computed based on vehicle simulations performed using Powertrain System Analysis Toolkit (PSAT) version 6.2, developed by DOEs Argonne National Labs [19]. In PSAT the simulation of IC and hybrid powertrains generate vehicle operational data from which IC vehicle and PHEV models are developed. The development of the vehicle classes and the PSAT simulations are documented in [20] which at the time of this thesis has not been published. Full PSAT results are shown in Appendix 1, and this data is utilized to compute the results below.

Four vehicle classes were arbitrarily selected to provide a diverse vehicle fleet representative of what a real vehicle fleet could look like in the future. The following vehicles were used as inspiration for each class [20]:

Class 1: Honda Civic and Ford Focus.
Class 2: Honda Accord and Ford Taurus.
Class 3: Ford Explorer and Ford F-150.
Class 4: Chevrolet Suburban and Chevrolet Silverado.

Once the complete vehicle models had been selected, PSAT simulated the operation of the modeled vehicles over specified driving schedules. Three drive schedules Highway Fuel Economy Test (HWFET), Urban Dynamometer Driving Schedule (UDDS), and the updated federal test driving cycle (US06) were selected to generate varied results representative of an entire vehicle fleet [20]. First the PSAT IC vehicle results are described followed by the PSAT PHEV results.

3.1.1.1 Vehicle Fleet Performance Metrics

The PSAT IC vehicle simulations resulted in fuel efficiency, NO_x generated per mile driven, and CO_2 generated per mile driven for each vehicle class over each of the three drive cycles (Table A.5) [20]. To compute a single estimate, for each of the performance metrics (fuel efficiency, NO_x generated per mile driven, and CO_2 generated per mile driven), for each vehicle class (classes 1-4) a weighted average of the results for each drive cycle is computed. The US06 drive cycle represents more modern driving and as such is weighted 50%. The remaining 50% is split 55% UDDS and 45% HWFET analogous to the comprehensive EPA fuel efficiency. The resulting weighted average performance metric for each class is shown in Table 3.1.

Table 3.1. PSAT IC results for each vehicle class.

Class	1	2	3	4
MPG [mi./gal.], $IC_{MPG}^{(c)}$	27.58	23.52	15.17	11.89
NO_x generated per mile [kg/mi.], $IC_{NOx}^{(c)}$	1.643E-04	1.904E-04	2.778E-04	3.253E-04
CO_2 generated per mile [kg/mi.], $IC_{CO2}^{(c)}$	0.3300	0.3884	0.6016	0.7656

Next, the PHEV PSAT results are described. No mass production PHEVs are currently available thus the performance metrics including energy required per mile, gasoline efficiency, and EAP generated per mile are approximated based on PSAT simulation results [20].

PSAT simulations were performed for each vehicle class over each drive cycle and varying the amount of drive energy supplied from the vehicles battery [20]. The variable amount of driving energy supplied from the vehicles battery was defined as $k_{PHEV}(k_{PHEV} \in [0,1])$ [20]. This parameter is defined such that, $k_{PHEV} = 0$ represented a charge sustaining hybrid i.e. on average all of the drive energy came from gasoline and $k_{PHEV} = 1$ represented a pure battery electric vehicle (BEV) i.e. all of the drive energy came from electricity [20].

The vehicle simulation methodology utilizes randomly generated vehicle design parameters including k_{PHEV}. To facilitate simulating PHEV operation without a priori knowledge of the exact value of k_{PHEV} performance metric functions (3.1 - 3.4) are approximated based on the discrete PSAT results (Tables A.1 - A.4). The method to compute the functional relations is described next.

$$E^{(c)}(k_{PHEV}) = A_E^{(c)} \cdot (k_{PHEV})^{B_E^{(c)}} \tag{3.1}$$

$$1/MPG^{(c)}(k_{PHEV}) = A_{GPM}^{(c)} \cdot (1 - k_{PHEV})^{B_{GPM}^{(c)}} \tag{3.2}$$

$$NO_x^{(c)}(k_{PHEV}) = A_{NOx}^{(c)} \cdot (1 - k_{PHEV})^{B_{NOx}^{(c)}} \tag{3.3}$$

$$CO_2^{(c)}(k_{PHEV}) = A_{C02}^{(c)} \cdot (1 - k_{PHEV})^{B_{CO2}^{(c)}} \tag{3.4}$$

Each performance metric function is a function of the vehicle design parameter k_{PHEV} and the vehicle class-c. In (3.1), $E^{(c)}(k_{PHEV})$ is the required energy per mile driven [kWh/mi.] and values of the function parameters $A_E^{(c)}$ [kWh/mi.] and $B_E^{(c)}$ are given in Table 3.2. In (3.2), $MPG^{(c)}(k_{PHEV})$ is the fuel efficiency [mi./gal.] and values of the function parameters $A_{GPM}^{(c)}$ [gal./mi.] and $B_{GPM}^{(c)}$ are given in Table 3.3. In (3.3), $NO_x^{(c)}(k_{PHEV})$ is the generated NO_x per mile driven [kg/mi.] and values of the function parameters $A_{NOx}^{(c)}$ [kg/mi.] and $B_{NOx}^{(c)}$ are given in Table 3.4. In (3.4), $CO_2^{(c)}(k_{PHEV})$ is the

generated CO_2 per mile driven [kg/mi.] and values of the function parameters $A_{C02}^{(c)}$ [kg/mi.] and $B_{C02}^{(c)}$ are given in Table 3.5.

Table 3.2. PHEV grid energy per mile function parameters for each vehicle class.

Class	A_E [kWh/mi.]	B_E
1	0.3790	0.4541
2	0.4288	0.4179
3	0.6720	0.4040
4	0.8180	0.4802

Table 3.3. PHEV fuel efficiency (1/MPG) function parameters for each vehicle class.

Class	A_{GPM} [gal./mi.]	B_{GPM}
1	0.0268	1.901
2	0.0329	1.892
3	0.0505	1.884
4	0.0547	1.844

Table 3.4. PHEV NO_x generated per mile function parameters for each vehicle class.

Class	A_{NOx} [kg/mi.]	B_{NOx}
1	1.341E-04	1.752
2	1.642E-04	2.113
3	2.209E-04	1.751
4	2.500E-04	1.501

Table 3.5. PHEV CO_2 generated per mile function parameters for each vehicle class.

Class	A_{CO2} [kg/mi.]	B_{CO2}
1	0.2423	1.916
2	0.2954	1.895
3	0.4555	1.875
4	0.4907	1.839

The function parameters (Tables 3.2 - 3.5) are estimated from the discrete PSAT results (Tables A.1 - A.4) using a weighted nonlinear least squares approximation method. Specifically, MATLABs function *lsqnonlin* [21] is used to compute the approximation function parameters.

Each drive cycle PSAT data and resulting weighted average performance metric function for the Class 2 data is shown in Figure 3.3 for the grid electric energy, in Figure 3.4 for the fuel efficiency, in Figure 3.5 for the NO_x generated per mile, and in Figure 3.6 for the CO_2 generated per mile. In Figures 3.3 - 3.6 the discrete drive cycle data [20] is shown with data markers and dashed lines, the weighted continuous approximations are shown with a solid line.

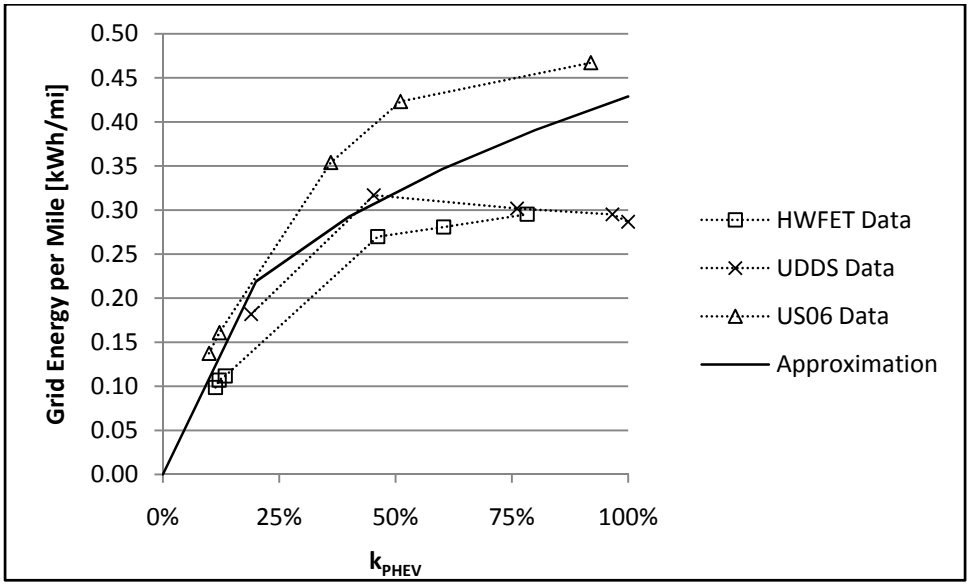

Figure 3.3. Class 2 PSAT discrete data and weighted average for the required grid energy performance metric.

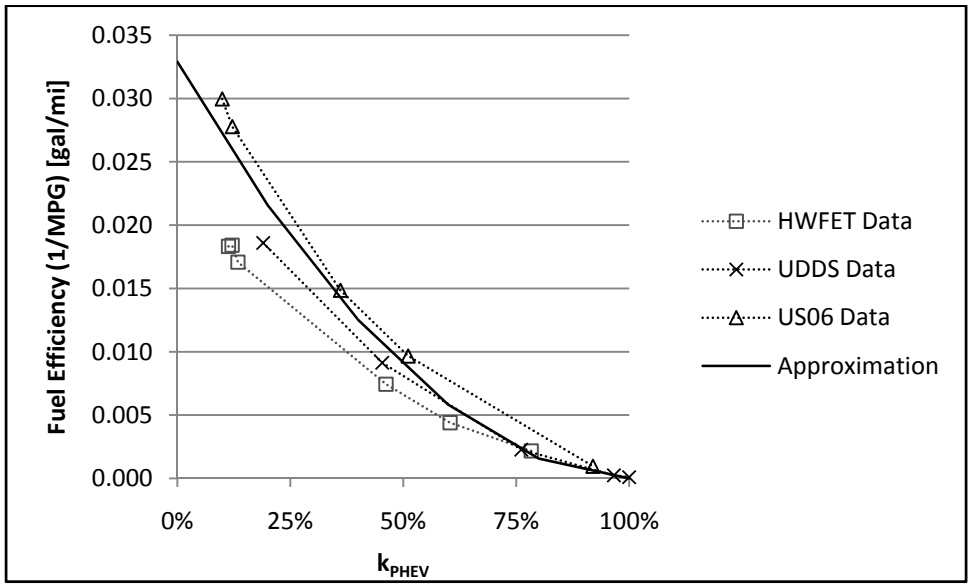

Figure 3.4. Class 2 PSAT discrete data and weighted average for the fuel efficiency performance metric.

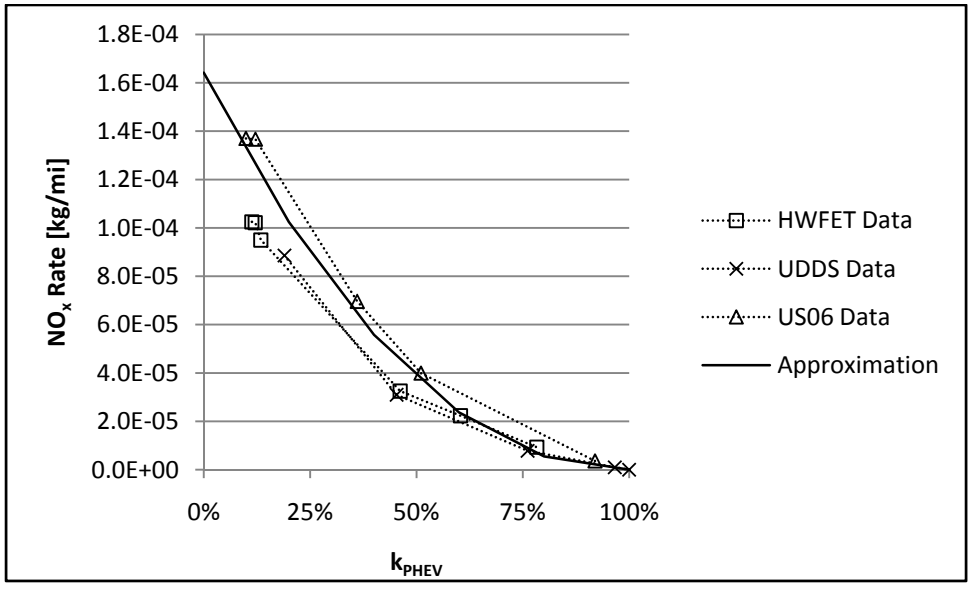

Figure 3.5. Class 2 PSAT discrete data and weighted average for the NO_x rate performance metric.

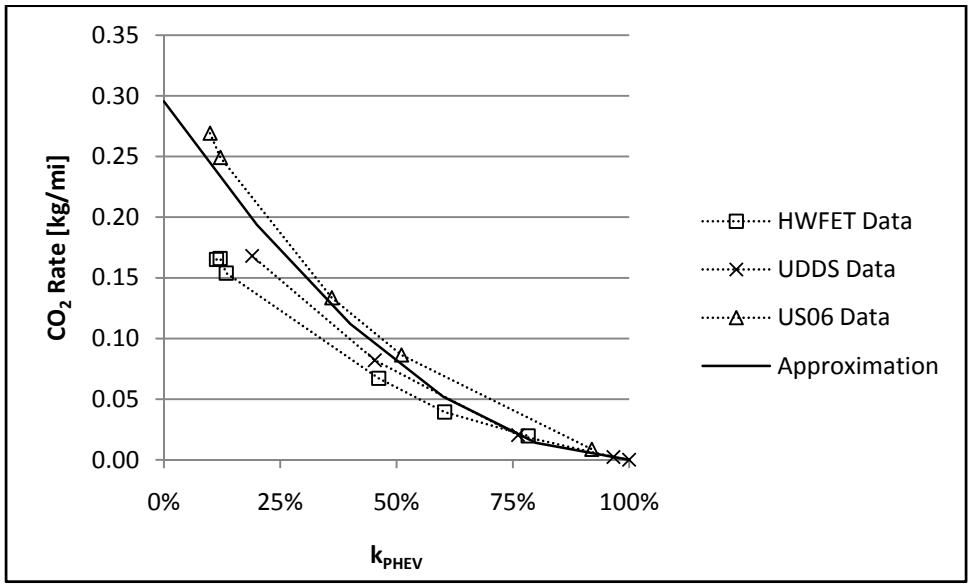

Figure 3.6. Class 2 PSAT discrete data and weighted average for the CO_2 rate performance metric.

The weighted average performance metric functions (3.1 - 3.4) are computed with the same weighting as the IC data results (50% US06, 27.5% UDDS, and 22.5% HWFET). The most accurate approximation of the PHEV energy per mile (3.1) for each class is a power trend line. In Figure 3.3 the approximated power function (3.1) closely matches the PSAT discrete data over the entire range of k_{PHEV} and when evaluated at $k_{PHEV} = 0$ evaluates to zero electrical energy required per mile driven as expected for a charge sustaining HEV. All other performance metrics are approximated with shifted power functions. In figures 3.4 through 3.6 the shifted approximation functions closely match the PSAT discrete data over the entire range of k_{PHEV}. These approximation functions (3.2 - 3.4) are shifted so that at $k_{PHEV} = 1$, and these functions then evaluate to zero. Thus, a BEV ($k_{PHEV} = 0$) requires no gasoline per mile driven (3.2) and produces no NO_x (3.3) nor CO_2 (3.4) per mile driven.

The weighted average performance metric function (3.1 - 3.4) for each vehicle class are shown in Figure 3.7 for the grid energy per mile approximations (3.1), in Figure

3.8 for the fuel efficiency approximations (3.2), in Figure 3.9 for the NO_x rate approximations (3.3), and in Figure 3.10 for the CO_2 rate approximations (3.4).

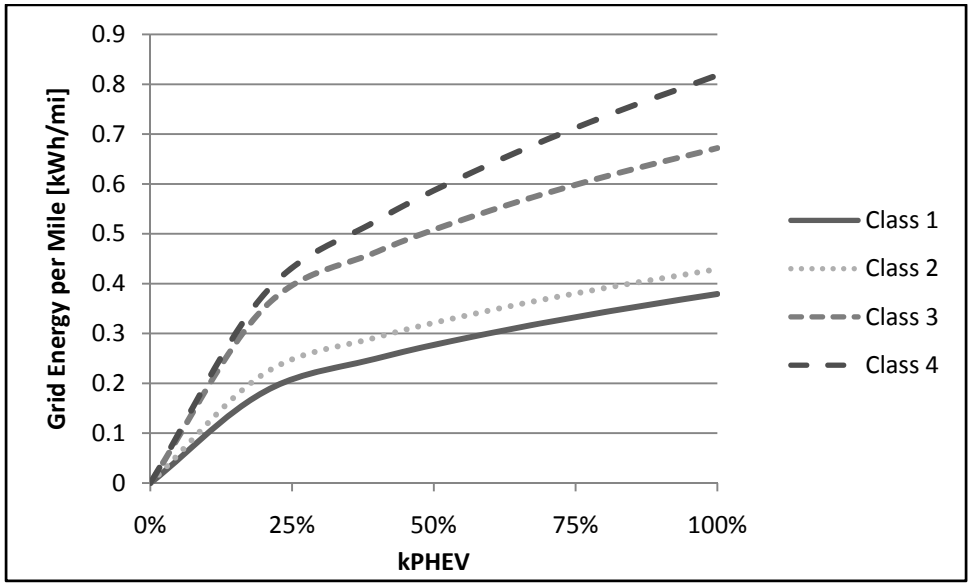

Figure 3.7. Average PHEV grid energy per mile approximation for each PHEV class.

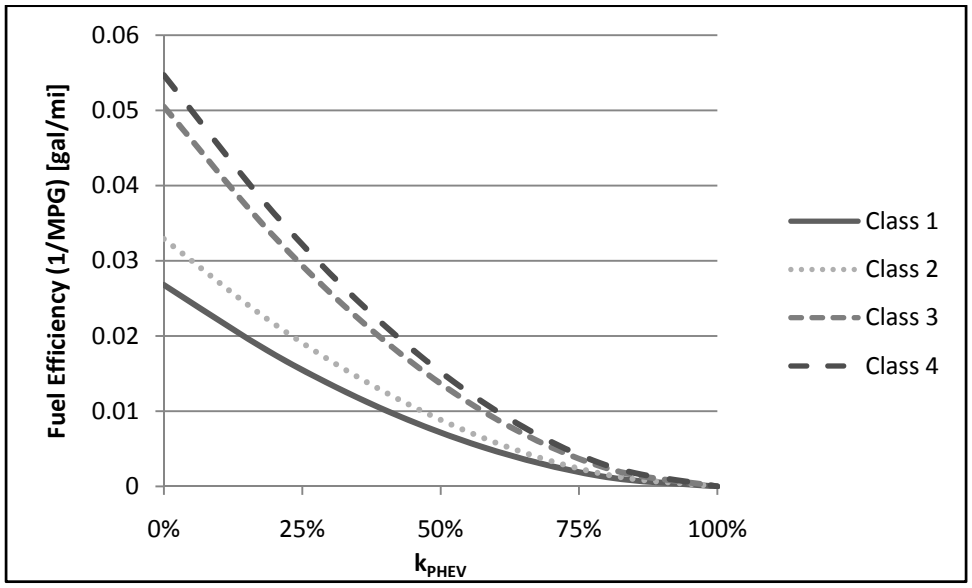

Figure 3.8. Average PHEV fuel efficiency approximations for each PHEV class.

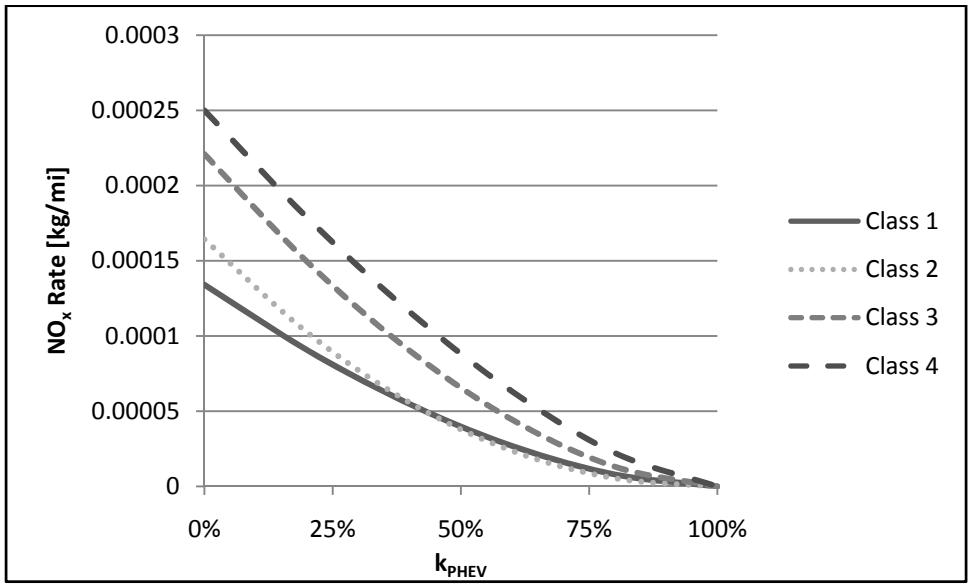

Figure 3.9. Average PHEV NO_x rate approximation and for each PHEV class.

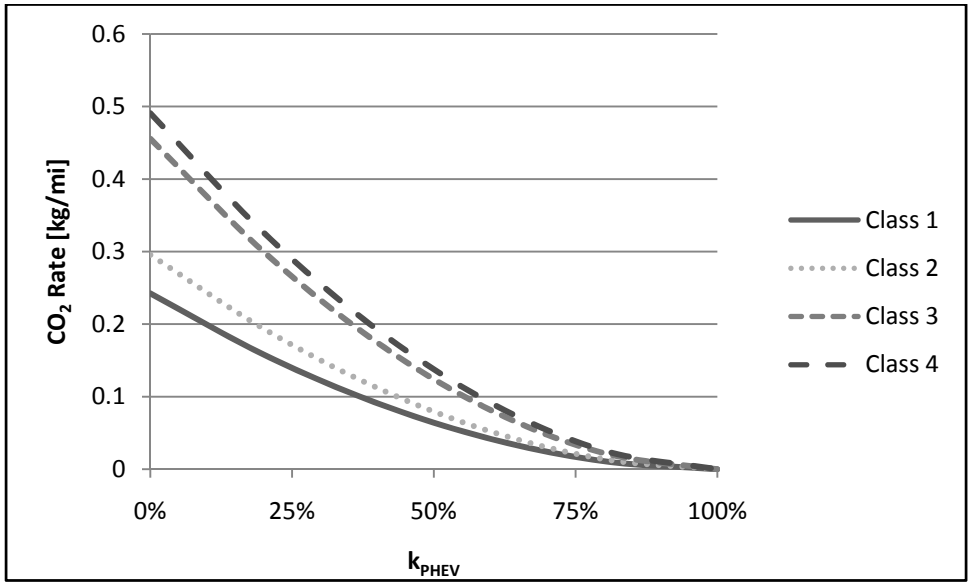

Figure 3.10. Average PHEV CO_2 rate approximation and for each PHEV class.

In figures 3.7 through 3.10 all of the weighted approximations follow a strict ranking by class, except the NO_x rate approximation functions (Figure 3.9) for PHEV classes 1 and 2. There is a crossover between these two classes of NO_x rate approximation functions at approximately 50% k_{PHEV}. This result is realistic because the two vehicle classes are similar in size and performance.

The two-mode PHEV control strategy is optimized to maximize the benefits of PHEVs for an optimal trip length of M_E^* miles. The two modes are a charge depleting mode and a charge sustaining mode ($k_{PHEV} = 0$). The charge depleting mode is used initially when the vehicles battery is relatively fully charged. On trips (times between charging) longer then M_E^*, after the battery is depleted (to a specified lower level) the charge sustaining mode is utilized. The charge sustaining mode relies on gasoline to maintain a constant average state-of-charge where on average all the energy used to drive the PHEV comes from gasoline. The driving distance in the charge depleting mode is called the charge depleting distance $M_E^{(c)}$ (miles). The charge depleting distance for each vehicle class-c ($c \in \{1,2,3,4\}$), $M_E^{(c)}$, is calculated, in (3.5), as a function of the useable battery capacity, $BC^{(c)}$ [kWh], assumed to be a random variable (RV) within the battery capacity ranges defined in Table 3.6 for each vehicle class, and the vehicles required grid energy per mile, $E^{(c)}(k_{PHEV})$.

$$M_E^{(c)} = BC^{(c)}/E^c(k_{PHEV}) \tag{3.5}$$

Table 3.6. Battery capacity range for each vehicle class [kWh].

Class	$BC_{\max}^{(c)}$ [kWh]	$BC_{\min}^{(c)}$ [kWh]
1	12	8
2	14	10
3	21	17
4	23	19

From $BC^{(c)}$ (Table 3.6) and M_E^* a formula for the vehicle design parameter k_{PHEV} can be derived. Substituting (3.1) into (3.5) results in

$$M_E^{(c)} = BC^{(c)}/\left[A_E^{(c)} \cdot \left(k_{PHEV}^{(c)}\right)^{B_E^{(c)}}\right] \tag{3.6}$$

which can be rearranged to solve for $k_{PHEV}^{(c)}$ as

$$k_{PHEV}^{(c)} = \left[BC^{(c)} / \left(A_E^{(c)} \cdot M_E^*\right)\right]^{1/B_E^{(c)}} \quad (3.7)$$

The ranges of $k_{PHEV}^{(c)}$ for each vehicle class can be computed from (3.7), an M_E^* value of 40 miles, and the battery capacity ranges in Table 3.6. An M_E^* value of 40 is selected to provide typical results for approximately 75% of average U.S. driver's daily commutes [22]. The computed ranges of k_{PHEV} are shown in Table 3.7. The parameter $k_{PHEV}^{(c)}$ represents the percentage of energy per mile on average which comes from a PHEV in class-c battery in the assumed vehicle control strategy during the charge depleting mode.

Table 3.7. Computed k_{PHEV} range for each vehicle class.

Class	$k_{PHEV,\max}^{(c)}$	$k_{PHEV,\max}^{(c)}$
1	0.5976	0.2447
2	0.6151	0.2750
3	0.5428	0.3217
4	0.4800	0.3224

The values in Tables 3.6 and 3.7 form the basis of one of the three random vehicle fleet parameters described next.

3.1.1.2 Vehicle Operation Distributions

The following three vehicle parameters are based on random distributions.

1. PHEV vehicle class populations.
2. PHEV design parameters k_{PHEV} and battery capacity.
3. Daily driving distance, departure time, and arrival time.

This section of the thesis introduces the RV distributions for each of the vehicle parameters, motivates why the particular distribution type and parameters are selected, and describes the method used to generate the RVs in the simulation program.

The vehicle fleet is distributed into the four vehicle classes based on the assumed vehicle class distribution $p^{(c)}$. The number of vehicles in each vehicle class is the total

number of vehicles in the power system area, N_T, times the percentage of vehicles in each class, $p^{(c)}$, shown in Table 3.8.

Table 3.8. IC vehicle class distribution [20].

Class 1	Class 2	Class 3	Class 4
0.20	0.30	0.30	0.20

The first RV distribution is the number of PHEVs in each vehicle class. The level of PHEV penetration is defined as P_{PHEV}. The total number of PHEVs with P_{PHEV} penetration is $N_T \cdot P_{PHEV}$. The number of PHEVs in each vehicle class is normally distributed with mean $\mu^{(c)}$ and variance $\left(\sigma^{(c)}\right)^2$. Where $\mu^{(c)}$ is $N_T \cdot P_{PHEV} \cdot p^{(c)}$ and $\left(\sigma^{(c)}\right)^2$ is $\alpha_p \cdot \mu^{(c)}$ (by default $\alpha^{(c)}$ is 1%). The normal distribution is selected because normal distributions often occur naturally. Thus, this distribution realistically models random consumer behavior. The specific values for mean and variance are arbitrarily selected.

The Box-Műller method, in (3.8) is used to compute normally distributed RVs [23]

$$N = \sqrt{-2 \cdot \ln (U_1)} \cos (2 \cdot \pi \cdot U_2) \tag{3.8}$$

where, N is a standard normal value (a normal RV with a mean of zero and a variance of one), U_1 and U_2 are independent and identically distributed (IID) pseudo random numbers distributed uniformly over the range (0,1]. U_1 and U_2 are generated using the C function *rand()*. The vehicle class population is then computed

$$N_{PHEV}^{(c)} = \mu^{(c)} + \sigma^{(c)} \cdot N \tag{3.9}$$

where the result $N_{PHEV}^{(c)}$ is normally distributed with mean $\mu^{(c)}$ and standard deviation $\sigma^{(c)}$.

The next set of RV distributions is the vehicle design parameters $k_{PHEV}^{(c)}$ and usable battery capacity $BC^{(c)}$ [kWh]. The random vehicle design parameters are assumed to be distributed according to a bivariate normal distribution with mean vector $\vec{\mu}$ and covariance matrix $\boldsymbol{\Sigma}$. The bivariate normal distribution is selected because of the ability to include parameter correlation. Using the specified ranges of k_{PHEV} and $BC^{(c)}$, given in Tables 3.6 and 3.7, $\vec{\mu}$ and $\boldsymbol{\Sigma}$ are calculated. The correlation between $k_{PHEV}^{(c)}$ and $BC^{(c)}$ ρ is arbitrarily set to 0.8. This correlation represents the intuitive relationship between the design parameters $k_{PHEV}^{(c)}$ and $BC^{(c)}$. The correlation coefficient is arbitrarily selected with added consideration that $\boldsymbol{\Sigma}$ be positive definite so that a Cholesky decomposition [24] of $\boldsymbol{\Sigma}$ can be computed.

As an example of how the bivariate normal values are generated, the calculations for the Class 2 vehicle design parameters are shown below in detail. First, the bivariate distribution parameters $\vec{\mu}^{(2)}$ and $\boldsymbol{\Sigma}^{(2)}$ are calculated

$$\vec{\mu}^{(2)} = \begin{bmatrix} \left(k_{PHEV,\max}^{(2)} + k_{PHEV,\min}^{(2)}\right)/2 \\ \left(BC_{\max}^{(2)} + BC_{\min}^{(2)}\right)/2 \end{bmatrix} \tag{3.10}$$

$$= \begin{bmatrix} (0.6151 + 0.2750)/2 \\ (14 + 10)/2 \end{bmatrix} = \begin{bmatrix} 0.4451 \\ 12 \end{bmatrix}$$

$$\sigma_{kPHEV}^{(2)} = \left(k_{PHEV,\max}^{(2)} - k_{PHEV,\min}^{(2)}\right)/4 \tag{3.11}$$

$$= 0.6151 - 0.2750/4 = 0.0850$$

$$\sigma_{BC}^{(2)} = \left(BC_{\max}^{(2)} - BC_{\min}^{(2)}\right)/4 \tag{3.12}$$

$$= (14 - 10)/4 = 1 \text{ kWh}$$

$$\boldsymbol{\Sigma}^{(2)} = \begin{bmatrix} \sigma_{kPHEV}^2 & \rho \cdot \sigma_{kPHEV} \cdot \sigma_{BC} \\ \rho \cdot \sigma_{kPHEV} \cdot \sigma_{BC} & \sigma_{BC}^2 \end{bmatrix} \tag{3.13}$$

$$= \begin{bmatrix} 0.0882^2 & 0.8 \cdot 0.0882 \cdot 1 \\ 0.8 \cdot 0.0882 \cdot 1 & 1^2 \end{bmatrix}$$

$$= \begin{bmatrix} 0.0072 & 0.0680 \\ 0.0680 & 1 \end{bmatrix}$$

Next, the Cholesky decomposition is used to decompose the covariance matrix into a lower triangular matrix $\boldsymbol{B}$, where

$$\boldsymbol{\Sigma} = \boldsymbol{B} \cdot \boldsymbol{B}^T \tag{3.14}$$

and specifically, for Class 2

$$\boldsymbol{B}^{(2)} = \begin{bmatrix} 0.0850 & 0 \\ 0.8 & 0.6 \end{bmatrix}$$

Then, a vector of two standard normal values $\vec{N}$ is generated using (3.8). Finally, the desired multivariate normal distribution is calculated

$$\vec{X}_{VD} = \begin{bmatrix} k_{PHEV}^{(2)} \\ BC^{(2)} \end{bmatrix} = \vec{\mu} + \boldsymbol{B} \cdot \vec{N} \tag{3.15}$$

Similar calculations are performed for each vehicle class.

The last set of RVs are those associated with the daily vehicle performance: miles driven per day $M^{(v,d)}$ [mi], vehicle departure time$D_T^{(p)}$ [h], and vehicle arrival time $A_T^{(p)}$ [h]. The miles driven per day are distributed log-normal RVs with mean μ_m of 3.37 and standard deviation σ_m of 0.5 [25], the vehicle timing distributions are normally distributed RVs with parameters shown in Table 3.9. The parameter p in the distribution parameters mean $\mu_T^{(p)}$ [h] and variance $\left(\sigma_T^{(p)}\right)^2$ [h] indicates one of the four possible daily timing distributions: weekday departure, weekend departure, weekday arrival, or weekend arrival.

Table 3.9. Vehicle departure and arrival time distribution parameters.

	Departure		Arrival	
Parameter	Weekday	Weekend	Weekday	Weekend
$\mu_T^{(p)}$ [h]	7	9	18	15
$\left(\sigma_T^{(p)}\right)^2$ [h]	3	6	3	6

The log normal distribution is selected because of the correlation between the shape of a log normal histogram and the author's intuition. This intuition has been verified comparing sample generated results with known driving pattern statistics. The known driving statistics are average yearly total miles driven of 12,000 miles, 50% of drivers drive 25 miles per day or less, and 75% of drivers drive 45 miles or less [22]. Sample results computed by MATLAB using 328,500 log normal RVs (μ_m = 3.37 and σ_m = 0.5) show that the total yearly driving distance average is 12,018 miles, 48% of the vehicles drive 25 miles or less each day, and 83% of the vehicles drive 45 miles or less each day, which closely approximate the driving performance results from [22].

In the probabilistic simulation program the log normal RVs are generated using a standard normal RV, N, generated using (3.8). Then, the value $M^{(v,d)}$ is computed from

$$M^{(v,d)} = e^{(\mu_m + \sigma_M \cdot N)} \tag{3.16}$$

where $M^{(v,d)}$ is a RV representing the total miles vehicle-v on day-d drove and is distributed log normal with mean μ_m and standard deviation σ_M. Vehicle-v is a particular vehicle sampled randomly from the total vehicle fleet N_T. The total number of vehicles in the sample population is n, where n is much less then N_T, because generating data for N_T vehicles for the entire simulation period is computationally prohibitive. Day-d is a particular day of the simulation. The total number of days simulated is D.

For the time performance parameters, departure time and arrival time Gaussian distributions are selected as a best estimate of random consumer behavior. Different timing distributions are used to model the potential different consumer behaviors on weekdays versus weekends.

As before a standard normal value, N, is computed using (3.8). Then, the value $X_T^{(p)}$ is computed

$$X_T^{(p)} = \left\lfloor \mu_T^{(p)} + \sigma_T^{(p)} \cdot N \right\rfloor \tag{3.17}$$

where the result $X_T^{(p)}$ is a normally distributed integer with mean $\mu_T^{(p)}$ and standard deviation $\sigma_T^{(p)}$. The value $X_T^{(p)}$ represents either the arrival time $A_T^{(p)}$ or the departure time $D_T^{(p)}$ depending on the values used for the mean and standard deviation.

The arrival time $A_T^{(v,d)}$ for vehicle-v on day-d must occur after the departure time $D_T^{(v,d)}$ for vehicle-v on day-d. To achieve this specification, an acceptance-rejection method is used. Let A_T^* be a particular generated arrival time and D_T^* be a particular generated departure time. Each generated pair (A_T^*, D_T^*) is checked, and if $A_T^* \leq D_T^*$ then a new pair is generated. The process is repeated until $A_T^* > D_T^*$ and the generated pair is accepted.

3.1.1.3 Gasoline Usage Statistics

Three steps are required to compute of the amount of gasoline for a vehicle fleet with a specified level of PHEV penetration:

1. Compute the amount of gasoline which a fleet of N_T IC vehicles will consume, G_{IC} [gal.].
2. Compute the amount of gasoline which a fleet of $N_T \cdot P_{PHEV}$ PHEVs will consume, G_{PHEV} [gal.].
3. Compute the total gasoline usage, G [gal.].

The total gasoline G_{IC} used by a fleet of N_T IC vehicles is computed assuming the average gasoline used by the vehicle sample population, $\overline{G_{IC}^{(c)}}$ [gal./veh.], is equal to the average gasoline used by the population average, so that

$$\overline{G_{IC}^{(c)}} = 1/n \cdot \sum_{v=1}^{n} \left(T^{(v)} / IC_{MPG}^{(c)} \right) \tag{3.18}$$

where $T^{(v)}$ is the total number of miles driven by vehicle-v over the simulation period and $IC_{MPG}^{(c)}$ is the fuel efficiency of an IC vehicle in class-c. Thus, G_{IC} is the sum of the product of the total number of vehicles in class-c times the average gasoline used per vehicle in class-c for each vehicle class. Hence

$$G_{IC} = N_T \cdot \sum_{c=1}^{4} \left(p^{(c)} \cdot \overline{G_{IC}^{(c)}} \right) \tag{3.19}$$

To calculate the amount of gasoline a fleet of PHEVs uses is more complicated because the rate at which PHEVs use fuel, in the assumed control strategy, depends on the daily driving distance. If $M_E^{(c)}$ is greater than or equal to $M^{(v,d)}$, then the entire daily driving distance is performed in charge depleting mode. Under this condition the daily required gasoline, $D_G^{(v,d,c)}$ [gal.], is

$$D_G^{(v,d,c)} = M^{(v,d)} / MPG^{(c)}(k_{PHEV}) \tag{3.20}$$

Where $MPG^{(c)}(k_{PHEV})$ is the fuel efficiency of a PHEV with design variable k_{PHEV} in class-c in the charge depleting mode. However, if $M_E^{(c)}$ is strictly less than $M^{(v,d)}$ then the distance $\left(M^{(v,d)} - M_E^{(c)} \right)$ must be completed in charge sustaining mode, and $D_G^{(v,d,c)}$ is

$$D_G^{(v,d,c)} = M_E^{(c)} / MPG^{(c)}(k_{PHEV}) + \left(M^{(v,d)} - M_E^{(c)} \right) / MPG^{(c)}(0) \tag{3.21}$$

where the first term in the sum represents gasoline used in charge depleting mode and the second term represents gasoline used in charge sustaining mode (where $MPG^{(c)}(0)$ is the fuel efficiency of a PHEV in class-c in the charge sustaining mode).

From $D_G^{(v,d,c)}$ the yearly gasoline usage, $Y_G^{(v,c)}$ [gal.], is computed by summing over each day in the simulation

$$Y_G^{(v,c)} = \sum_{\mathrm{d}=1}^{\mathrm{D}} D_G^{(v,d,c)} \tag{3.22}$$

Next, the sample vehicle population average gasoline usage, $\overline{Y_G^{(c)}}$ [gal./veh.], is computed

$$\overline{Y_G^{(c)}} = 1/n \cdot \sum_{v=1}^{n} Y_G^{(v,c)} \tag{3.23}$$

Then, the total gasoline G_{PHEV} used by a fleet of $N_T \cdot P_{PHEV}$ PHEVs is the sum of the product of the number of vehicles in each class times the average gasoline usage per vehicle for each vehicle class

$$G_{PHEV} = N_T \cdot P_{PHEV} \cdot \sum_{c=1}^{4} \left(p^{(c)} \cdot \overline{Y_G^{(c)}} \right) \tag{3.24}$$

assuming, again, that the sampled PHEV population average gasoline usage is equal to the total PHEV population gasoline usage.

Finally, the total gasoline usage, G, is the sum of the gasoline used by the IC vehicles and the gasoline used by the PHEVs, G_{PHEV}. The gasoline used by the IC vehicles is the percentage of IC vehicles in the total vehicle fleet times G_{IC}. The percentage of IC vehicles in the population is $(1 - P_{PHEV})$. Thus,

$$G = (1 - P_{PHEV}) \cdot G_{IC} + G_{PHEV} \tag{3.25}$$

Thus far, the described methodology computes the performance of a fleet of N_T vehicles with a penetration percentage of P_{PHEV}. The next step in the probabilistic simulation program is to compute the load curves used in the power system simulation algorithm.

3.1.2 Calculate Load Curves

Two forms of load curves are used, namely the chronological load curve and the NILDC [18]. The chronological form depicts the load as a function of time. The second form, computed from the first, depicts a probabilistic description of the electric load. First the chronological load curve is computed using the base case electric load and the

additional electric load due to PHEV charging. Second the chronological load curve is converted into the NILDC.

In each simulated experiment the base case electric load demand is based on data in [26] and the peak electric load of the power system in the experiment. The data in [26] describes the electric load demand as a percentage of the peak for each hour of a year. The electric load representing PHEV charging is added to the base case electric load. Next, the method to calculate the added electric load demand due to PHEV charging is described.

To compute the additional energy required to charge the PHEV fleet requires five calculations:

1. Compute the daily recharge energy required by the PHEV from the grid, $D_E^{(v,d,c)}$ [kWh].
2. Compute the daily recharge length, $C_T^{(v,d)}$ [h].
3. Generate the recharge voltage, $V^{(v,c)}$ [V].
4. Compute the recharge current, $I^{(v,d,c)}$ [A].
5. Compute the total recharge power, p_v [MW], per hour.

First, $D_E^{(v,d,c)}$ is computed. This value depends on $M^{(v,d)}$ and $M_E^{(c)}$. If $M^{(v,d)}$ is greater than or equal to $M_E^{(c)}$ then the required grid energy is $BC^{(c)}$. Otherwise $D_E^{(v,d,c)}$ is the product of $M^{(v,d)}$ and $E^{(c)}(k_{PHEV})$.

$$D_E^{(v,d,c)} = \begin{cases} BC^{(c)} & M^{(v,d)} \geq M_E^{(c)} \\ M^{(v,d)} \cdot E^{(c)}(k_{PHEV}) & M^{(v,d)} < M_E^{(c)} \end{cases} \tag{3.26}$$

Second, $C_T^{(v,d)}$ is computed. This value is the number of hours between arriving home on day-d and leaving on day-$d+1$ (note that on day-D, the last day of the simulation, the arrival time on day-D and the departure time on day-1 is used).

$$C_T^{(v,d)} = \left(24 - A_T^{(v,d)}\right) + D_T^{(v,d+1)} \tag{3.27}$$

Third, $V^{(v,c)}$ is generated. This value is a discrete RV, and is set at 120 volts for 70% of the vehicles and is set at 240 volts for 30% of the vehicles.

Fourth, $I^{(v,d,c)}$ is computed. This value is limited by the maximum current available, I^* [A], from the charging circuit, where I^* is 15 A from a 120 V service and 30 A from a 240 V service.

$$I^{(v,d,c)} = \min\left\{\left(D_E^{(v,d,c)} \cdot 1000\right)/\left(V^{(v,c)} \cdot C_T^{(v,d)}\right), I^*\right\} \tag{3.28}$$

where $D_E^{(v,d,c)} \cdot 1000$ is the energy [Wh] required by the PHEV-v on day-d in class-c, and $V^{(v,c)} \cdot C_T^{(v,d)}$ is the charging voltage [V] for the PHEV-v in class-c times the number of hours the PHEV-v on day-d will be charged. The charging voltage is held constant for each vehicle in the simulation period assuming that PHEV owners will not change their charging circuit over the simulation period. The charging time is held constant for each class for simplicity. Thus, the quotient

$$\left(D_E^{(v,d,c)} \cdot 1000\right)/\left(V^{(v,c)} \cdot C_T^{(v,d)}\right)$$

is the current demanded for the required energy at the charging voltage level for the number of hours the PHEV will be charging. Additionally, using the min{·} function results in $I^{(v,d,c)}$ not exceeding the service capacity.

Finally, the required recharge power is the energy required every hour of the charging period and is stored in an array, $LDC[h_c]$, where h_c is the simulation hour. The array is initialized to all zeros and computed by looping through each vehicle in the sampled population and each vehicle class adding the product of the number of vehicles in the present class times the required grid power in MW for each charging hour for each day of the simulation.

$$p_v = \left(N_{PHEV}^{(c)} \cdot V^{(v,c)} \cdot I^{(v,d,c)}\right)/(n \cdot 10^6) \tag{3.29}$$

This procedure is outlined in Figure 3.11.

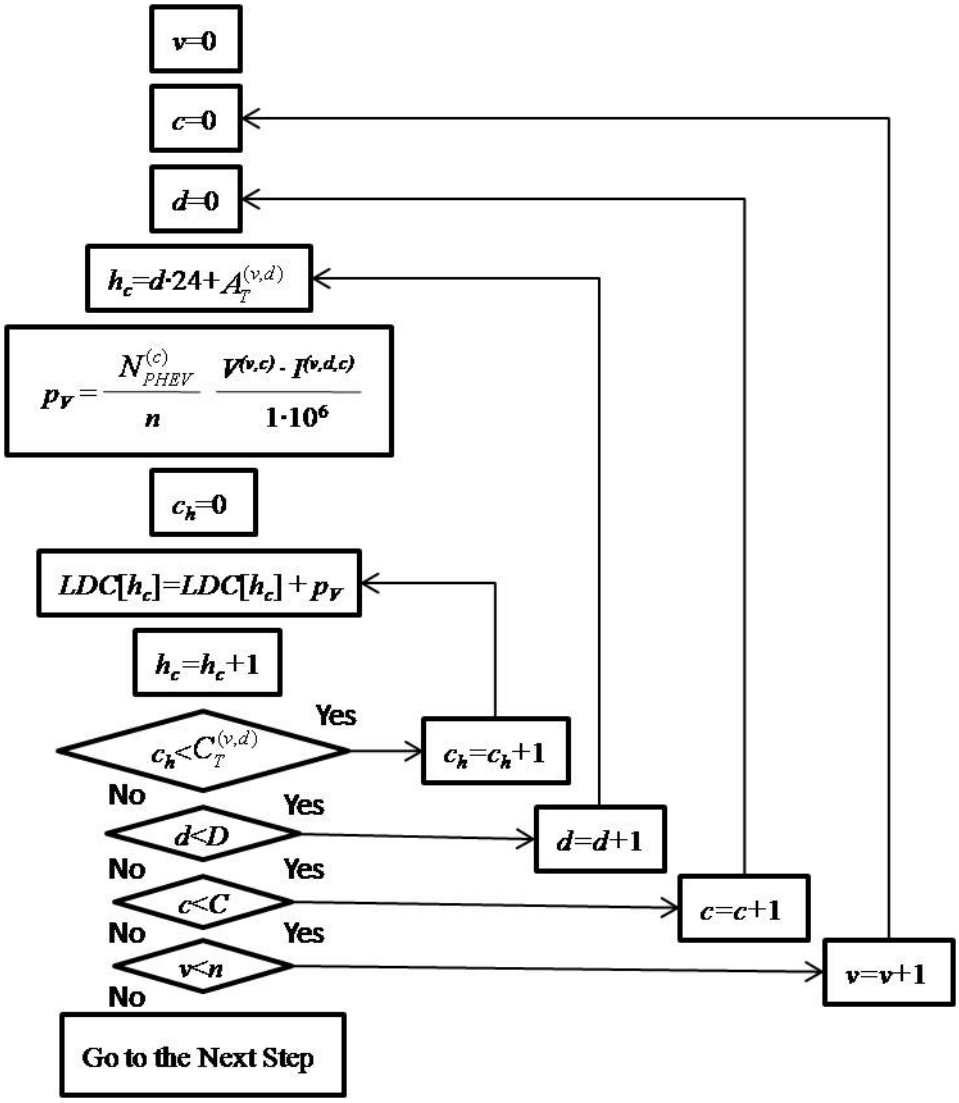

Figure 3.11. PHEV required grid energy calculation block diagram.

The chronological electric load model is converted into a probability distribution function (inverted) of the load for the purposes of the probabilistic simulation method. In general, a NILDC describes the length of time for which the load is greater than a specified value, which ranges from the system minimum load to the maximum load [18].

To convert from the chronological load demand curve to the NILDC requires that the range of possible load levels from the system minimum to the system maximum load

be broken up into a specified number of increments. For each increment the number of hours during which the load is greater than or equal to that level is counted. Then, the resulting count for each increment is normalized by the total length of the simulation in hours. The resulting curve has horizontal axis units of power and vertical axis units of probability. The vertical axis probability is the probability that the load is greater than or equal to the horizontal axis power level.

3.1.3 Power System Simulation Using the Probabilistic Production Costing (PPC) Power System Simulation Procedure

PPC power system simulation procedure provides the following functionality, "Given the forecasted electric load demand for the time period under consideration and a list of available generating units of the system, simulate the operation of the system in order to forecast energy generated by units, cost, and required fuel, taking into account the effects of scheduling functions within the time period considered and the random forced outages of the units" [18], where units indicates generators in power plants.

The forecasted electric load demand is the NILDC introduced in the last section. The list of available generating units is described below. The forced outage rate (FOR) of the available generating units is defined as a function of the mean time to failure (MTTF) and mean time to repair (MTTR)

$$\mathrm{FOR} = \mathrm{MTTF}/(\mathrm{MTTF} + \mathrm{MTTR}) \tag{3.30}$$

Given a forecasted electric load demand and list of available generators, the expected value of each of the following quantities can be computed for each available generating unit:

1. Total energy produced.
2. Total fuel cost.
3. Total amount of fuel utilized.
4. Total EAP generated.

The calculation of the above power system quantities is based on a probabilistic methodology fully developed in [18]. In [18] the "arbitrary dispatch criterion" utilized is an economic dispatch criterion. Thus, when additional load needs to be met the generator selected to meet the demand is chosen by the least expensive option available.

The PPC power system simulation procedure is utilized to compute both the base case power system results and the PHEV scenario results. Because the electric load due to PHEV charging is based on RVs repeated simulations of the PHEV scenarios is used to compute average system production results.

3.1.4 Calculate EAP Statistics

Next, the method used to compute the total system EAP results is described. The results from the vehicle and power system simulations are combined to compute the total system EAP.

The vehicle EAP is computed in a similar fashion to that of the gasoline consumption, replacing the fuel efficiency with EAP rates, denoted by $P^{(c)}(k_{PHEV})$, as a general term for either, $NO_x^{(c)}(k_{PHEV})$ or $CO_2^{(c)}(k_{PHEV})$, the NO_x and CO_2 emission rates of a PHEV utilizing design variable k_{PHEV} in class-c respectively. First, the total EAP generated by the fleet of IC vehicles is described, followed by a description of the EAP generated by the fleet of PHEVs.

The total EAP generated by a fleet of N_T IC vehicles is computed, assuming the sample vehicle population average EAP generated, $\overline{EAP_{IC}^{(c)}}$ [kg/veh.], is equal to the average EAP generated by the entire vehicle population

$$\overline{EAP_{IC}^{(c)}} = 1/n \cdot \sum_{v=1}^{n}\left(T^{(v)}/IC_{EAP}^{(c)}\right) \tag{3.31}$$

where $T^{(v)}$ is the total number of miles driven by vehicle-v over the simulation period and $IC_{MPG}^{(c)}$ is the fuel efficiency of an IC vehicle in class-c. Thus, the total vehicle fleet EAP generated, EAP_{IC} [kg], is the sum of the product of the total number of vehicles in class-c times the average EAP generated per vehicle in class-c for each vehicle class. Hence

$$EAP_{IC} = N_T \cdot \sum_{c=1}^{4} \left(p^{(c)} \cdot \overline{EAP_{IC}^{(c)}} \right) \tag{3.32}$$

The method used to compute the total EAP generated by a fleet of PHEVs is described next. First, the daily amount of EAP generated, $D_{EAP}^{(v,d,c)}$ [kg], is computed. If $M_E^{(c)}$ is greater than or equal to $M^{(v,d)}$ then

$$D_{EAP}^{(v,d,c)} = M^{(v,d)} \cdot P^{(c)}(k_{PHEV}) \tag{3.33}$$

however, if $M_E^{(c)}$ is strictly less than $M^{(v,d)}$ then

$$D_{EAP}^{(v,d,c)} = M_E^{(c)} \cdot P^{(c)}(k_{PHEV}) + \left(M^{(v,d)} - M_E^{(c)} \right) \cdot P^{(c)}(0) \tag{3.34}$$

where the first term in the sum represents the EAP produced in charge depleting mode and the second term is the EAP produced in charge sustaining mode.

Second, the yearly EAP generated, $Y_{EAP}^{(v,c)}$ [kg], is computed by summing over each day in the simulation

$$Y_{EAP}^{(v,c)} = \sum_{d=1}^{D} D_{EAP}^{(v,d,c)} \tag{3.35}$$

Third, the sample vehicle population average yearly EAP generated, $\overline{Y_{EAP}^{(c)}}$ [kg/veh.], is computed

$$\overline{Y_{EAP}^{(c)}} = 1/n \cdot \sum_{v=1}^{n} Y_{EAP}^{(v,c)} \tag{3.36}$$

Next, the total EAP generated by a fleet of PHEVs, EAP_{PHEV} [kg], is calculated. This value is the sum of the product of the number of vehicles in each class times the average EAP generated per vehicle class over each vehicle class, and is given by

$$EAP_{PHEV} = N_T \cdot P_{PHEV} \sum_{c=1}^{4} \left(p^{(c)} \cdot \overline{Y_{EAP}^{(c)}} \right) \quad (3.37)$$

Finally, the total EAP generated, EAP [kg], is the sum of the EAP produced by both the IC vehicles and the PHEVs

$$EAP = (1 - P_{PHEV}) \cdot EAP_{IC} + EAP_{PHEV} \quad (3.38)$$

The simulation methodology thus far described is facilitated with the use of a graphical user interface (GUI) with access to all the required input data and simulations results.

3.2 Primary Energy Source Utilization Experiments

This section describes how the three experiments are performed. The experiments are conducted using the probabilistic simulation of an integrated power system with distributed PHEVs methodology to quantify the impact which charging PHEVs will have on primary energy source utilization. In the first two experiments the level of PHEV penetration is increased from 0% (Base Case), to 5%, 10%, 20% and 40%. Here P_{PHEV} percent penetration is defined as

$$P_{PHEV} = N_{\text{PHEVs}}/N_{\text{T}} \quad (3.39)$$

where N_{PHEVs} is the total number of PHEVs in the simulation. In the first experiment the power system used to charge the vehicles is the 1979 Reliability Test System (RTS) [26]. In the second experiment the power system is the average generating mix used in the United States. The third experiment keeps the number of PHEVs constant and varies the RTS generating mix. The RTS generating mix is changed such that the total generating capacity is constant but the ratio of clean generating capacity (nuclear and hydro) is increased.

In each experiment the results include primary energy source utilization shifts and pollution shifts. The total cost for consumers is computed for the first experiment only.

3.2.1 Reliability Test System (RTS) Experiment

The RTS model was developed in [26] "to provide a basis for reporting on analysis methods". It contains nearly all the power system data for the probabilistic simulation of an integrated power system with distributed PHEVs methodology; the only data not included in [26] is generator emission data. The remainder of this subsection describes the power system data used in the RTS experiment in this investigation and the results of the experiment.

3.2.1.1 RTS Experiment Data

The RTS system utilizes five fuel types (#6 oil, #2 oil, coal, nuclear, and hydro) and 32 different generators. These 32 generators consist of nine different generator types.

The cost and heat content of each fuel type (Table 3.10) is based on data in [26]. The cost data has been updated to typical current prices.

Table 3.10. Fuel type data [26].

Fuel Type	Fuel Costs [$/kg]	Fuel Energy Density [kcal/kg]
#6 Oil	0.6	11,200
#2 Oil	0.65	12,000
Coal	0.05	6,000
Nuclear	60,000	$200 \cdot 10^{19}$
Hydro	--	--

The hydro energy generation is treated as negative load when calculating the load demand curve. Thus, in Table 3.10 the hydro fuel cost and fuel energy density are not included because hydro fuel is not included in the economic dispatch calculation. The

relative cost of each fuel type is of significant importance because the generating unit dispatching is ordered based on economic ranking.

Generator unit reliability data (Table 3.11) includes MTTF, MTTR and resulting FOR.

Table 3.11. Generating unit reliability data [26].

Size of Unit [MW]	FOR	MTTF [h]	MTTR [h]
12	0.02	2,940	60
20	0.1	450	50
50	--	--	--
76	0.02	1,960	40
100	0.04	1,200	50
155	0.04	960	40
197	0.05	950	50
350	0.08	1,150	100
400	0.12	1,100	150

In Table 3.11 unit reliability for the hydro units is considered in the calculations of the hyrdo availability data.

Generator capacity data (Table 3.12) includes generator fuel type, maximum generating capacity, and minimum generating capacity.

Table 3.12. Generating unit generation capacity data [26].

Fuel	Capacity [MW]	
	Maximum	Minimum
#6 Oil	12	2.4
#2 Oil	20	16
Hydro	50	--
Coal	76	15.2
#6 Oil	100	25
Coal	155	54.25
#6 Oil	197	68.95
Coal	350	140
Nuclear	400	100

In Table 3.12, the hydro capacity is treated as negative load and as such no minimum capacity is required.

Additional data utilized in the PPC power system simulation procedure is heat and emission rate functions for all of the available generating units in the system. This data is described next.

The generator heat rate function (3.40), is used as a cost function modeling the amount of fuel needed to meet a specific power demand for each generator. A linear least square method is used to calculate the heat rate coefficients a_h, b_h, and c_h for each generator. In the heat rate function

$$h(P) = a_h + b_h \cdot P + c_h \cdot P^2 \tag{3.40}$$

P [MW] represents the generated power and $h(P)$ [kcal/h] is the required heat rate.

The data used to compute each heat rate functions is found in [26]. The least square approximation solves the general matrix equation

$$\vec{Y} = \boldsymbol{A} \cdot \vec{X} \tag{3.41}$$

with solution

$$\vec{X} = (\boldsymbol{A}^T \cdot \boldsymbol{A}) \cdot \boldsymbol{A}^T \cdot \vec{Y} \tag{3.42}$$

where $\vec{Y}$ is a vector of known data (heat rate) [kcal/h], $\boldsymbol{A}$ is a known observation matrix (power levels) [MW], and $\vec{X}$ is a vector of unknown data (generator coefficients).

An example of how the heat rate coefficients are calculated is provided for the 12 MW generating units. For the 12 MW generators the heat rate input at four levels of output power levels (2.4 MW, 6.0 MW, 9.6 MW, 12.0 MW) are known [26]

$$\vec{\mathrm{Y}} = \begin{bmatrix} \text{Heat Rate 1} \\ \text{Heat Rate 2} \\ \text{Heat Rate 3} \\ \text{Heat Rate 4} \end{bmatrix} = \begin{bmatrix} 9{,}434{,}880 \\ 19{,}504{,}800 \\ 28{,}788{,}480 \\ 36288000 \end{bmatrix} \tag{3.43}$$

$$\boldsymbol{A} = \begin{bmatrix} 1 & P_1 & P_1^2 \\ 1 & P_2 & P_2^2 \\ 1 & P_3 & P_3^2 \\ 1 & P_4 & P_4^2 \end{bmatrix} = \begin{bmatrix} 1 & 2.4 & 5.76 \\ 1 & 6 & 36 \\ 1 & 9.6 & 92.16 \\ 1 & 12 & 144 \end{bmatrix} \tag{3.44}$$

$$\vec{X} = \begin{bmatrix} a_h \\ b_h \\ c_h \end{bmatrix} \tag{3.45}$$

and the solution is computed

$$\vec{X} = (\boldsymbol{A}^T \cdot \boldsymbol{A}) \cdot \boldsymbol{A}^T \cdot \vec{Y}$$

$$= \left(\begin{bmatrix} 1 & 1 & 1 & 1 \\ 2.4 & 6 & 9.6 & 12 \\ 5.76 & 36 & 92.16 & 144 \end{bmatrix} \cdot \begin{bmatrix} 1 & 2.4 & 5.76 \\ 1 & 6 & 36 \\ 1 & 9.6 & 92.16 \\ 1 & 12 & 144 \end{bmatrix} \right)$$

$$\cdot \begin{bmatrix} 1 & 1 & 1 & 1 \\ 2.4 & 6 & 9.6 & 12 \\ 5.76 & 36 & 92.16 & 144 \end{bmatrix} \cdot \begin{bmatrix} 9{,}434{,}880 \\ 19{,}504{,}800 \\ 28{,}788{,}480 \\ 36{,}288{,}000 \end{bmatrix}$$

$$= \begin{bmatrix} 303{,}340 \\ 355{,}040 \\ 15{,}047 \end{bmatrix}$$

Figure 3.12 shows the 12 MW generator discrete heat rate data and the continuous function computed using the results of linear least square method outlined above.

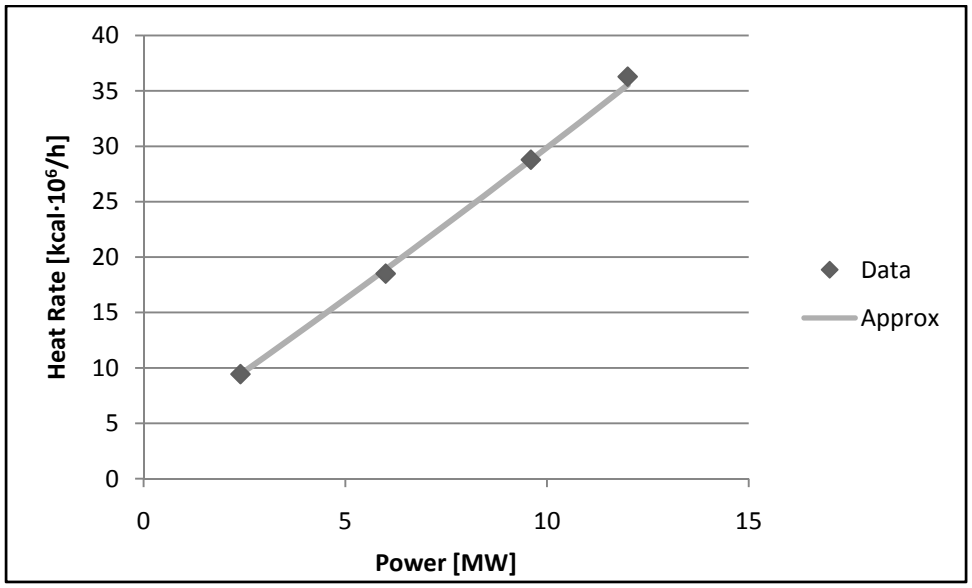

Figure 3.12. 12 MW unit heat rate data [26] and approximation.

Figure 3.12 shows a good agreement between the discrete data and the computed heat rate function. Similar linear least square calculations are performed for each generator using the discrete data outlined in [26] with results shown in Table 3.13.for all nine generator types.

Table 3.13. Generating unit heat rate coefficients [26].

Size [MW]	$a_h \left[\frac{kcal}{h}\right]$	$b_h \left[\frac{kcal}{MWh}\right]$	$c_h \left[\frac{kcal}{(MW)^2 h}\right]$
12	3,330,000	2,550,000	15,050
20	10,080,000	3,150,000	0
50	--	--	--
76	21,090,000	2,550,000	2,376
100	31,360,000	1,963,000	2,413
155	43,410,000	1,947,000	1,401
197	33,000,000	2,194,000	328.5
350	81,530,000	1,873,000	822.3
400	90,960,000	2,245,000	116.0

In Table 3.13, the c_h coefficient for the 20 MW units is zero because only two heat rate data points are published in [26]. The resulting heat rate curve is linear. Again, the hydro units are treated as negative load and as such require no heat rate equation in Table 3.13.

Next, the calculation of emission rate functions is described. The generator emission rate function (3.46) is used as a cost function modeling the amount of EAP generated at a specific power level. Again, a linear least square method is used to calculate the emission rate coefficients a_e and b_e for each generator.

$$e(P) = a_e + b_e \cdot P \tag{3.46}$$

In this equation, P [MW] represents the generated power and $e(P)$ [kg/h] is the emission rate.

Due to the lack of published emission data for the RTS generators in [26] the generator pollution statistics in [27], are utilized to approximate linear emission rate functions for each generator type in the RTS system (Table 3.14). From this data [27] the following procedure is utilized to compute the emission rate functions. First, the pollution statistics [27] are converted and normalized from thousands of tons per year (NO_x) and millions of tons per year (CO_2) to kg per MWh per year. Second, the average pollution, $R_{\text{Pollutant}}$ [kg/MWh], rate is scaled by the average power capacity, P_{ave} [MW], for each of the seven pollution generating plants utilized in the RTS power system (hydro and nuclear produce neither NO_x nor CO_2). Finally, assuming each plants pollution production would increase 20% from the minimum capacity, P_{min} [MW], to the maximum capacity P_{max} [MW], a linear emission rate function is approximated.

Table 3.14. TVA generator statistics [27].

Plant	Energy Produced [billions of kWh]	NO_x [thousands of tones/year]	CO_2 [millions of tones/year]
Allen	4.9	17.4	5.7
Bull Run	6	28	4.6
Cumberland	18.97	18.4	19
Gallatin	4.7	23.4	7.7
John Saviers	5.25	30.1	5.1
Johnsonville	5.68	86.8	9
Kingston	10	55.5	35.8

The environmental air pollutants NO_x and CO_2 are analyzed based on the availability of both power plant emission data and vehicle emission data. Both are necessary so that a comparison can be made in terms of total system EAP. The total system EAP is the EAP produced by both the power system and vehicle fleets for scenarios with and without PHEV charging.

An example of how the emission rate coefficients are calculated is provided for the 12 MW generating units below, where the linear least square variables $\vec{Y}$, $\boldsymbol{A}$, and $\vec{X}$ are

$$\vec{Y} = \begin{bmatrix}\text{Emission Rate 1}\\ \text{Emission Rate 2}\\ \text{Emission Rate 3}\end{bmatrix} = \begin{bmatrix}0.9 \cdot R_{\text{Pollutant}} \cdot P_{\text{ave}}\\ R_{\text{Pollutant}} \cdot P_{\text{ave}}\\ 1.1 \cdot R_{\text{Pollutant}} \cdot P_{\text{ave}}\end{bmatrix} = \begin{bmatrix}20.88\\ 23.18\\ 25.50\end{bmatrix}$$

$$\boldsymbol{A} = \begin{bmatrix}1 & P_{\text{min}}\\ 1 & P_{\text{ave}}\\ 1 & P_{\text{max}}\end{bmatrix} = \begin{bmatrix}1 & 2.4\\ 1 & 7.2\\ 1 & 12\end{bmatrix}$$

$$\vec{X} = \begin{bmatrix}a_e\\ b_e\end{bmatrix}$$

Thus,

$$\vec{X} = (\boldsymbol{A}^T \cdot \boldsymbol{A}) \cdot \boldsymbol{A}^T \cdot \vec{Y}$$

and the 12 MW units NO_x rate coefficients are

$$= \left(\begin{bmatrix}1 & 1 & 1\\ 2.4 & 7.5 & 12\end{bmatrix} \cdot \begin{bmatrix}1 & 2.4\\ 1 & 7.2\\ 1 & 12\end{bmatrix}\right) \cdot \begin{bmatrix}1 & 1 & 1\\ 2.4 & 7.5 & 12\end{bmatrix} \cdot \begin{bmatrix}20.88\\ 23.18\\ 25.50\end{bmatrix}$$

$$= \begin{bmatrix}19.72\\ 0.4832\end{bmatrix}$$

Similar calculations are performed for each RTS generator, for both NO_x and CO_2 rate function coefficients, with results shown in Table 3.15.

Table 3.15. Generating unit emission rate coefficients.

Size [MW]	NO_x		CO_2	
	$a_e \left[\frac{kg}{h}\right]$	b_e	$a_e \left[\frac{kg}{h}\right]$	b_e
12	19.72	0.4832	6,459	158.31
20	7.621	3.810	1,252	626.0
50	--	--	--	--
76	179.9	0.6961	37,420	144.8
100	45.83	0.1467	47,320	151.4
155	374.4	0.9381	123,200	308.7
197	548.0	1.080	92,850	183.0
350	2,604	3.235	270,000	335.4
400	--	--	--	--

In Table 3.15, the hydro (50 MW) and nuclear (400 MW) generators produced no EAP, thus the rate function coefficients are set to zero.

The accuracy of the emission rate functions is subject to question, having been obtained from emission statistics for seven different Tennessee Valley Authority (TVA) generators [27]. Pollution results from the RTS using the described power system simulation procedure, are plotted in Figure 3.13 and compared with the TVA plant data.

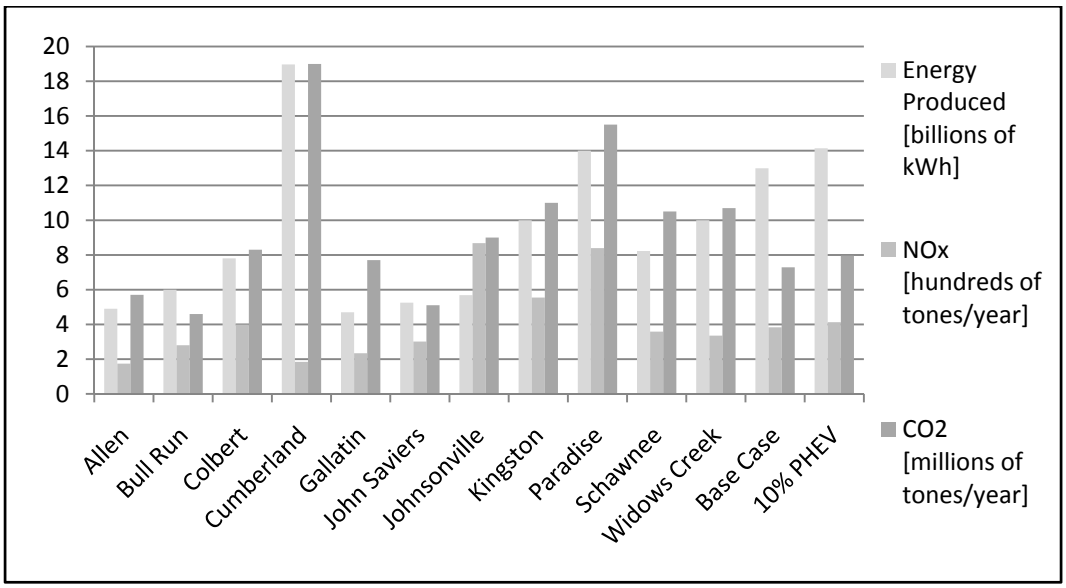

Figure 3.13. Pollution normalization justification.

Figure 3.13 shows the TVA generator statistics [27] and sample power system simulation procedure results. The sample power system simulation procedure results are shown for two scenarios the "Base Case" and "10% PHEV". The "Base Case" scenario is RTS power system simulation procedure results with no additional electric load due to PHEV charging. Whereas, the "10% PHEV" scenario is RTS power system simulation procedure results with the added electric load from replacing 10% of the light duty vehicles in the RTS area with PHEVs. These results show that for comparable annual energy production, between the TVA generator energy production statistics and the "Base

Case" and "10% PHEV" scenarios, the annual NO_x and CO_2 production, between these two sets of data, are on the same order of magnitude; suggesting that the approximated linear emission rate functions (Table 3.15) are realistic.

The base case load demand data is generated taking the product of the weekly peak (Table 3.16), daily peak (Table 3.17), and hourly peak (Table 3.18) data to create hourly load demand data for one year. The RTS system also includes six 50 MW hydro electric generating units. The hydro units are utilized 100% based on the availability (Table 3.19), thereby in effect treating the hydro generated energy as negative load. Thus, each hourly load is decreased by the hydro power available $H_P^{(q)}$ [MW] given by (3.47).

Table 3.16. Weekly peak load in percent of annual peak [26].

Week	Peak Load [%]	Week	Peak Load [%]	Week	Peak Load [%]
1	86.2	19	87	37	78
2	90	20	88	38	69.5
3	87.8	21	85.6	39	72.4
4	83.4	22	81.1	40	72.4
5	88	23	90	41	74.3
6	84.1	24	88.7	42	74.4
7	83.2	25	89.6	43	80
8	80.6	26	86.1	44	88.1
9	74	27	75.5	45	88.5
10	73.7	28	81.6	46	90.9
11	71.5	29	80.1	47	94
12	72.7	30	88	48	89
13	70.4	31	72.2	49	94.2
14	75	32	77.6	50	97
15	72.1	33	80	51	100
16	80	34	72.9	52	95.2
17	75.4	35	72.6		
18	83.7	36	70.5		

Table 3.17. Daily peak load in percent of weekly peak [26].

Day	Monday	Tuesday	Wednesday	Thursday	Friday	Saturday	Sunday
Peak Load [%]	93	100	98	96	94	77	75

Table 3.18. Hourly peak load in percent of daily peak [26].

Hour	Winter Weeks [%]		Summer Weeks [%]		Spring/Fall Weeks [%]	
	1-8 and 44-52		18-30		9-17 and 31-43	
	Weekday	Weekend	Weekday	Weekend	Weekday	Weekend
12(midnight)-1a	67	78	64	74	63	75
1a-2a	63	72	60	70	62	73
2a-3a	60	68	58	66	60	69
3a-4a	59	66	56	65	58	66
4a-5a	59	64	56	64	59	65
5a-6a	60	65	58	62	65	65
6a-7a	74	66	64	62	72	68
7a-8a	86	70	76	66	85	74
8a-9a	95	80	87	81	95	83
9a-10a	96	88	95	86	99	89
10a-11a	96	90	99	91	100	92
11a-12noon	95	91	100	93	99	94
12noon-1p	95	90	99	93	93	91
1p-2p	95	88	100	92	92	90
2p-3p	93	87	100	91	90	90
3p-4p	94	87	97	91	88	86
4p-5p	99	91	96	92	90	85
5p-6p	100	100	96	94	92	88
6p-7p	100	99	93	95	96	92
7p-8p	96	97	92	95	98	100
8p-9p	91	94	92	100	96	97
9p-10p	83	92	93	93	90	95
10p-11p	73	87	87	88	80	90
11p-12midnight	63	81	72	80	70	85

Table 3.19. Hydro energy per calendar quarter [26].

Quarter	Energy Availability [%]	Capacity Availability [%]
1	35	100
2	35	100
3	10	90
4	20	90

$$H_P^{(q)} = \left(E_A^{(q)} \cdot C_A^{(q)} \cdot H_E\right)/(2190 \cdot 1000) \quad (3.47)$$

In (3.47) $H_P^{(q)}$ is the power available from the hydro generators in quarter-q, $E_A^{(q)}$ [MWh] is the energy available in quarter-q, $C_A^{(q)}$ [MW] is the maximum capacity available in quarter-q, and H_E is 100% of the available energy from the hydro units (200 GWh [26]).

As described in [26] the peak load demand of the RTS system is 2850 MW. From the peak load demand and a number of average statistical assumptions the total number of vehicles in the RTS area is derived below.

The number of customers is calculated from an average electric monthly demand of 1,500 kWh. Based on an average month of 30 days, the average power demand per customer is calculated to be $[1{,}500/(30 \cdot 24)] = 2.083$ kW. The peak system electric load demand is 2,850 MW [26] assuming 75% of this load is comprised of residential demand the number of customers in the power system area is calculated to be $(2{,}850{,}000 \cdot 75\%/2.083) = 1.026$ million. Finally, the number of vehicles per electric customer is assumed to be 1.5, which results in a total number of vehicles (N_T) of 1.539 million.

3.2.1.2 RTS Experiment Results

Four simulations are considered for varying the percentage of PHEV penetration. The levels simulated are 5%, 10%, 20% and 40%. For each RTS experiment scenario the number of IC vehicles (N_{IC}) and PHEVs (N_{PHEV}) are shown in Table 3.20.

Table 3.20. Number of vehicles for each RTS simulation.

Simulation	BC	5%	10%	20%	40%
N_{PHEV}	0	76,950	153,900	307,800	615,600
N_{IC}	1,539,000	1,462,000	1,385,000	1,231,000	923,400

In Table 3.20 notice that for each simulation the total number of vehicles remains 1.539 million.

For each PHEV penetration level the simulation is performed 30 times each, with a sample population of 100 vehicles. Thirty repeated simulations are performed so that a distribution of the expected results can be analyzed. Similarly, 100 vehicles are used as a sample vehicle population so that the impact of the vehicle assumption distribution can be observed; whereas simulating all of the vehicles in the power system areas is computationally prohibitive.

Vehicle assumptions including vehicle design parameters $k_{PHEV}^{(c)}$ and $BC^{(c)}$, are generated based on the probabilistic models described above. A scatter plot of 30 generated values is shown in Figure 3.14.

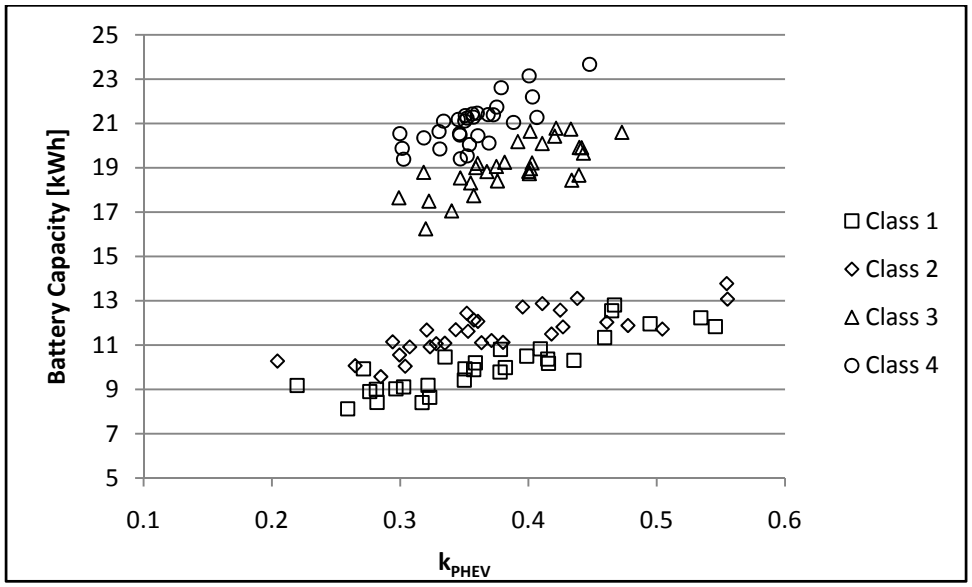

Figure 3.14. Typical vehicle design parameter scatter plot.

In Figure 3.14 two characteristics are apparent, namely the range of the vehicle design parameters and the correlation ($\rho = 0.8$) between the design parameters.

The base case electric load model [26] varies over the simulated year which is representative of typical electric load demand in a typical electric power system. Thus, the maximum power demand differs from the minimum power demand. The additional load due to PHEV charging is calculated with random charging times and random daily driving distances. One result of the probabilistic model of the added electric load due to PHEV charging is an increase in system maximum and minimum power demand. The increase in the maximum and minimum power demand is shown in Figure 3.15 for each of the simulated PHEV penetration levels. The maximum and minimum power demand for the PHEV scenarios are the average maximum and minimum power demand for the 30 PHEV penetration simulations.

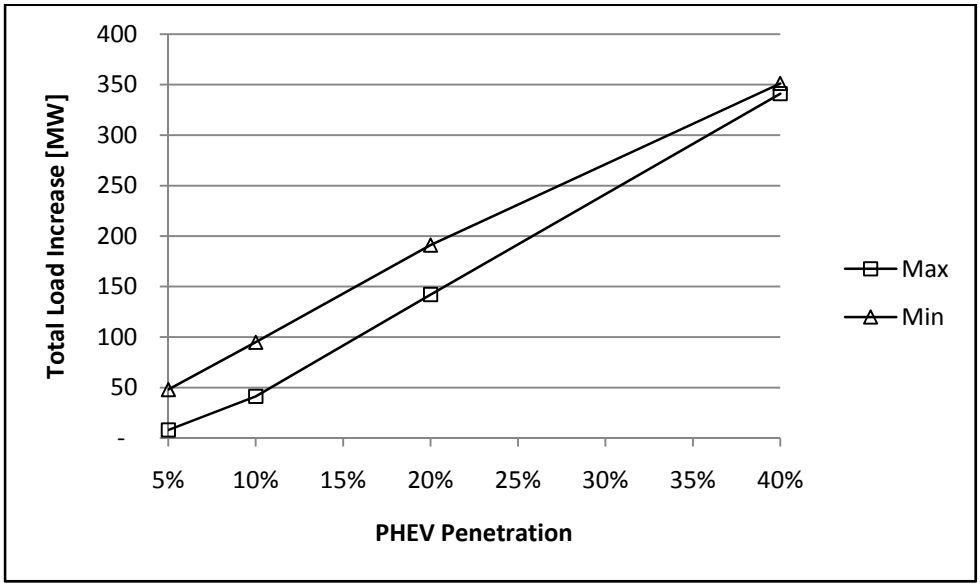

Figure 3.15. Increase in max and min power demand for each RTS scenario.

In Figure 3.15, the horizontal axis shows the percent of penetration of PHEVs and the vertical axis shows the *increase* in both maximum and minimum power demand for each percent PHEV penetration scenario simulated. Further, the base case result for maximum power demand is 2,834 MW and minimum power demand is 841 MW. Thus,

the 5% PHEV penetration scenario maximum power demand is approximately 2834 + 10 = 2844 MW. Where 2834 MW represents the base case maximum power demand and 10 MW (from Figure 3.15) represents the increase in maximum power demand for the 5% PHEV penetration scenario. Similarly, for the 5% PHEV penetration scenario minimum power demand is approximately 841 + 50 = 891 MW. Where 841 MW represents the base case minimum power demand and 50 MW (from Figure 3.15) represents the increase in minimum power demand for the 5% PHEV penetration scenario.

The curves in Figure 3.15 show that the increase in system maximum load is smaller than the increase in system minimum load for each PHEV penetration scenario. This result indicates that the addition of PHEVs into a typical power system, with no control over when the vehicles are charged, will act to flatten the electric load demand curve.

The PPC power system simulation procedure computes the expected amount of energy generated by each fuel type to meet a projected electric load demand. Based on the developed projected electric load the energy generated by each fuel type is shown in Figure 3.16. For the "Base Case" scenario (no additional electric load due to PHEVs) the energy generated per fuel type is deterministic because the "Base Case" electric load demand is deterministic. Whereas, for the PHEV penetration scenarios the energy generated per fuel type is the average energy generated by each fuel type over the 30 repeated simulations for each penetration level.

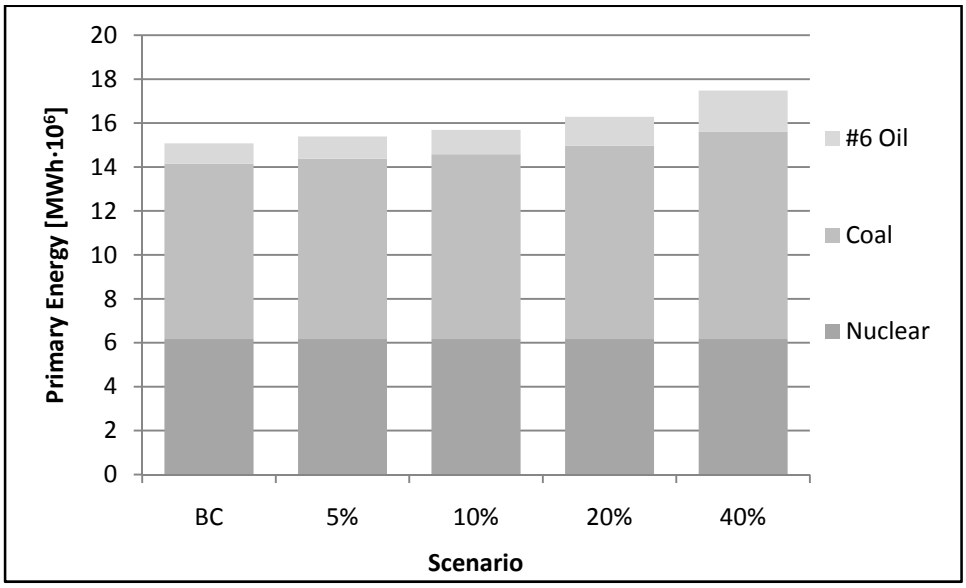

Figure 3.16. Primary energy generated for each RTS scenario.

In Figure 3.16, as expected the total generated energy increases as the penetration level of PHEVs increases. In Figure 3.16 the #2 oil, hydro, and unserviced energy energy productions are negligible (i.e. very small contribution to the total energy production) and are removed from the list of fuel types. The specific increase in each fuel types energy production for each PHEV penetration level is shown in Figure 3.17.

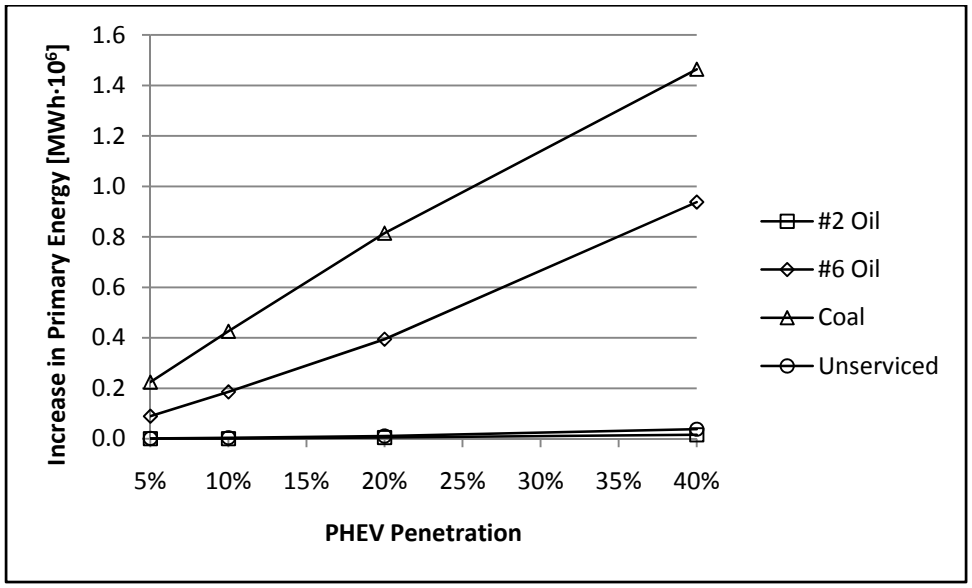

Figure 3.17. Increase in primary energy for each RTS PHEV penetration scenario.

In Figure 3.17, the increase in energy produced by each fuel type is computed by subtracting the base case fuel type energy production from the average PHEV scenario fuel type energy production ($\Delta =$ PHEV Scenario $-$ Base Case). The expected amount of nuclear and hydro energy production is constant, thus no increase in either is observed and both energy sources are removed from the list of power system fuel types in Figure 3.17. The significant increase in both #6 oil and coal indicates that these two fuel types are utilized to charge PHEVs for the particular power system generating mix studied.

The PPC power system simulation procedure computes expected energy statistics including loss of load probability (LOLP), total generated energy (GE), unserviced energy (UE), total fuel cost (TFC), and average electricity cost (AEC) amount of energy generated by each fuel type to meet a project electric demand. For each PHEV scenario the energy statistic results are the average energy statistic over the 30 simulations, as shown in Table 3.21.

Table 3.21. Energy statistics for each simulated RTS scenario.

	Base Case	5%	10%	20%	40%
LOLP	0.0070	0.0083	0.0099	0.0142	0.0296
GE [MWh]	15,080,000	15,400,000	15,710,000	16,340,000	17,580,000
UE [MWh]	9,029	10,82	13,200	20,000	47,020
TFC [k$]	202,700	215,100	228,1	256,500	323,000
AEC [¢/kWh]	1.34	1.40	1.45	1.57	1.84

In Table 3.21, each statistic increases proportionally with the number of PHEVs. From Tables 3.20 and 3.21 the added utility revenues can be calculated for each PHEV penetration level as shown in Table 3.22.

Table 3.22. Added RTS power system revenue.

Scenario	5%	10%	20%	40%
Increased Energy [MWh]	315,000	628,500	1,255,000	2,498,000
N_{PHEV}	76,950	153,900	307,800	615,600
Revenue [k$]	25,210	50,280	100,400	199,900
Revenue [$] per Vehicle per Year	327.60	326.70	326.20	324.70

The results shown in Table 3.22 are computed assuming that the retail electricity rate of 8 cents per kWh is constant all year long. In Table 3.22, the average power system revenue is $326 per PHEV per year.

The impact of displacing gasoline usage with increased utilization of electric energy, for the RTS, causes a slight increase in NO_x and significant decrease in CO_2 for all PHEV penetration scenarios. The percent change in EAP is shown in Figure 3.18.

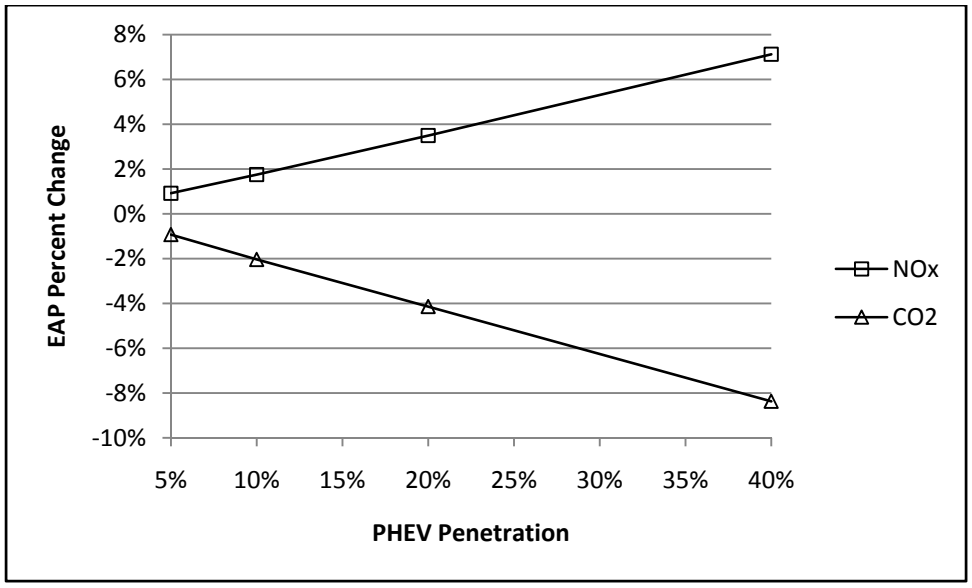

Figure 3.18. RTS percent change of EAP as a function of PHEV penetration.

The percent change at 5% PHEV penetration is 0.92% of NO_x and -0.93% of CO_2, which corresponds to an annual increase of 0.4986 million kg of NO_x and an annual decrease of 160.6 million kg of CO_2.

The gasoline utilization results reveal that the gasoline utilization decreases approximately linearly as PHEV penetration increases as shown in Figure 3.19.

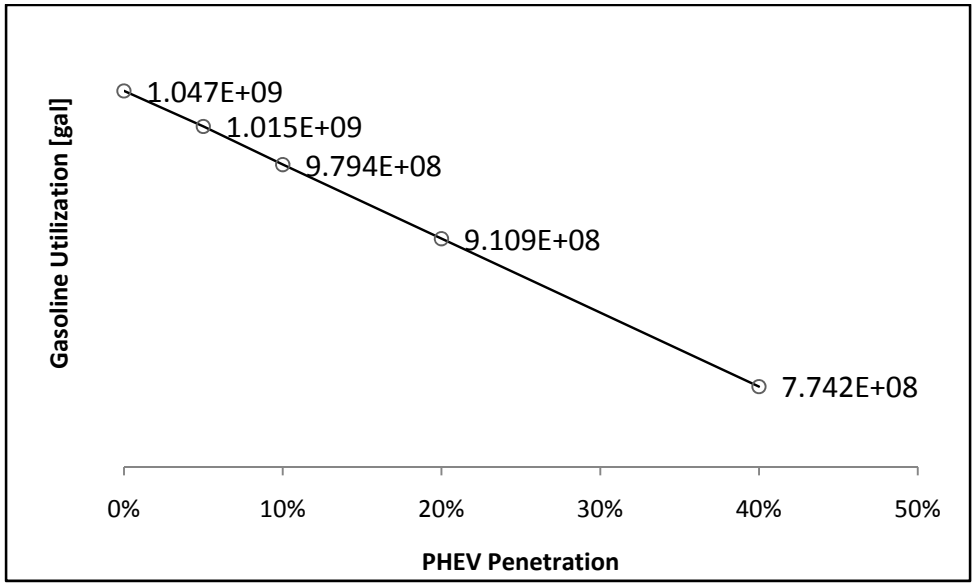

Figure 3.19. RTS gasoline utilization as a function of PHEV penetration.

Specifically, with a fleet of 1.539 million IC vehicles the average yearly gasoline utilization is 1,047 million gallons whereas with 40% of the vehicle fleet replaced with PHEV this utilization reduces to 774 million gallons, a reduction of 26.1%.

Based on the gasoline utilization (Figure 3.19) and the total generated energy (Table 3.21) the total fuel cost can be calculated for an average driver in each PHEV penetration level. The "Base Case" scenario yearly fuel cost consists of entirely gasoline purchases because no PHEVs are utilized, and the PHEV penetration scenarios total fuel cost includes electricity and gasoline purchases. It is assumed that gasoline costs $3.00 per gallon and electricity rate is 8 cents per kWh all year long. Finally, the average gasoline utilization for the base case scenario is used to compute the amount of gasoline used per IC vehicle in the PHEV scenarios, the results are shown in Table 3.23.

Table 3.23. RTS annual fuel cost.

Scenario	Base Case	5%	10%	20%	40%
Annual Fuel Cost [$]	2,042.00	1,089.00	1,041.00	1,037.00	1,035.00

In Table 3.23, a 65% reduction in fuel cost is achieved utilizing PHEVs over IC vehicles. This reduction in annual fuel cost is significantly influence by the cost effectiveness of electricity over gasoline.

3.2.2 United States System Experiment

Next, the second experiment, the U.S. experiment, is described. As with the RTS experiment the U.S. experiment varies the level of PHEV penetration. This experiment uses a generation mix representative of the entire U.S. Similarly, the peak electric load and number of vehicles in the power system area are set to values representing the entire U.S.

3.2.2.1 U.S. Experiment Data

Specifically, the data to generate PPC power system simulation procedure input data is the total U.S. generating capacity [28] (Table 3.24), the total U.S. generated energy production per fuel type [29] (Table 3.25), and the total U.S. power system EAP generated [30] (Table 3.26). PPC power system simulation procedure input data is composed so that the base case energy and EAP results match the statistics in Tables 3.25 and 3.26.

Table 3.24. Total U.S. generating capacity by fuel type [28].

Fuel Type	Generator Nameplate Capacity [MW]
Coal	336,040
Liquid and Coke Petroleum	62,394
Natural and Other Gas	452,052
Nuclear	105,764
Renewable/Other	131,541

Table 3.25. Net U.S. energy generating by fuel type [29].

Fuel Type	Net Generation By Fuel Source [GWh]
Coal	1,994,385
Liquid and Coke Petroleum	45,354
Natural and Other Gas	888,521
Nuclear	808,972
Renewable/Other	377,648

Table 3.26. Estimated EAP by each fuel type in 2007 for the entire U.S. [30].

Fuel Type	CO_2 [kg]	NO_x [kg]
Coal	16,018,807,896,000	22,956,252,000
Liquid and Coke Petroleum	536,895,358,000	1,258,970,000
Natural and Other Gas	3,458,905,616,000	3,402,814,000
Renewable/Other	118,031,404,000	1,582,196,000

Further, the RTS electric load demand distribution [26] is used, but changing the peak electric load demand to 764,476 [MW] [31]. The number of vehicles in the power system test area is set to 135.7 million [32].

3.2.2.2 U.S. Experiment Results

Four simulations are considered for varying the percentage of PHEV penetration. The penetration levels simulated are 5%, 10%, 20% and 40%. For each scenario the number of IC vehicles (N_{IC}) and PHEVs (N_{PHEV}) is shown in Table 3.27.

Table 3.27. Number of vehicles for each U.S. simulation.

Scenario	BC	5%	10%	20%	40%
N_{PHEV}	0	6,783,495	13,566,990	27,133,979	54,267,959
N_{IC}	135,669,897	128,886,402	122,102,907	108,535,918	81,401,938

In Table 3.27, for each PHEV penetration level the total number of vehicles remains 135.7 million.

Each PHEV penetration scenario is repeated 30 times each, with a sample population of 100 vehicles using the same vehicle assumptions as for the RTS experiment.

One result of the probabilistic model of the added electric load due to PHEV charging is an increase in system maximum and minimum power demand. The increase in the maximum and minimum power demand is shown in Figure 3.20 for each of the simulated PHEV penetration levels. The maximum and minimum power demand for the PHEV scenarios is the average maximum and minimum power demand for the 30 PHEV penetration simulations.

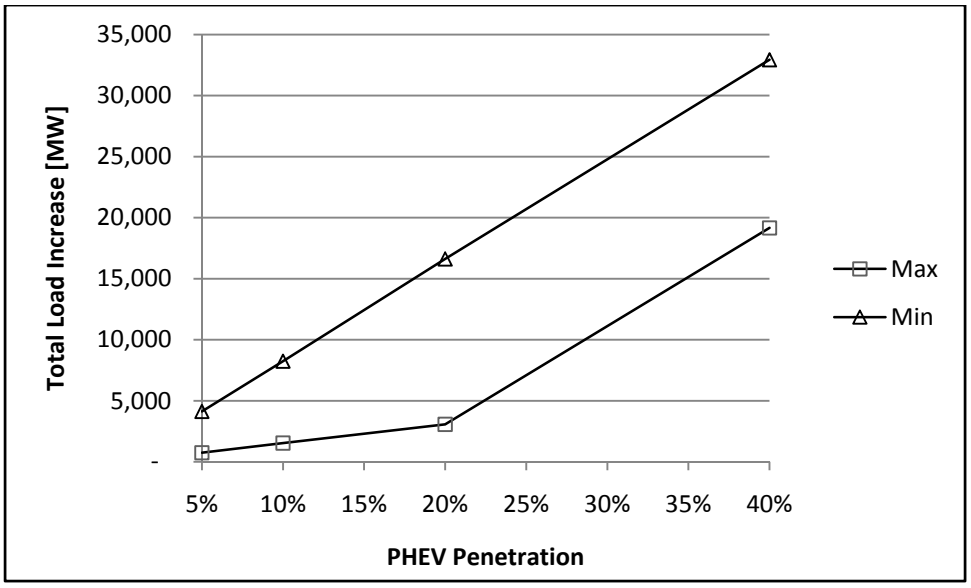

Figure 3.20. Increase in max and min power demand for each U.S. scenario.

As is the case for the RTS experiment the change in maximum and minimum power demand, the curves in Figure 3.20 show that the increase in system maximum load is smaller than the increase in system minimum load for each PHEV penetration scenario. This result indicates that the addition of PHEVs into a typical power system, with no control over when the vehicles are charged, will act to flatten the electric load demand

curve. Specifically, for the U.S. experiment the base case result for maximum power demand is 764,810 MW and the minimum power demand is 229,200 MW.

Based on the projected electric load, the energy generated by each fuel type is shown in Figure 3.21. For the PHEV penetration scenarios the energy generated per fuel type is the average energy generated by each fuel type over the 30 simulations.

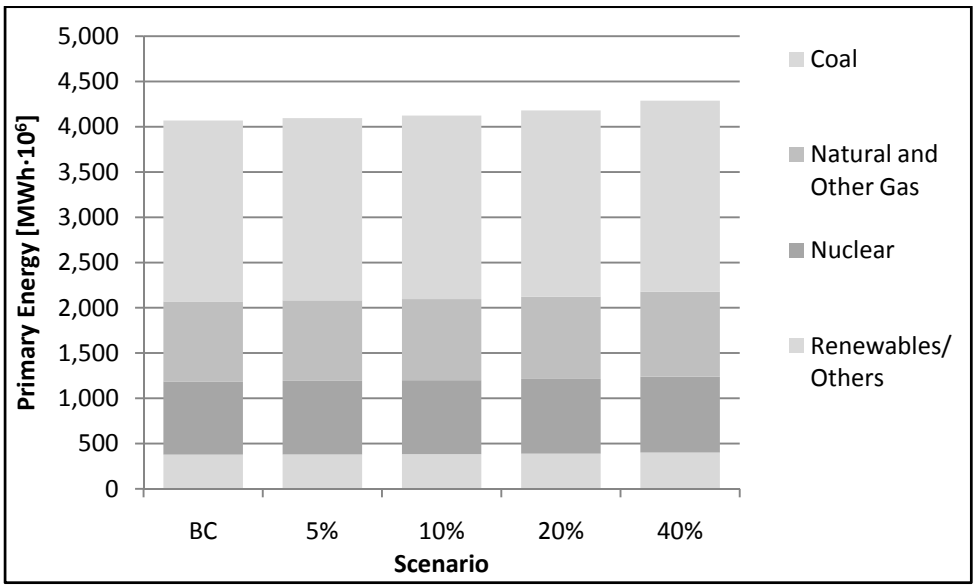

Figure 3.21. Primary energy generated for each U.S. scenario.

In Figure 3.21, as expected, the total generated energy increases as the level of PHEV penetration increases. In Figure 3.21, liquid and coke petroleum energy production is negligible (i.e. very small contribution to the total energy production) and is removed from the list of fuel types. The increase in fuel types energy production is shown in Figure 3.22 for each level of PHEV penetration.

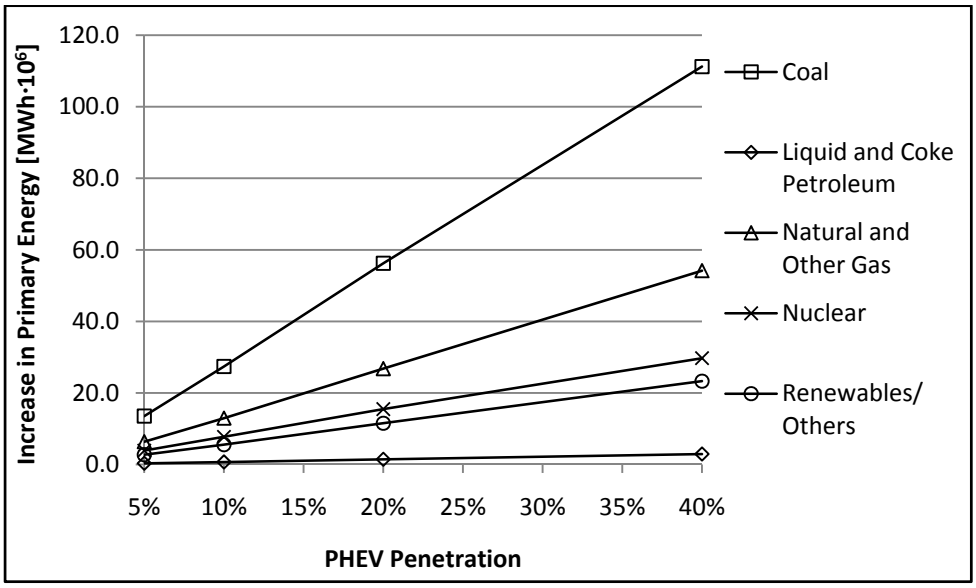

Figure 3.22. Increase in primary energy for each U.S. PHEV penetration scenario.

In Figure 3.22, the increase in energy produced by each fuel type is computed by subtracting the base case fuel type energy production from the average PHEV scenario fuel type energy production ($\Delta =$ PHEV Scenario $-$ Base Case). The significant increase in coal and natural gas energy production indicates that these two fuel types are utilized to charge PHEVs for the particular power system generating mix studied.

Due to a lack of generating unit reliability and fuel cost data the power system simulation procedure energy statistic results for the U.S. experiment simulations are not applicable.

The impact of displacing gasoline usage with increased utilization of electric energy, using the average U.S. power system, results in the percent change in NO_x and CO_2 shown is shown in Figure 3.23.

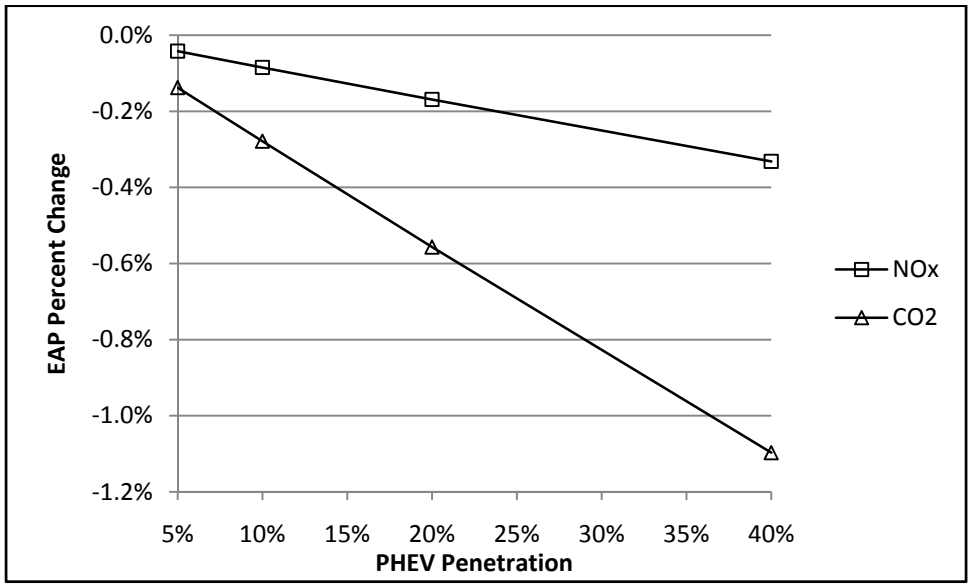

Figure 3.23. U.S. percent change of EAP as a function of PHEV penetration.

The percent change at 40% PHEV penetration is -0.33% of NO_x and -1.10% of CO_2, which corresponded to annual decrease of 98 million kg of NO_x and an annual decrease of 230,133 million kg of CO_2. This represents a significant reductions in both pollutants considered.

The gasoline utilization results reveal that the gasoline utilization decreases approximately linearly as PHEV penetration increases as shown in Figure 3.24.

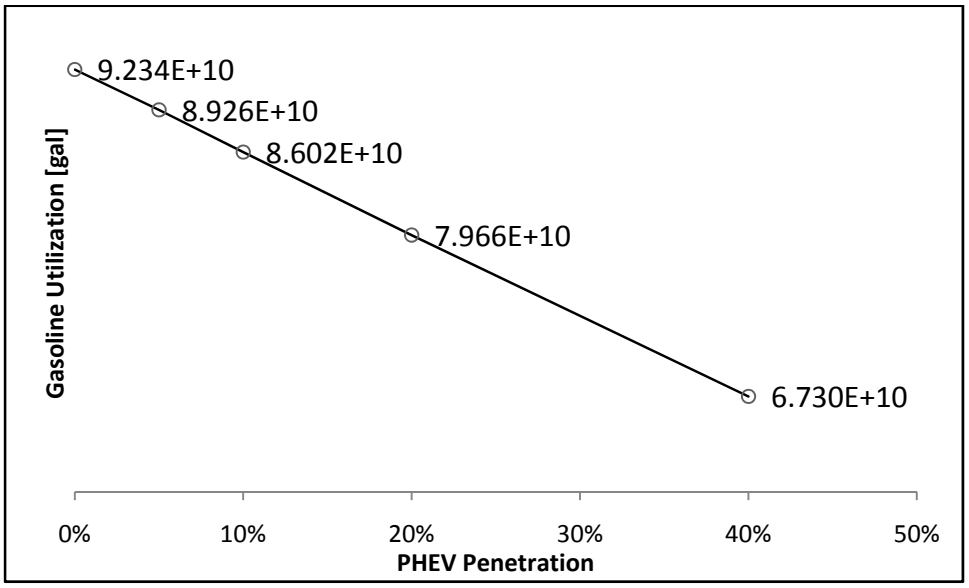

Figure 3.24. U.S. gasoline utilization as a function of PHEV penetration.

Specifically, with a fleet of 135.7 million IC vehicles the average yearly gasoline utilization is 92,340 million gallons whereas with 40% of the vehicle fleet replaced with PHEV this utilization reduces to 67,300 million gallons a reduction of 37.2%.

3.2.3 Modified Reliability Test System

Next, the third experiment, the modified RTS experiment, is described. In the third experiment the penetration level of PHEVs is constant and the RTS electric power generation capacity mix varies. The generating mix varies such that the total generating capacity is constant but the ratio of clean generating capacity increases. All other PPC power system simulation procedure input data is identical to the first experiment.

3.2.3.1 Modified RTS Experiment Data

Five simulation scenarios are considered (called RTS, C1, C2, C3, and C4) each with 5% penetration of PHEV in the RTS power system area, representing 76,950 PHEVs (1,462,050 IC vehicles, thus 1.539 million vehicles in total). The total generating

capacity of each set of generators, where a set is comprised of all available generator using the same fuel type, is shown in Figure 3.25.

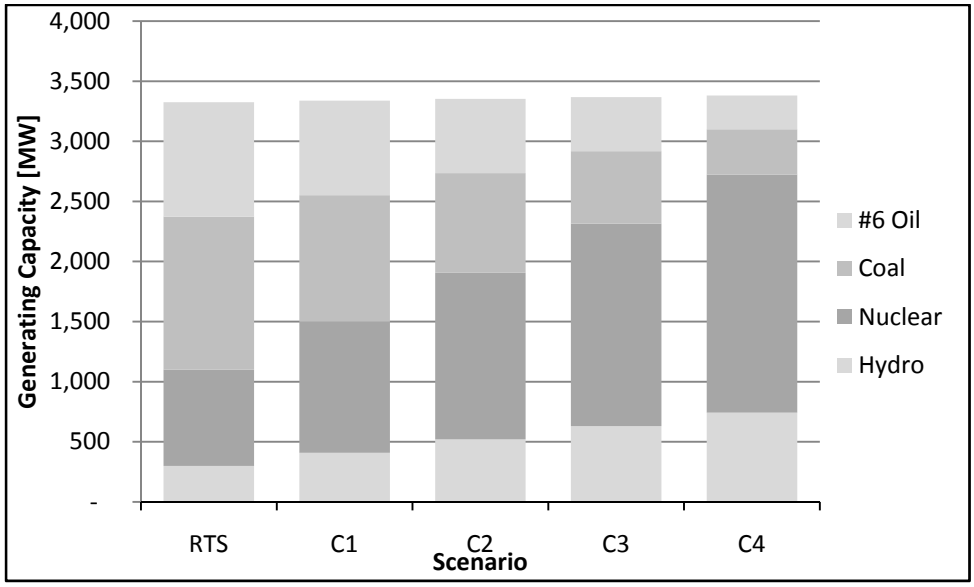

Figure 3.25. Clean energy experiment scenario generation capacities.

In Figure 3.25, the first column is the original RTS power generating capacity mix, and each subsequent column indicates the modified power generating mix capacity for each fuel type. In Figure 3.25, the #2 oil generating capacity is negligible and is removed from the list of fuel types. The generating capacity available from all nuclear and hydro (non-EAP producing) generators increases and the capacity available from #2 oil, #6 oil, and coal (all others fuel types) generators decreases; thus, the total generating capacity for each scenario is constant 3,405 MW.

3.2.3.2 Modified RTS Experiment Data

The percentage of non-EAP producing capacity and energy production is shown in Table 3.28 for each modified RTS scenario.

Table 3.28. Clean energy capacity and generated energy summary.

Percentage of Non-EAP Producing	RTS	C1	C2	C3	C4
Capacity	32.31%	44.00%	56.00%	68.00%	80.00%
Energy Generated	40.79%	55.40%	69.42%	80.71%	89.41%

Clearly, as the level of non-EAP producing capacity increases the energy generated by the non-EAP producing energy sources also increases. The amount of energy generated by each power system fuel type is shown in Figure 3.26.

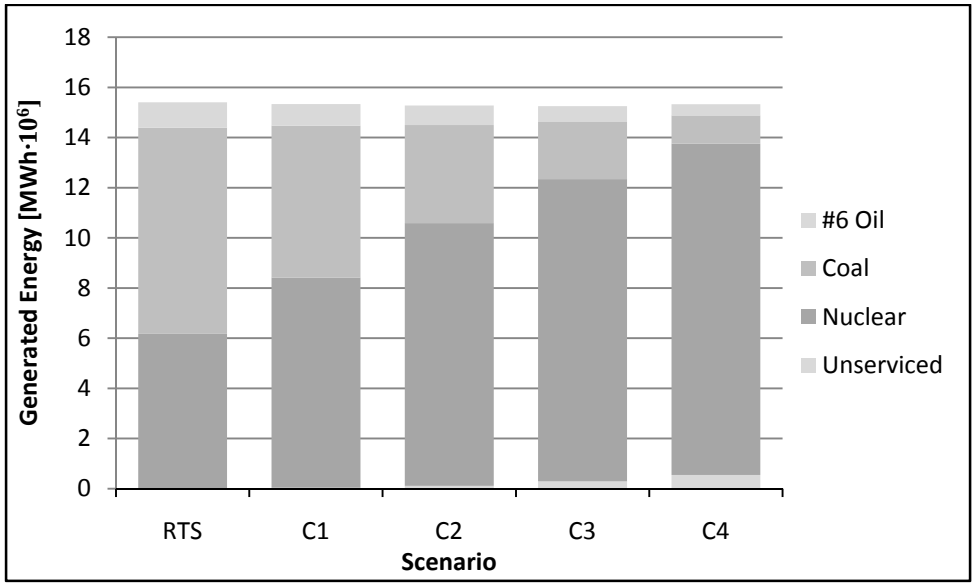

Figure 3.26. Clean energy experiment scenario generated energy.

In Figure 3.26, #2 oil and hydro energy production are negligible (i.e. very small contribution to the total energy production) and are removed from the list of fuel types. In Figure 3.26, as the level of nuclear energy reaches significant levels, scenarios C3 and C4 (78% and 85% respectively), the amount of unserviced energy becomes noticeable (2% and 4% respectively). This result is due to the relatively high forced outage rate (FOR) for the nuclear generators (Table 3.11). The specific percentage increase for each fuel type is shown in Figure 3.27.

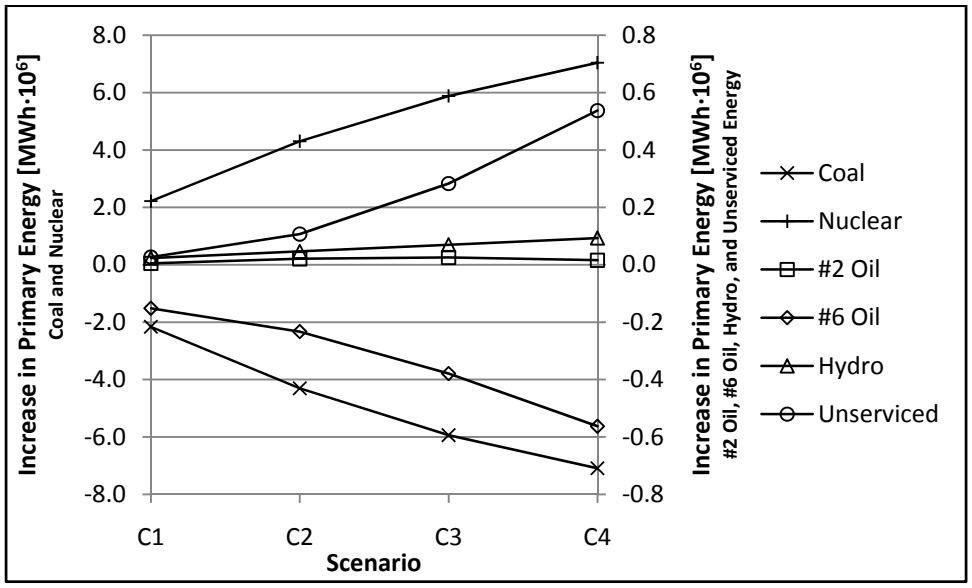

Figure 3.27. Clean energy experiment scenario increase in primary energy.

In Figure 3.27, the percentage increase for #2 oil, #6 oil, hydro, and unserviced energy are an order of magnitude smaller than that of the percent increase of coal and nuclear energy, for this reason the percentage in #2 oil, #6 oil, hydro and unserviced energy are plotted on a secondary (right-hand side) vertical axis, with a different scale then the primary (left-hand side) vertical axis..

This experiment indicates that nuclear energy is used to replace the energy originally derived by coal energy. The other three fuel types, #2 oil, #6 oil and hydro energy combined only produce less that 8% of the total generated energy for each scenario. The resulting change in EAP is shown in Figure 3.28.

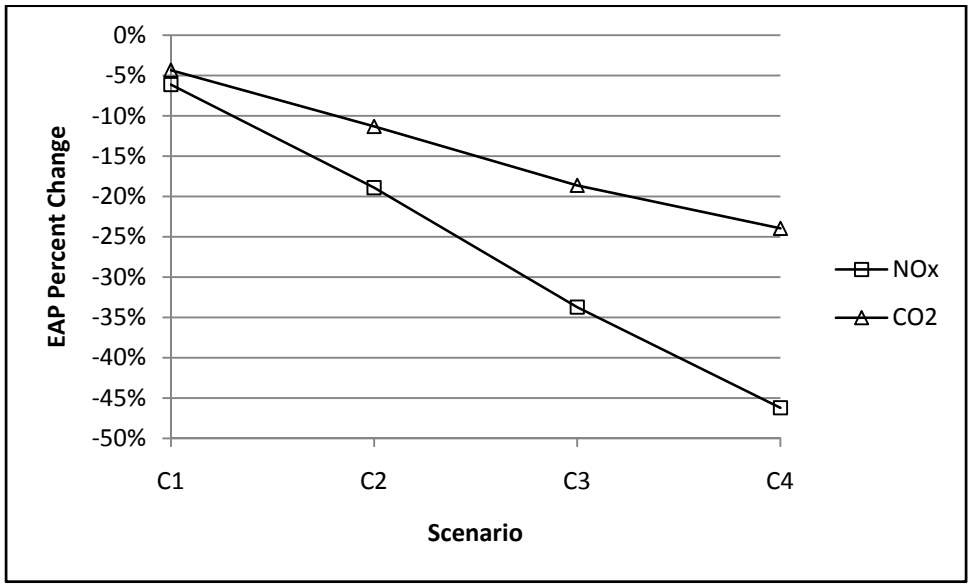

Figure 3.28. Clean energy experiment change in EAP for each simulated scenario.

Not surprisingly as the amount of energy produced from non-EAP producing sources increases, the total amount of EAP decreases significantly.

3.3 Conclusion

The use of PHEVs represents a feasible near term solution to the correlated global crisis of increased use of petroleum and increased generation of EAP. The impact of PHEV use in the context of these two issues is addressed in this chapter.

The change in primary energy source utilization due to PHEV charging is evaluated using the PPC power system simulation procedure [18]. For this research the PPC power system simulation procedure is augmented with a PHEV model. The PHEV model allows the amount of added electric energy demand to charge a fleet of PHEVs to be calculated. The results of this methodology include expected energy generated with and without the added electric load demand required to charge PHEVs, the expected EAP produced by the vehicle fleet and power system with and without PHEV charging, and fuel costs for IC vehicles and PHEVs.

Three experiments are presented. The first uses the 1979 RTS [26] to charge varying levels of PHEV penetration. The second uses the U.S. average generation mix to charge varying levels of PHEV penetration. The third varies the relative capacity of EAP producing and non-EAP producing generation in the RTS power system and simulated the primary energy utilized to charge 5% penetration of PHEVs.

The probabilistic simulation of an integrated power system with distributed PHEVs results depend on the integrated power system generation mix. The percent of the total generating capacity for each fuel type utilized in the original RTS system [26] is shown in Figure 3.29, the U.S. average generation [28] mix is shown in Figure 3.30, and the generating capacity of each fuel type for the five clean energy scenarios are shown in Figure 3.25.

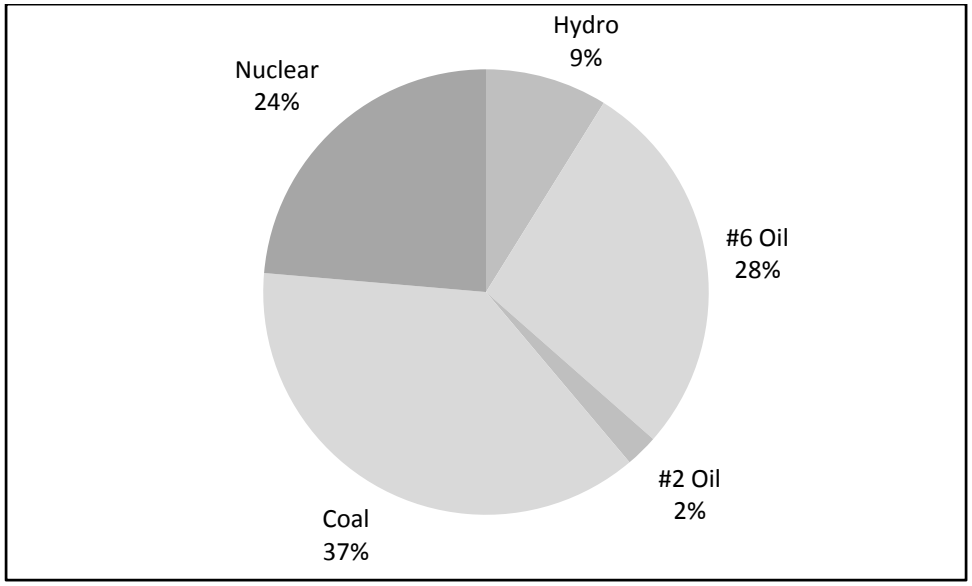

Figure 3.29. RTS generating capacity [26].

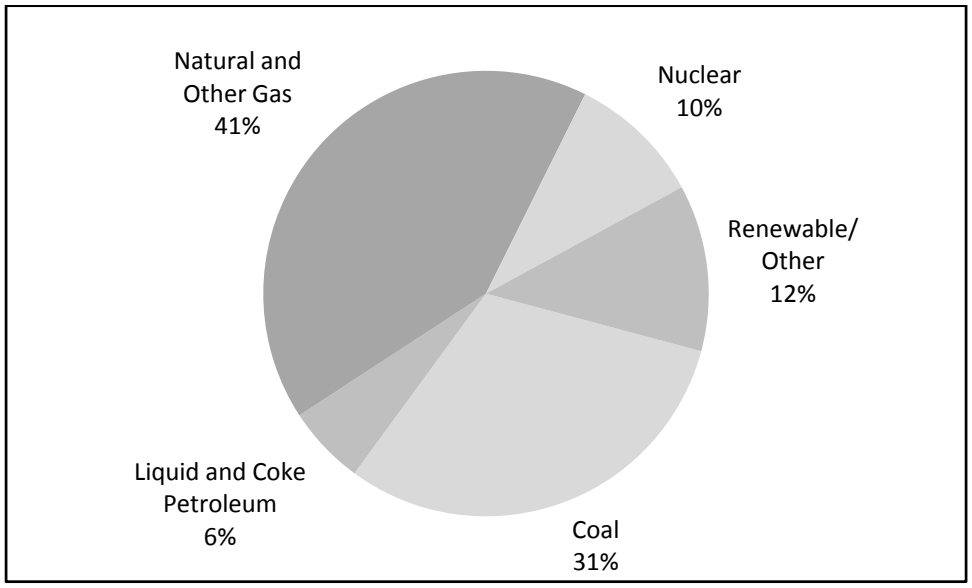

Figure 3.30. U.S. total generating capacity [28].

The expected energy production from each fuel type for the base case, no PHEVs included in the light duty vehicle fleet, and a scenario where 5% of the light duty vehicle fleet in the power system area is replaced with PHEVs, are shown in Table 3.29. In Table 3.29 the percentage change is given by

$$\text{Percent Change} = [(5\%\ \text{PHEV} - \text{Base Case})/\text{Base Case Total}] \cdot 100\% \quad (3.48)$$

where the base case total amount of generated energy is used to normalize the change in energy production so that the relative size of each fuel types contribution to the total energy generated is accounted for. Without this normalization the RTS simulation results percent increase in #2 oil energy production would be 17.71% and the percent increase in #6 oil energy production would be 9.67%, thereby incorrectly indicating a higher increase in #2 oil over #6 oil because the contribution of #2 oil is so small compared to all other fuel types. The modified RTS simulation results in Table 3.29 are the C1 scenario results. In the C1 scenario results the non-EAP producing capacity (nuclear and hydro) is increased to provide 44% of the total system capacity up from 32.31% in the original

RTS generating capacity [26]. This scenario represents the smallest increase in clean production capacity simulated in the modified RTS experiment.

Table 3.29. Change in primary energy source utilization.

		Base Case [GWh]	5% PHEV Penetration [GWh]	Percent Change
RTS Simulations	#6 Oil	924	1,014	0.59%
	#2 Oil	5	6	0.01%
	Coal	7,988	8,212	1.47%
	Nuclear	6,167	6,167	0%
	Hydro	194	194	0%
U.S. Power System Simulations	Coal	2,000,000	2,014,000	0.33%
	Liquid and Coke Petroleum	45,530	45,880	0.01%
	Natural and Other Gas	882,800	889,200	0.16%
	Nuclear	808,600	812,500	0.09%
	Renewables/Others	377,900	380,700	0.07%
Modified RTS Simulations	#6 Oil	1,014	862	-0.97%
	#2 Oil	6	11	0.03%
	Coal	8,212	6,052	-13.85%
	Nuclear	6,167	8,384	14.22%
	Hydro	194	217	0.15%

In the RTS simulations the #6 oil and coal are utilized to meet the additional load created by PHEV charging, and the nuclear and hydro energy are fully utilized thus no increase in energy utilization of these fuel types is possible. In the U.S. power system simulations coal is utilized to meet the additional load created by PHEV charging. The modified RTS simulations introduce additional nuclear and hydro generation capacity compared to the RTS simulations. The modified RTS simulations result in a significant increase in nuclear energy generation and a slight increase in hydro energy generation.

In addition to the expected energy production, expected NO_x and CO_2 EAP production are also calculated. The total system EAP is the EAP produced by both the electric power system and the light duty vehicle fleet in the power system area. Table

3.30 shows EAP results for each experiments base case and 5% PHEV penetration simulations and the modified RTS experiment C1 scenario. Here the percent decrease is normalized by the base case results, as is the standard percent reduction calculation.

Table 3.30. Total system EAP.

		Base Case [kg]	5% PHEV Penetration [kg]	Percent Decrease
RTS Simulations	NO_x	4.432E+07	4.472E+07	-0.92%
	CO_2	1.736E+10	1.720E+10	0.93%
U.S. Power System Simulations	NO_x	2.959E+10	2.958E+10	0.04%
	CO_2	2.097E+13	2.095E+13	0.14%
Modified RTS Simulations	NO_x	4.472E+07	4.198E+07	6.13%
	CO_2	1.720E+10	1.645E+10	4.34%

In the RTS simulations, an increase of 0.92% of NO_x represents an annual increase of 0.4986 million kg of NO_x; whereas, a decrease of 0.93% of CO_2 represents a decrease of 160.6 million kg of CO_2. Similarly in the U.S. simulations, a decrease of 0.04% of NO_x represents an annual decrease of 12.40 million kg of NO_x; further, a decrease of 0.14% of CO_2 represents a decrease of 28,900 million kg of CO_2. In the modified RTS simulations significant EAP reduction are simulated, a decrease of 6.13% of NO_x represents an annual decrease of 2.742 million kg of NO_x; further, a decrease of 4.34% of CO_2 represents a decrease of 745.9 million kg of CO_2.

The fuel cost of a PHEV includes gasoline and electricity purchasing. The average annual fuel cost is compared for PHEV versus IC vehicles in the RTS experiment. Assuming a constant gasoline price of $3.00 per gallon and electricity rate of 8 cents per kWh all year long, it is found that PHEV fuel costs are 65% less expensive then IC vehicle fuel costs.

The results from Chapter 3 indicate that PHEVs offer cleaner transportation (depending on the generation mix used to charge the vehicles) with decreased gasoline

utilization at a lower cost to consumers. The cost to pay for these three advantages in terms of impact on distribution transformers is discussed in Chapter 4.

CHAPTER 4

IMPACT OF PHEV CHARGING ON DISTRIBUTION TRANSFORMERS

This chapter examines the impact that charging plug-in hybrid electric vehicles (PHEVs) will have on distribution transformers. Distribution systems, and specifically the distribution transformer, are designed for specific load carrying capability based on typical load consumption patterns. When PHEVs are deployed the pattern of electric power demand will change. The power system may or may not be capable of handling the new pattern and level of demand.

To examine the impact that PHEV charging will have on distribution transformers, simulations of daily load flows are performed using random electric loads. Two scenarios are examined, the first provides a baseline comparison of the transformer percent loss of life (LOL) with no electric load due to PHEV, the second scenario provides the transformer LOL including PHEV charging in addition to the normal household electrical demand.

A center-tapped single phase transformer model is used to compute the expected transformer currents and an electro-thermal transformer model of the distribution transformer is used to compute the expected distribution transformer hourly hot-spot temperature.

Random distributions for both the normal house hold electric load demand and additional electric load demand for PHEV charging are utilized. Repeated simulations in both scenarios provide a distribution of the expected LOL results.

The remainder of this chapter is organized as follows:

1. The random transformer electrical load distribution is described.
2. The PHEV electrical load distribution is described.
3. The center-tapped single phase transformer model is described.
4. The electro-thermal transformer model is described.
5. The method of computing the transformer LOL is described.
6. The simulation methodology is described.
7. The transformer LOL results are compared.

4.1 Random Feeder Electrical Load

Two assumptions used to compute the random electric load representing the average electric demand for a three house distribution circuit are (1) the hourly peak real power demand, $P^{(h)}$ [W], is a normally distributed random variable (RV) with mean and variance as a function of the daily hour and (2) the hourly power factor ($p.f.^{(h)}$) for each hour is a discrete RV with probability mass function

$$\mathrm{P}\{p.f.^{(h)} = x\} = \begin{cases} 0.3 & \text{if } x = 0.9 \\ 0.4 & \text{if } x = 0.95 \\ 0.3 & \text{if } x = 1 \end{cases} \tag{4.1}$$

The assumed time distribution for the average hourly peak load is shown in Figure 4.1.

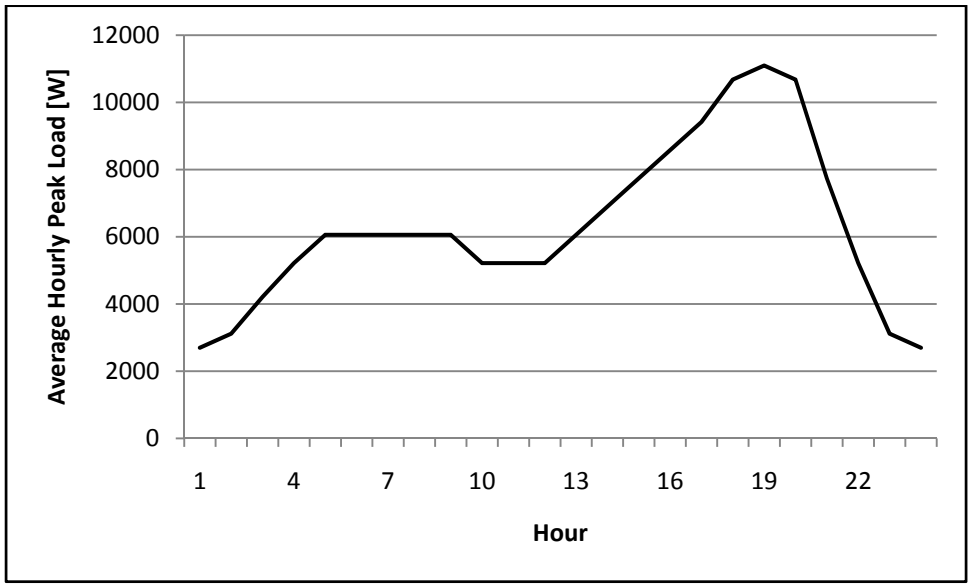

Figure 4.1. Hourly mean peak real power.

In Figure 4.1, this curve represents the mean value for the hourly real power demand at the distribution transformer over a typical day. The real power generated using this mean value is the real power electric load demand for three houses. The validity of this curve is checked by computing the average total daily electric energy demand represented by this curve. The resulting average daily electric energy computed is 151.2 kWh which is consistent with an assumed average household monthly electric load demand of 1,500 kWh.

From the hourly mean peak real power, $\mu_P^{(h)}$ [W] the real power variance is computed as

$$\sigma_P^{(h)} = \mu_p^{(h)}/4 \tag{4.2}$$

From the generated real power quantity $\left(P^{(h)}\right)$ and power factor $\left(p.f.^{(h)}\right)$ the reactive power demand, $Q^{(h)}$ [VAR] is computed as

$$\mathrm{Q^{(h)}} = \sin\left[\cos^{-1}\left(p.f.^{(h)}\right)\right] \cdot \left(P^{(h)}/p.f.^{(h)}\right) \tag{4.3}$$

4.2 PHEV Electrical Load

The added electric load due to PHEV charging is assumed to 90% of the estimated PHEV-40 battery capacity, where PHEV-X indicates a PHEV which is capable of driving X miles using the battery alone. This electric load represents the useful capacity of the total PHEV battery capacity. This scenario models the situation where a PHEV returns home with a completely discharged battery. A fully discharged battery represents the largest possible demand from the PHEV, representing a worst case scenario in terms of added electric load demand to the distribution transformer. Further, it is assumed that the vehicle begins charging as soon as it is plugged in.

The method to compute the required power and time when the vehicle is connected to the power system is computed by the following three steps:

1. The vehicles arrival, A_T [h], and departure times, D_T [h], are randomly generated.
2. The vehicles added electric energy load, BC [Wh], is randomly generated.
3. The additional real, P [W], and reactive, Q [VAR], power demand power demand is computed.

The arrival (A_T) and departure (D_T) times are assumed to be normally distributed RVs. The distribution parameters (Table 4.1) are the weekday distribution parameter values previously defined (Table 3.9). In Table 4.1, the parameter p in the distribution parameters mean, $\mu_T^{(p)}$ [h], and variance, $\left(\sigma_T^{(p)}\right)^2$ [h], indicates one of the two possible daily timing distributions: weekday departure or weekday arrival.

Table 4.1. PHEV timing distribution parameters.

Parameter	Departure	Arrival
$\mu_T^{(p)}$	7	18
$\left(\sigma_T^{(p)}\right)^2$	3	3

The vehicles added electric energy load (BC) is assumed to be a normally distributed RV with a mean (μ_{BC}) of 16,000 Wh and a standard deviation (σ_{BC}) of 4,000 Wh. These parameters are selected to include all four vehicle classes previously defined. Finally, the vehicle charger is assumed to have a power factor of 0.99. All RVs are assumed to be independent.

From these distributions the added charging power (4.4) and reactive power, (4.5) can be computed.

$$P = BC/[(24 - A_T) + D_T] \tag{4.4}$$

$$Q = (P/0.99)\sin[cos^{-1}(0.99)] \tag{4.5}$$

In (4.4) $(24 - A_T) + D_T$ is the total time, in hours, that the vehicle will be charging.

4.3 Center-Taped Single-Phase Distribution Transformer Model

The typical residential distribution system distribution transformer model is used to compute the expected transformer currents for a specified electric load demand. The model, shown in Figure 4.2, is fully described in [33]. The specific scenario modeled here is a single phase distribution transformer feeding three typical houses. The transformer is a 7.960 kV to 120/240 V transformer rated at 15 kVA. The transformer has a series resistance (R_A) and reactance (X_A) of 0.007 p.u. and 0.035 p.u. respectively.

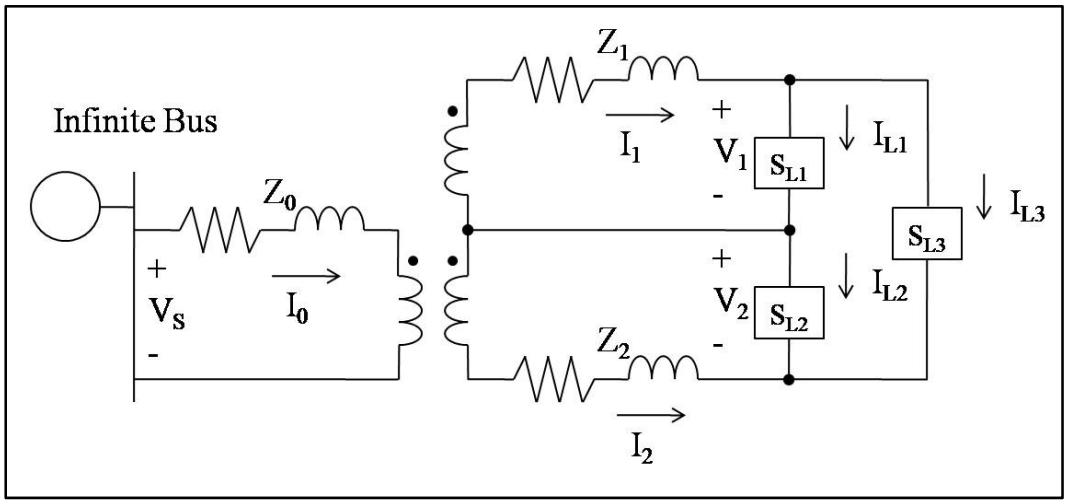

Figure 4.2. Center-tapped single phase transformer model [33].

To compute the winding impedances Z_0, Z_1, and Z_2 the interlaced transformer design equations are used [33]

$$Z_{\text{p.u.0}} = 0.5 \cdot R_A + j \cdot 0.8 \cdot X_A \tag{4.6}$$

$$Z_{\text{p.u.1}} = Z_{\text{p.u.2}} = R_A + j \cdot 0.4 \cdot X_A \tag{4.7}$$

The per-unit impedance values are converted to actual units by multiplying them by the per-unit base impedances

$$Z_{\text{base high voltage}} = (V_s^2 / S_{\text{transformer rated}}) \tag{4.8}$$

$$= 7{,}960^2 / 15{,}000 = 4224\ \Omega$$

$$Z_{\text{base low voltage}} = 240^2 / 15{,}000 = 3.84\ \Omega \tag{4.9}$$

Thus,

$$Z_0 = Z_{\text{base high voltage}} \cdot Z_{\text{p.u.0}} \tag{4.10}$$

$$= 4{,}224 \cdot (0.5 \cdot 0.007 + j \cdot 0.8 \cdot 0.035)$$

$$= 14.78 + j \cdot 118.3\ \Omega$$

$$Z_1 = Z_2 = Z_{\text{base low voltage}} \cdot Z_{\text{p.u.1}} \tag{4.11}$$

$$= 3.84 \cdot (0.007 + j \cdot 0.4 \cdot 0.035)$$

$$= 0.0269 + j \cdot 0.0538\ \Omega$$

The turns ratio (n_t) is the ratio of the primary and secondary voltages

$$n_t = 7960/120 = 66.33 \tag{4.12}$$

Finally, the total complex power is distributed between the two 120 V circuits (S_{L1} and S_{L2} [VA]) and the 240 V circuit (S_{L3} [VA]) assuming that 60% of the power demand in a typical household is 120 V (split evenly between the two 120 V lines) and the remaining 40% is 240 V. Thus,

$$S_{L1} = S_{L2} = 0.3 \cdot \left(P^{(h)} + j \cdot Q^{(h)}\right) \tag{4.13}$$

$$S_{L3} = 0.4 \cdot \left(P^{(h)} + j \cdot Q^{(h)}\right) \tag{4.14}$$

To compute the winding currents I_0, I_1, and I_2 in Figure 4.2 an iterative process from [33] is utilized. These currents form the input to the electro-thermal transformer model, which is in turn used to compute the expected distribution transformer temperature, and thus the distribution transformer LOL. The method outlined in [33] to compute the transformer currents is an iterative process consisting of a forward sweep and a backward sweep. As an example of this method the transformer currents are computed in detail below for the average assumed electric load including average real power $\bar{P}$ [W], average power factor $\overline{p.f.}$, and average reactive power $\bar{Q}$ [VAR]

$$\bar{P} = E\left\{P^{(h)}\right\} = 1/24 \cdot \sum_{h=1}^{24} P^{(h)} = 6{,}298 \text{ W} \tag{4.15}$$

$$\overline{p.f.} = E\left\{p.f.^{(h)}\right\} = 1 \cdot 0.3 + 0.95 \cdot 0.4 + 0.9 \cdot 0.3 = 0.95 \tag{4.16}$$

$$\bar{Q} = \sin(\cos^{-1}(0.95)) \cdot 6298/0.95 = 2{,}070 \text{ VAR} \tag{4.17}$$

Thus, the average electric load demand at the transformer, representing the total demand for three average houses, is $\overline{S_{L1}}$ (120 V load number 1), $\overline{S_{L2}}$ (120 V load number 2), and $\overline{S_{L3}}$ (240 V load)

$$\overline{S_{L1}} = \overline{S_{L2}} = 0.3 \cdot (6{,}298 + j \cdot 2{,}558) = 1{,}889 + j \cdot 621.0 \text{ VA}$$

$$\overline{S_{L3}} = 0.4 \cdot (6{,}298 + j \cdot 2{,}558) = 2{,}519 + j \cdot 828.0 \text{ VA}$$

The first step to compute the transformer currents is to assume no average low voltage line currents

$$\begin{bmatrix}\bar{I}_1\\ \bar{I}_2\end{bmatrix} = \begin{bmatrix}0\\0\end{bmatrix}\ \text{A} \tag{4.18}$$

Next, the average load voltages are computed

$$\begin{bmatrix}\bar{V}_1\\ \bar{V}_2\end{bmatrix} = \left(n_t \cdot \begin{bmatrix}1 & 0\\ 0 & 1\end{bmatrix}\right)^{-1} \cdot \left(\begin{bmatrix}V_s\\ V_s\end{bmatrix} - \begin{bmatrix}Z_1 + \frac{1}{n_t^2}Z_0 & -\frac{1}{n_t^2}Z_0\\ \frac{1}{n_t^2}Z_0 & -Z_2 - \frac{1}{n_t^2}Z_0\end{bmatrix} \cdot \begin{bmatrix}\bar{I}_1\\ \bar{I}_2\end{bmatrix}\right) \tag{4.19}$$

$$= \begin{bmatrix}0.0151 & 0\\ 0 & 0.0151\end{bmatrix} \cdot \left(\begin{bmatrix}7960\\ 7960\end{bmatrix} - \begin{bmatrix}0.0303 + j \cdot 0.0807 & -0.0034 - j \cdot 0.0269\\ 0.0034 + j \cdot 0.0269 & -0.0303 - j \cdot 5.3518\end{bmatrix} \cdot \begin{bmatrix}0\\0\end{bmatrix}\right)$$

$$= \begin{bmatrix}120\\120\end{bmatrix}\ \text{V}$$

Then, the average load currents are computed

$$\begin{bmatrix}\overline{I_{L1}}\\ \overline{I_{L2}}\\ \overline{I_{L3}}\end{bmatrix} = \begin{bmatrix}\left(\frac{\overline{S_{L1}}}{V_1}\right)^*\\ \left(\frac{\overline{S_{L2}}}{V_2}\right)^*\\ \left(\frac{\overline{S_{L3}}}{V_1+V_2}\right)^*\end{bmatrix} = \begin{bmatrix}15.75 - j \cdot 5.175\\ 15.75 - j \cdot 5.175\\ 10.50 - j \cdot 3.450\end{bmatrix}\ \text{A} \tag{4.20}$$

Next, the average line currents are computed

$$\begin{bmatrix}\bar{I}_1\\ \bar{I}_2\end{bmatrix} = \begin{bmatrix}1 & 0 & 1\\ 0 & -1 & -1\end{bmatrix} \cdot \begin{bmatrix}\overline{I_{L1}}\\ \overline{I_{L2}}\\ \overline{I_{L3}}\end{bmatrix} = \begin{bmatrix}26.24 - j \cdot 8.625\\ -26.24 + j \cdot 8.625\end{bmatrix}\ \text{A} \tag{4.21}$$

Finally, the average load voltages are computed. Now using the average load currents computed in the preceding step

$$\begin{bmatrix}\bar{V}_1\\ \bar{V}_2\end{bmatrix} = \begin{bmatrix}120.0 - j \cdot 0.0382\\ 120.0 - j \cdot 0.0382\end{bmatrix}\ \text{V} \tag{4.22}$$

This process is repeated until the error (e) falls below a specified tolerance $(e < 0.001)$ [33]

$$\begin{bmatrix}7960 \cdot e\\ 7960 \cdot e\end{bmatrix} =$$

$$\begin{bmatrix} V_s \\ V_s \end{bmatrix} - \left(n_t \cdot \begin{bmatrix} 1 & 0 \\ 0 & 1 \end{bmatrix} \cdot \begin{bmatrix} \overline{V_1} \\ \overline{V_2} \end{bmatrix} + \begin{bmatrix} n_t \cdot Z_1 + \frac{1}{n_t^2} Z_0 & -\frac{1}{n_t^2} Z_0 \\ \frac{1}{n_t^2} Z_0 & -n_t \cdot Z_2 - \frac{1}{n_t^2} Z_0 \end{bmatrix} \cdot \begin{bmatrix} \overline{I_1} \\ \overline{I_2} \end{bmatrix} \right)$$

$$= \begin{bmatrix} 0.0 \\ 0.0 \end{bmatrix} \text{ V}$$

Once the iterative process converges the average high voltage winding current can be computed

$$\begin{bmatrix} \overline{I_0} \\ \overline{I_0} \end{bmatrix} = \frac{1}{n_t} \begin{bmatrix} 1 & -1 \\ 1 & -1 \end{bmatrix} \begin{bmatrix} \overline{I_1} \\ \overline{I_2} \end{bmatrix} \tag{4.23}$$

$$= \begin{bmatrix} 0.0151 & -0.0151 \\ 0.0151 & -0.0151 \end{bmatrix} \cdot \begin{bmatrix} 26.24 - j \cdot 8.625 \\ -26.24 + j \cdot 8.625 \end{bmatrix}$$

$$= \begin{bmatrix} 0.7912 - j \cdot 0.2601 \\ 0.7912 - j \cdot 0.2601 \end{bmatrix} \text{ A}$$

The electro-thermal transformer model, described next, computes the expected transformer winding temperature based on real valued currents, and thus the following magnitudes of the complex current values are used

$$\begin{bmatrix} |\overline{I_0}| \\ |\overline{I_1}| \\ |\overline{I_2}| \end{bmatrix} = \begin{bmatrix} 0.8328 \\ 27.62 \\ 27.62 \end{bmatrix} A$$

4.4 Electro-Thermal Transformer Model

Different electro-thermal transformer models of transformers have been experimentally developed in [34] and [35], and a similar model is used here to calculate the hot-spot temperature of a distribution transformer for random daily load patterns. Variations of the model used in this thesis, shown in Figure 4.3, have also been used by others in [36] and [37] and is a simplified electro-thermal transformer model of a center-tapped single phase convection cooled distribution transformer.

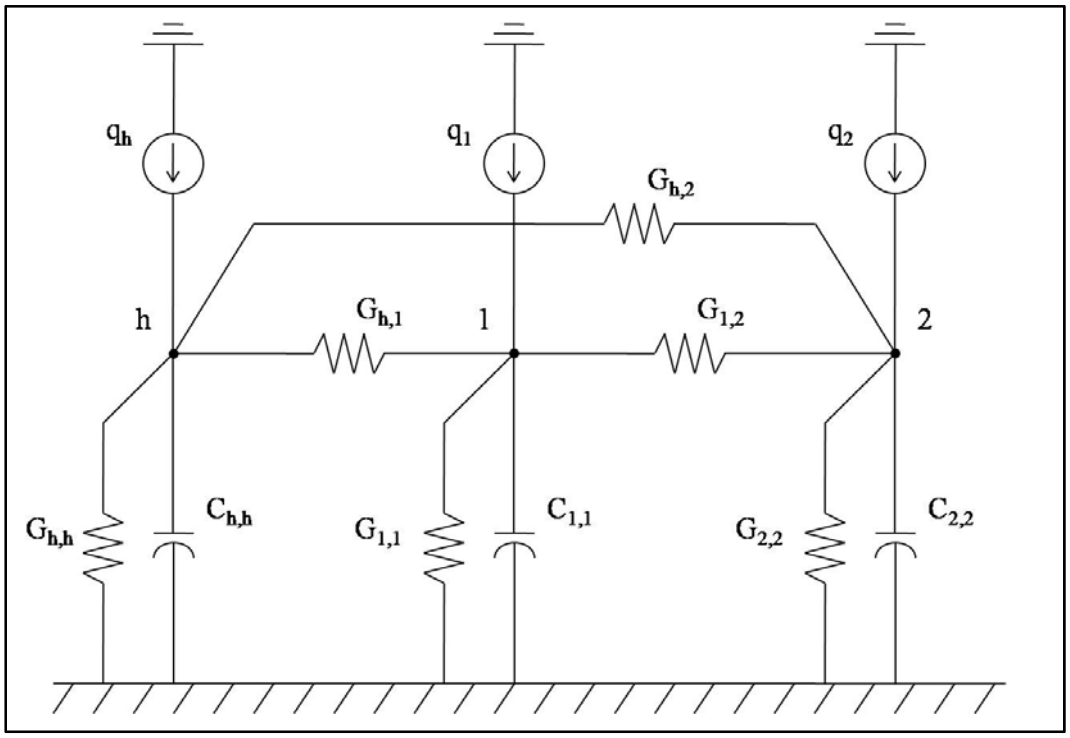

Figure 4.3. Electro-thermal transformer model.

The nodes in Figure 4.3 represent:

- The high voltage winding (node h).
- The low voltage winding center tap 1 (node 1).
- The low voltage winding center tap 2 (node 2).

Each circuit element represents a thermal phenomenon: the conductance components represent heat transfer within and between the transformer windings (estimated from temperature gradients between transformer windings [38]); the capacitive components represent transformer winding thermal inertia (computed from the winding mass and winding specific heat constant [38]); and the current sources represent heat sources in the form of ohmic losses in each of the transformer windings.

The dynamics of the transformer winding temperatures [38] are described by the following differential equation

$$\boldsymbol{C} \cdot d\vec{T}/dt = -\boldsymbol{G} \cdot \vec{T} + \vec{Q} \tag{4.24}$$

where $\boldsymbol{C}$ [joules/˚C] is the thermal capacitance matrix

$$\boldsymbol{C} = \begin{bmatrix} C_{h,h} & 0 & 0 \\ 0 & C_{1,1} & 0 \\ 0 & 0 & C_{2,2} \end{bmatrix} \tag{4.25}$$

$\vec{T}$ [˚C] is the components temperature vector

$$\vec{T} = [T_h \quad T_1 \quad T_2]^T \tag{4.26}$$

$\vec{Q}$ [W] is the heat input vector

$$\vec{Q} = [Q_h \quad Q_1 \quad Q_2]^T \tag{4.27}$$

which represent ohmic losses in the transformer windings and as such can be modeled as the following function of the winding currents and resistances

$$\vec{Q} = [14.78 \cdot I_h^2 \quad 0.0269 \cdot I_1^2 \quad 0.0269 \cdot I_2^2]^T \tag{4.28}$$

and $\boldsymbol{G}$ [W/˚C] is the thermal conductance matrix, which represents the thermal conductance among the three windings

$$\boldsymbol{G} = \begin{bmatrix} G_{h,h} + G_{h,1} + G_{h,2} & -G_{h,1} & -G_{h,2} \\ -G_{h,1} & G_{1,1} + G_{h,1} + G_{1,2} & -G_{1,2} \\ -G_{h,2} & -G_{1,2} & G_{2,2} + G_{h,2} + G_{1,2} \end{bmatrix} \tag{4.29}$$

The numeric values of the circuit parameters chosen were analytical computed and experimentally verified [39]

$$\boldsymbol{C} = \begin{bmatrix} 468 & 0 & 0 \\ 0 & 375 & 0 \\ 0 & 0 & 365 \end{bmatrix} \frac{\text{joules}}{\text{°C}}$$

$$\boldsymbol{G} = \begin{bmatrix} 0.78 + 2.1 + 2.0 & -2.1 & -2.0 \\ -2.1 & 0.44 + 2.1 + 3.5 & -3.5 \\ -2.0 & -3.5 & 0.46 + 2.0 + 3.5 \end{bmatrix} \frac{\text{W}}{\text{°C}}$$

A trapezoidal integration method is used to calculate the solution of (4.24). In particular, the integration within the time interval $[t-u, t]$ is

$$\vec{T}(t) = (\boldsymbol{C} + \boldsymbol{G} \cdot u/2)^{-1} \cdot (C - \boldsymbol{G} \cdot u/2) \cdot \vec{T}(t-u) + (\boldsymbol{C} + \boldsymbol{G} \cdot u/2)^{-1} \cdot \vec{Q} \cdot u \tag{4.30}$$

where u is the time step of the integration.

The input to the above model is the transformer currents I_h, I_1, and I_2 over a specific time period, typically one day. The result from the trapezoidal integration is the estimated transformer temperature with respect to ambient temperature over the simulated time span. An assumed flat daily temperature profile is used for simplicity (20℃).

4.5 Transformer Loss-of-Life (LOL) Calculation

The process of insulation degradation, for oil filled transformer, is a function of three phenomenon (1) temperature, (2) moisture, and (3) oxygen content [40]. The second two consist of water and oxygen contamination of the transformer oil and can be controlled through "oil preservation systems" [40] and thus are not considered in this analysis. The following method outlined in [40] is used to compute the LOL.

The LOL, P_L [%], is a function of the equivalent life, E_L [h], and the normal insulation life, N_L [h], [40]

$$P_L = (E_L \cdot 100)/N_L \tag{4.31}$$

where E_L is computed as a function of the aging acceleration factor, θ_u,

$$E_L = \sum_{u=1}^{U}(\theta_u \cdot \Delta t_u) \tag{4.32}$$

and θ_u is computed as a function of the aging rate constant, B [K], and the transformer hot-spot temperature, $\tilde{T}_u$ [˚C], at time u

$$\theta_u = \exp\{B/383 - B/(\tilde{T}_u + 273)\} \tag{4.33}$$

The LOL calculations are computed for a typical day based on hourly increments, thus U [h] is 24 and Δt_u is 1 hour. The LOL calculation variables E_L and θ_u are computed for each hour of the simulated day based on the simulated hot-spot temperature

$\tilde{T}_u$ in that hour (the maximum simulated transformer winding temperature for a given hour).

The LOL constants N_L and B are selected based on historically accepted values. The historical perspective on the insulation life values and LOL calculations is quite interesting, and the values in Table 4.2 for normal insulation life and in Table 4.3 for aging rate constant are surrounded in ambiguity; however, in [40] a conclusion is drawn that the "chemical test measurement of degree of polymerization is a much better indication of cellulosic insulation mechanical characteristics than loss of tensile strength," therefore the normal insulation life used is 150,000 hours (17.1 years) and the aging rate constant used is 14,580 K.

Table 4.2. Normal insulation life times [40].

Basis	Normal Insulation Life [h]
50% retained tensile strength of insulation (former IEEE Std. C57.92-1981)	65,000
25% retained tensile strength of insulation	135,000
200 retained degree of polymerization in insulation	150,000
Interpretation of distribution transformer functional life test (former IEEE std. C57.91-1981 criterion)	180,000

Table 4.3. Aging rate constant [40].

Basis	Aging rate constant [K]
50% retained tensile strength of insulation (former IEEE Std. C57.92-1948)	14,830
50% retained tensile strength of insulation (former IEEE Std. C57.92-1981)	16,054
DT life tests (former IEEE Std. C57.92-1981)	14,594
250 retained degree of polymerization in insulation	14,580

Normal LOL, using the normal insulation life and aging rate constant selected, for operation of a constant 110 ˚C for 24 hours is 0.016%. Intuitively, this indicates that a transformer which withstood a 24 hour period with hot-spot temperature of 110 ˚C aged

the equivalent of 0.016% of its useful life. Notice that 24 hours is 0.016% of 150,000 hours.

4.6 Transformer Impact Simulation Procedure

A block diagram of the simulation procedure is shown in Figure 4.4.

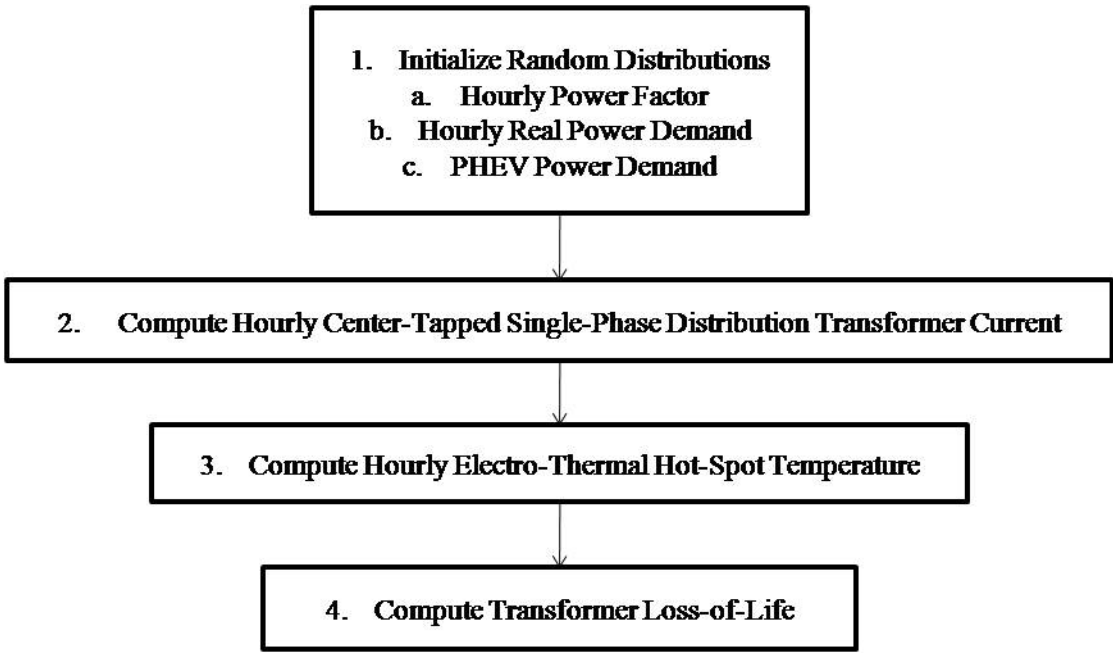

Figure 4.4. Transformer impact simulation block diagram.

The first step in Figure 4.4 is to generate all RVs used in the simulation procedure. The first RV generated is the hourly household power factor, this is a discrete value, and to generate this RV an inverse transform method is used [23]. The cumulative distribution function of the RV is inverted and evaluated using uniform (0, 1) values to generate the random power factor values.

$$F^{-1}(U) = \begin{cases} 0.9 & 0 \le U < 0.3 \\ 0.95 & 0.3 \le U < 0.7 \\ 1 & 0.7 \le U \le 1 \end{cases} \tag{4.34}$$

where U is a RV distributed uniform (0, 1) and is generated using the C function *rand()*.

The second and third RVs are generated using the Box-Műller method, (3.8). The second RV, the hourly real power demand is computed by

$$P^{(h)} = \mu^{(h)} + \sigma^{(h)} \cdot N \tag{4.35}$$

The third RV, the PHEV power demand is computed using (4.4). This value represents the added grid electric energy required for one PHEV.

The second step in Figure 4.4 is to compute the transformer current based on the assumed distribution transformer electric load demand. The methodology assumes that the distribution transformer electric load demand is constant for each hour of the simulated day. The iterative process, to compute the transformer currents for the simulated day, is repeated twice for every hour of the simulated day, once for the base case scenario and again for the PHEV scenario. The final result of the iterative process is the transformer currents for the specified load.

The third step in Figure 4.4 is to compute the transformer hot-spot temperature for every hour of the simulated day. Here hot-spot temperature is defined as the maximum winding temperature in a given hour. A step length of 10 seconds is used in the trapezoidal integration method described above. Thus, the transformer currents, from the center-tapped single phase distribution transformer, are sampled every 10 seconds as input to the electro-thermal transformer model simulation. The final result of this simulation is the hot-spot temperature of the distribution transformer, which is the maximum temperature observed from each hour of the simulated day.

The fourth step in Figure 4.4 computes the transformer LOL. Using the described method the LOL is computed for each simulated day for both scenarios, without PHEV charging (base case) and with PHEV charging (PHEV scenario).

Sample results are described below to clarify the procedure. The sample results consist of one day with the base case feeder demand (feeder demand with no electric load due to PHEV charging), and one day with the added electric load demand of charging three PHEVs. The input to the sample results are the average hourly peak load shown in Figure 4.1, and the average PHEV required grid electric energy of three PHEVs charged over the average arrival and departure times. Figure 4.5 shows the base case feeder load (called "BC Feeder Demand"), required PHEV grid electric energy due to three PHEVs (called "PHEV Feeder Demand"), and total feeder load with added PHEV electric load (called "Total Load with PHEVs").

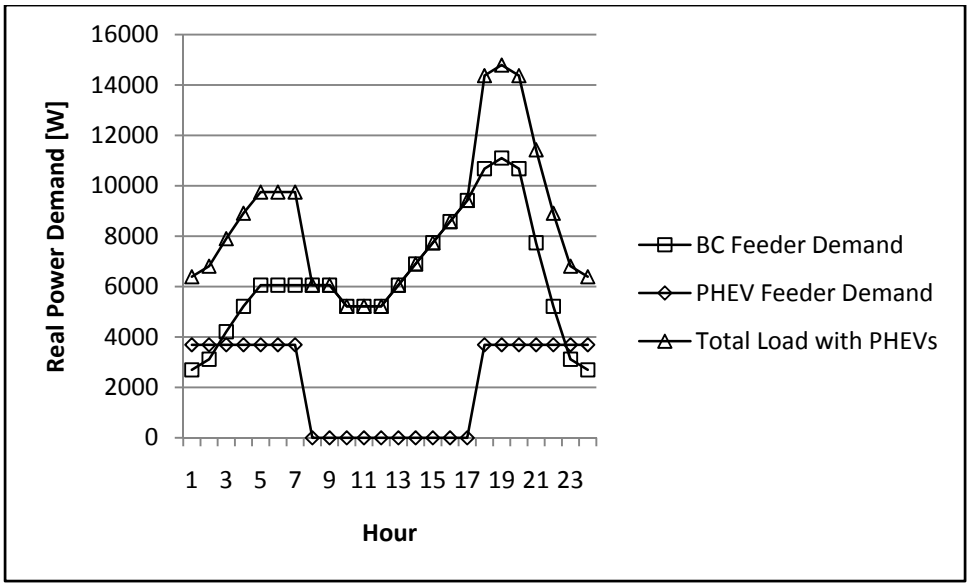

Figure 4.5. Sample scenario feeder load data.

In Figure 4.5 the total load with PHEVs is the hour by hour sum of the PHEV feeder demand and the base case feeder demand. The total load with PHEVs has a maximum real power demand of 14,792 W which is an increase of 33% over the base case feeder demand; moreover the total load with PHEVs has a minimum real power demand of 5,200 W, which is an increase of 93% over the base case feeder demand.

The next step in the transformer impact simulation is to compute the expected distribution transformer winding currents. This calculation includes two scenarios: one with no additional load due to PHEV charging (called "BC") and a second with the added electric load due to PHEVs (called "PHEV"). Both scenarios winding current results include two low voltage winding currents and one high voltage winding current. Because the load on both the low voltage windings is balanced, the low voltage winding current results are the same; for this reason and for simplicity, only one low voltage winding current result (called "Low V") and the high voltage winding current result (called "High V") are shown for both scenarios in Figure 4.6.

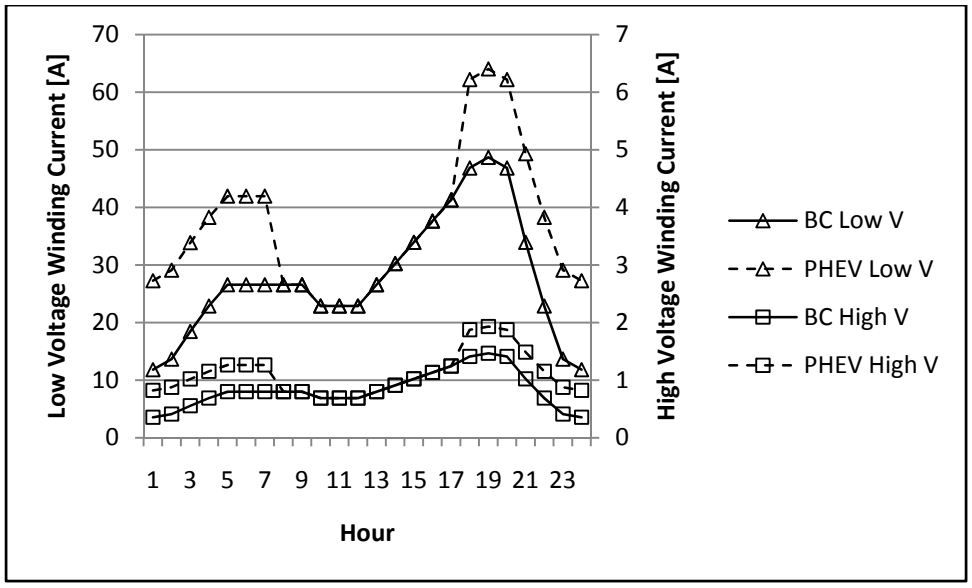

Figure 4.6. Sample scenario winding currents.

In both scenarios the high voltage winding currents are significantly smaller in amplitude then the low voltage winding currents; thus, in Figure 4.6 the high voltage winding currents are plotted for the secondary (right-hand side) vertical axis using a different scale than the primary (left-hand side) vertical axis.

The next step in the transformer impact simulation is to compute the expected distribution transformer winding temperature for both scenarios ("BC" and "PHEV"). The electro-thermal transformer model is utilized to compute these expected temperatures. The results of the electro-thermal transformer model using the winding currents in Figure 4.6 are shown in Figure 4.7. Again, because the load on the low voltage windings is balanced, the currents in the low voltage windings are the same and thus the low voltage winding temperatures are the same. For this reason and for simplicity only one low voltage winding temperature (called "Low V") and the high voltage winding temperature (called "High V") are shown in Figure 4.7.

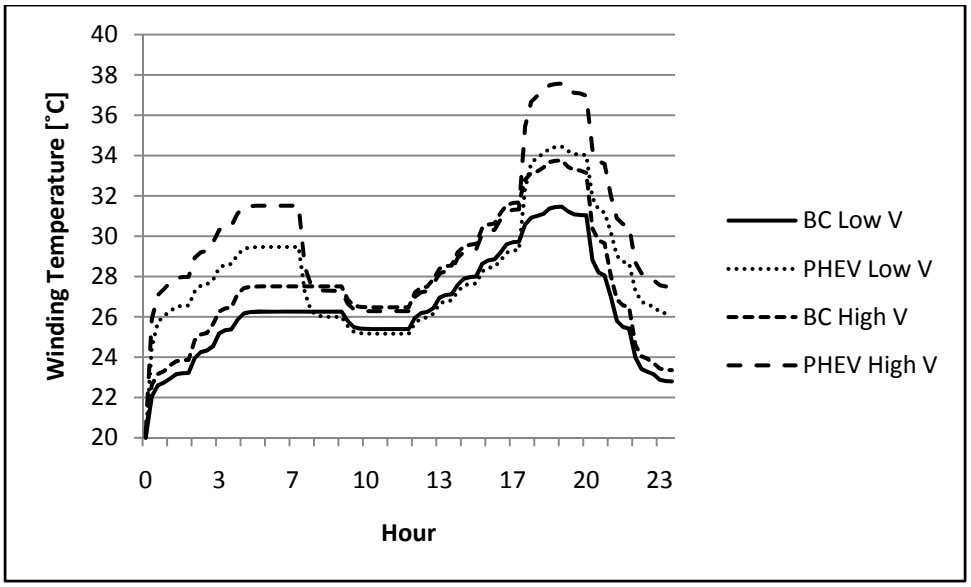

Figure 4.7. Sample scenarios winding temperatures.

Notice that, the significantly smaller high voltage winding current then the low voltage winding currents in Figure 4.6 result in similar amplitude temperature results for both high and low voltage winding temperatures. This change is due to the significantly larger high voltage winding resistance of 14.78 Ω, see (4.10) than the low voltage winding resistance of 0.0269 Ω, see (4.11).

The next step in the transformer impact simulation is to compute the hot-spot winding temperature for both scenarios ("BC" and "PHEV"). The hot spot temperature is the maximum winding temperature in a given hour. Based on the winding temperatures in Figure 4.7, the windings hot-spot temperatures is computed and shown in Figure 4.8.

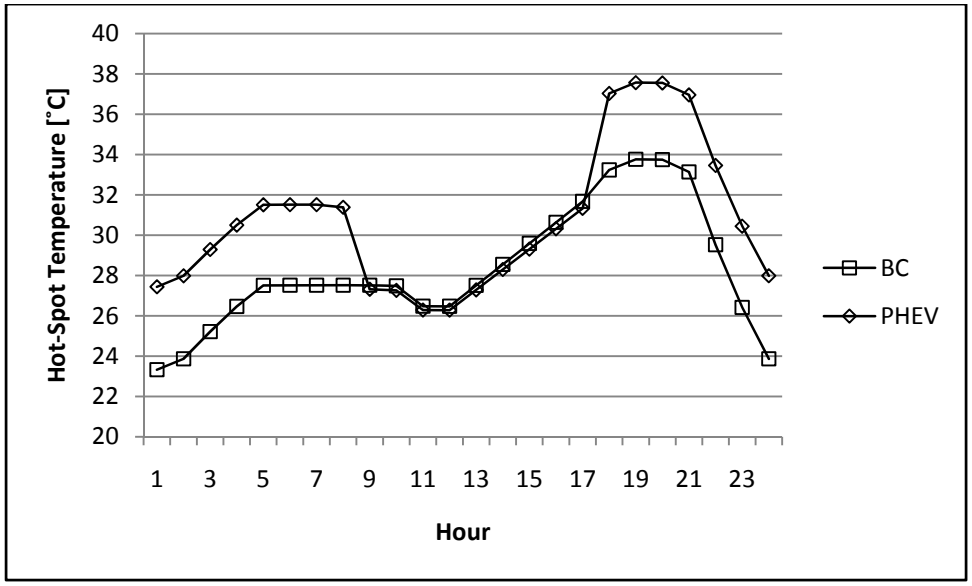

Figure 4.8. Sample scenarios hot-spot temperature.

The last step in the transformer impact simulation is to compute the distribution transformer LOL for both scenarios. Finally, from the hot-spot temperatures the aging acceleration values are computed shown in Table 4.4 and the resulting LOL are, 5.8891E-07% and 9.0037E-07%, for the base case and PHEV feeder demand respectively shown in Figure 4.5.

Table 4.4. Hot-spot temperature results and LOL calculation.

Hour	BC $\tilde{T}_u$	BC θ_u	PHEV $\tilde{T}_u$	PHEV θ_u
1	23.33	1.460E-05	27.44	2.863E-05
2	23.87	1.596E-05	27.98	3.126E-05
3	25.22	1.994E-05	29.29	3.853E-05
4	26.47	2.445E-05	30.50	4.670E-05
5	27.51	2.895E-05	31.51	5.476E-05
6	27.52	2.898E-05	31.51	5.481E-05
7	27.52	2.898E-05	31.51	5.481E-05
8	27.52	2.898E-05	31.38	5.370E-05
9	27.52	2.898E-05	27.32	2.807E-05
10	27.48	2.884E-05	27.26	2.782E-05
11	26.48	2.451E-05	26.29	2.375E-05
12	26.47	2.448E-05	26.28	2.373E-05
13	27.51	2.895E-05	27.29	2.793E-05
14	28.55	3.424E-05	28.30	3.287E-05
15	29.59	4.044E-05	29.31	3.865E-05
16	30.63	4.771E-05	30.32	4.539E-05
17	31.68	5.622E-05	31.33	5.324E-05
18	33.24	7.173E-05	37.03	1.285E-04
19	33.76	7.785E-05	37.57	1.394E-04
20	33.75	7.766E-05	37.55	1.390E-04
21	33.14	7.066E-05	36.96	1.271E-04
22	29.53	4.002E-05	33.46	7.428E-05
23	26.41	2.425E-05	30.45	4.631E-05
24	23.87	1.597E-05	27.99	3.127E-05

The hot-spot temperatures estimated by the sample results indicate average results. The developed probabilistic model varies the electric load above and below the average with variance as a function of the average peak real power, see (4.2), thus the sample results provide validation of the developed probabilistic simulation.

The LOL values computed indicate that in the simulated 24 hour period the transformer aged only 8.837E-4, and 1.350E-3 years for the base case and PHEV feeder demand respectively. This amount of aging is 5.889E-07% and 9.004E-07% (base case and PHEV feeder demand respectively) of the total expected life of 150,000 hours. There

are two reasons for the smallness of these results. First, the transformer is oversized for the modeled electric load. Second, the ambient temperature used is very conservative. The nameplate rating of the modeled transformer is 15 kVA. The peak average electric load is 11.1 kW. This indicates that there is $26\% = (1 - 11.1/15) \cdot 100\%$ spare transformer capacity for the peak average load. The ambient temperature assumed is 20 ˚C (≈ 68 ˚F) and is very conservative for warm temperate climate summer temperatures.

The amplitude of the LOL is not the focus of this study. Rather the relative increase in LOL which is the increase in transformer degradation caused by the additional electrical load caused by PHEV charging. The percent increase for the sample results is 52.89%. This shows that the sample results indicate that the life time of an average transformer will be decreased by 53% because of the added stress of charging three PHEVs. Next, results are presented which show the LOL results using the developed probabilistic models. It is expected that the probabilistic model results will on average approximate the sample results.

4.7 Transformer Impact Results

Each simulated day results in slightly different LOL values and therefore the LOL results are presented in histograms. Two LOL histograms are provided as visual evidence that the LOL results are normally distributed. The expectation is that the LOL results should follow a normal distribution due to the law of large numbers. The base case LOL results from 100 simulated days are shown in Figure 4.9. The PHEV scenario with the added electric load due to one PHEV in the distribution system is shown in Figure 4.10. The results for the added electric load due to two and three PHEVs are quite similar and are not shown.

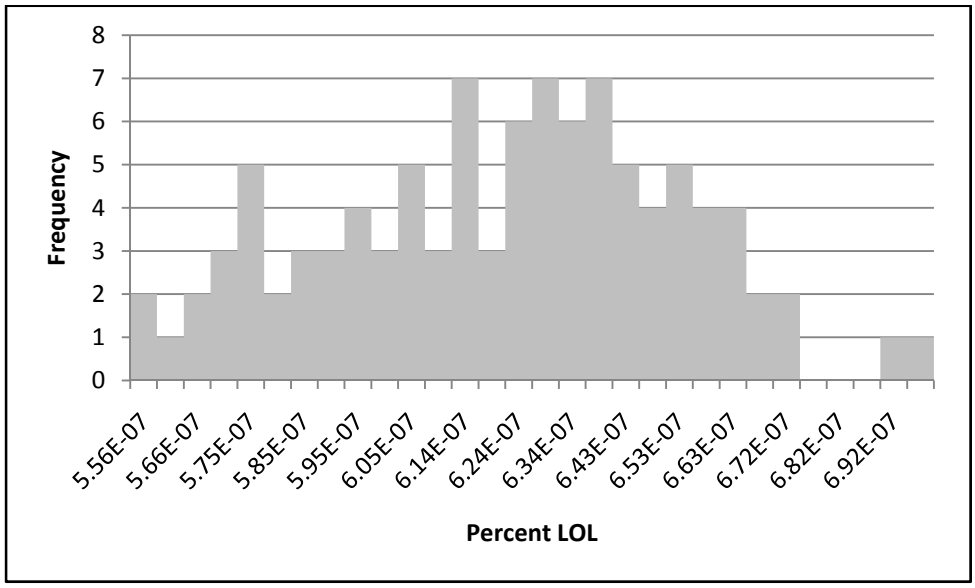

Figure 4.9. Base case LOL histogram.

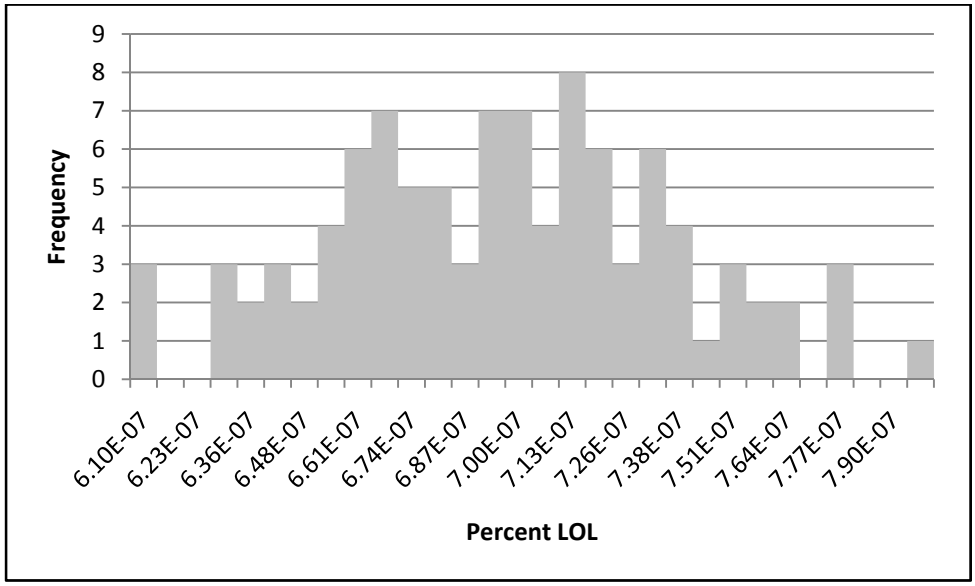

Figure 4.10. Single PHEV charging LOL histogram.

The simulation results are further characterized using a normal distribution maximum likelihood estimator (MLE)

$$\hat{\mu} = 1/\mathrm{N} \cdot \sum_{i=1}^{N} x_i \tag{4.36}$$

where N is the number of repeated simulations (100) and x_i represent the LOL result from iteration-i. This equation is valid assuming that the LOL results will follow a

normal distribution. From the mean MLE results for each of the four scenarios simulated, the percent change in average LOL is computed, indicating the impact PHEV charging will have on distribution transformers.

Table 4.5 compares all four scenarios mean MLE results. The calculated values for $\hat{\mu}$ show a percent change of 11.99% (from 6.212E-07% to 6.957E-7%) when adding one PHEV, 28.84% (from 6.212E-07% to 8.004E-7%) when adding two PHEVs, and 43.75% (from 6.212E-07% to 8.930E-7%) when adding three PHEVs.

Table 4.5. LOL MLE results.

	$\hat{\mu}$
Base Case	6.212E-07
One PHEV	6.957E-07
Two PHEVs	8.004E-07
Three PHEVs	8.930E-07

Also, the change in LOL comparing the probabilistic results versus the deterministic sample results from Section 4.6 show a 5.49% change in base case results (computed as $\left[1 - \left(6.212\text{E-}07/5.889\text{E-}07\right) \cdot 100\%\right]$ where 6.212E-07 is the base case $\hat{\mu}$ in Table 4.5 and the 5.8891E-07 is the deterministic sample base case LOL result), and a 0.82% change in the three PHEV scenario (computed as $\left[1 - \left(8.930\text{E-}07/9.004\text{E-}07\right) \cdot 100\%\right]$ where 8.930E-07 is the three PHEV scenario $\hat{\mu}$ in Table 4.5 and the 9.004E-07 is the deterministic sample three PHEV scenario.

4.8 Conclusion

To examine the impact that PHEV charging will have on distribution transformers, simulations of daily load flows are performed using random electric loads. Two scenarios are examined, the first provides a baseline comparison of the transformer

LOL with no PHEV electric load, and the second scenario provides the transformer LOL including PHEV charging in addition to the normal household electrical demand.

A center-tapped single phase transformer model is used to compute the expected transformer currents and an electro-thermal transformer model of the distribution transformer is used to compute the expected distribution transformer hourly hot-spot temperature.

On average it is assumed that the average daily electric demand experienced by a distribution transformer for three typical houses is 150 kWh. The average added electric load due to PHEVs is on average 16 kWh. The percent increase in feeder load and percent increase in average LOL are shown in Table 4.6.

Table 4.6. Increase in average electric load and resulting average transformer LOL.

	Percent Increase	
	Average Electric Load	Transformer LOL
One PHEV	10.67%	11.99%
Two PHEVs	21.33%	28.84%
Three PHEVs	32.00%	43.74%

The results in Table 4.6 show that adding the additional electric load demand to distribution transformers will have a measurable effect on the expected life of the distribution transformer. Specifically, if it is assumed that an average distribution transformer would operate for 150,000 hours (17.1 years), then the added impact of one PHEV decreases this expected lifetime to 132,015 hours (15.1 years). Similarly, the added impact of two PHEVs decreases it to 106,740 hours (12.2 years) and the added impact of three PHEVs decreases this expected lifetime to 84,390 hours (9.6 years).

CHAPTER 5

CONCLUSION

Plug-in hybrid electric vehicles (PHEVs) are a vehicle designed similar to a traditional hybrid electric vehicle (HEV) with more dependence on the electric drive system. PHEVs have the added ability, over HEVs, to recharge from the electric power system. The wide spread adoption of PHEVs has the potential benefit to (1) generate a lucrative new semi-dispatchable load for the electric utility industry and (2) diversify the transportation sector energy usage by displacing petroleum usage with electric energy.

Two power system level impacts of PHEV charging are investigated in this thesis. The first investigation quantifies the primary energy source utilization due to PHEV charging and the second quantifies the impact of PHEV charging on distribution transformers. In Chapter 3 the primary energy source utilization describes which power system fuel types are utilized to meet the added electric load demand created by PHEV charging. Additionally, the tradeoff between vehicle tailpipe environmental air pollution (EAP) and power system EAP is compared when PHEVs are used to replace varying levels of the light duty vehicle fleet in a given power system area. Finally, the annual fuel cost is computed for conventional internal combustion (IC) vehicles, which includes only gasoline purchasing, and that of PHEVs, which includes gasoline and electricity purchasing. The results from Chapter 3 indicate that PHEVs offer cleaner transportation (depending on the generation mix used to charge the vehicles) with decreased gasoline utilization at a lower cost (in terms of annual fuel costs) to consumers.

In Chapter 4 the impact of PHEV charging on distribution transformers is quantified using a transformer insulation percent loss-of-life (LOL) calculation. Two models are utilized to compute the data required for the LOL calculation, namely a center-tapped model and a simplified electro-thermal transformer model. The center-tapped single phase transformer model simulates the transformer winding currents for random daily load demand values. The electro-thermal model simulates the winding temperature as a function of the winding currents. The LOL calculation is based on the hourly transformer hot-spot temperature which is defined as the maximum winding temperature for each hour of the simulation period. The transformer LOL results indicate that adding the additional electric load demand to distribution transformers has a measurable effect on the expected life of the distribution transformer.

Future work which could follow this thesis includes:

- Model verification of the probabilistic consumer behavior including miles driven per day, arrival time and departure time random variables.
- Additional simulations of the effect that real time electric price signals could have on PHEV charging and primary energy source utilization.
- Power system data of existing power system could provide experimental results for existing power systems.
- Additional development of the transformer impact chapter could include investigations into the impact of ambient temperature profiles, the impact of vehicle charging time, and the impact of transformer sizing.

APPENDIX A

PSAT SIMULATION RESULTS

The data in this appendix is taken from [20]. From this data the vehicle, both internal combustion (IC) and plug-in hybrid electric (PHEV), performance metrics are computed. The IC vehicle performance metrics include fuel efficiency, NO_x generated per mile driven, and CO_2 generated per mile driven. The PHEV performance metrics include energy required per mile, gasoline efficiency, NO_x generated per mile driven, and CO_2 generated per mile driven. The methodology used to compute the performance metrics is described in Chapter 3.

PHEV simulations were performed using the Powertrain System Analysis Toolkit (PSAT). PSATs Matlab/Simulink/State-Flow models, of conventional vehicle and hybrid powertrain components, of various architectures, were assembled and simulated to generate operational data for PHEVs [20].

Once the complete vehicle models had been selected, PSAT allowed for the simulated operation of the developed vehicles over specified driving schedules with a variable amount of driving energy supplied from the vehicles battery [20].

PHEV PSAT results for each vehicle class are shown in Tables A.1 - A.4. IC PSAT results are shown in Table A.5.

Table A.1. Vehicle class 1 PHEV PSAT results [20].

Driving Schedule	k_{PHEV}	Electric Energy Per Mile [kWh/mi.]	GPM [gal./mi.]	NO_x Per Mile [kg/mi.]	CO_2 Per Mile [kg/mi.]
HWFET	0.1156	0.0807	0.0146	7.720E-05	0.1316
	0.2183	0.1471	0.0125	5.100E-05	0.1123
	0.7196	0.2508	0.0023	6.700E-06	0.0208
	1.000	0.2626	0.0001	0.00	0.00
UDDS	0.1461	0.1167	0.0162	7.080E-05	0.1457
	0.2757	0.1973	0.0123	4.790E-05	0.1109
	0.5193	0.2666	0.0059	2.040E-05	0.0528
	1.000	0.2235	0.0001	0.00	0.00
US06	0.1141	0.1281	0.0235	1.273E-04	0.2115
	0.1803	0.1820	0.0196	1.016E-04	0.1760
	0.4114	0.3162	0.0107	4.920E-05	0.0963
	0.9463	0.4341	0.0006	2.300E-06	0.0052

Table A.2. Vehicle class 2 PHEV PSAT results [20].

Driving Schedule	k_{PHEV}	Electric Energy Per Mile [kWh/mi.]	GPM [gal./mi.]	NO_x Per Mile [kg/mi.]	CO_2 Per Mile [kg/mi.]
HWFET	0.1131	0.0987	0.0183	1.025E-04	0.1651
	0.1210	0.1070	0.0184	1.022E-04	0.1659
	0.1340	0.1117	0.0171	9.500E-05	0.1538
	0.4617	0.2698	0.0074	3.250E-05	0.0671
	0.6035	0.2808	0.0044	2.230E-05	0.0393
	0.7829	0.2952	0.0022	9.300E-06	0.0197
UDDS	0.1898	0.1818	0.0186	8.860E-05	0.1680
	0.4534	0.3168	0.0091	3.100E-05	0.0820
	0.7613	0.3016	0.0023	7.800E-06	0.0203
	0.9664	0.2950	0.0002	1.000E-06	0.0022
	1.0000	0.2866	0.0001	0.00	0.00
US06	0.0992	0.1374	0.0300	1.370E-04	0.2692
	0.1215	0.1609	0.0278	1.367E-04	0.2492
	0.3608	0.3539	0.0149	6.960E-05	0.1336
	0.5108	0.4232	0.0097	3.990E-05	0.0864
	0.9199	0.4672	0.0010	3.600E-06	0.0087

Table A.3. Vehicle class 3 PHEV PSAT results [20].

Driving Schedule	k_{PHEV}	Electric Energy Per Mile [kWh/mi.]	GPM [gal./mi.]	NO_x Per Mile [kg/mi.]	CO_2 Per Mile [kg/mi.]
HWFET	0.0482	0.0780	0.0364	1.307E-04	0.3287
	0.2976	0.2950	0.0165	5.250E-05	0.1484
	0.4217	0.3790	0.0123	3.800E-05	0.1108
	0.7746	0.4143	0.0029	9.400E-06	0.0257
	1.000	0.4247	0.0001	0.00	0.00
UDDS	0.0596	0.1145	0.0427	1.612E-04	0.3850
	0.3006	0.3927	0.0216	7.370E-05	0.1949
	0.6990	0.3889	0.0039	1.240E-05	0.0357
	1.000	0.3872	0.0001	0.00	0.00
US06	0.0530	0.1165	0.0492	2.436E-04	0.4436
	0.1872	0.3362	0.0344	1.549E-04	0.3108
	0.3516	0.5259	0.0228	8.750E-05	0.2064
	0.4718	0.6694	0.0176	6.400E-05	0.1595
	0.7168	0.7204	0.0066	2.260E-05	0.0605

Table A.4. Vehicle class 4 PHEV PSAT results [20].

Driving Schedule	k_{PHEV}	Electric Energy Per Mile [kWh/mi.]	GPM [gal./mi.]	NO_x Per Mile [kg/mi.]	CO_2 Per Mile [kg/mi.]
HWFET	0.0630	0.1024	0.0361	1.746E-04	0.3254
	0.2503	0.2985	0.0212	9.000E-05	0.1909
	0.5925	0.4820	0.0078	3.240E-05	0.0706
	0.9096	0.5155	0.0012	4.600E-06	0.0109
UDDS	0.0719	0.1494	0.0461	1.892E-04	0.4158
	0.3406	0.4816	0.0221	7.720E-05	0.1987
	0.7526	0.4819	0.0037	1.320E-05	0.0338
	1.000	0.5189	0.0001	0.00	0.00
US06	0.0577	0.1360	0.0532	2.642E-04	0.4770
	0.3484	0.5736	0.0253	1.342E-04	0.2280
	0.4982	0.6986	0.0165	8.500E-05	0.1497
	0.6900	0.7606	0.0080	3.860E-05	0.0726
	0.8776	0.8530	0.0028	1.270E-05	0.0253

Table A.5. IC PSAT results [20].

Class	Drive Schedule	MPG [mi./gal.]	NO_x Per Mile[kg/mi.]	CO_2 Per Mile [kg/mi.]
1	HWFET	33.21	9.190E-05	0.2715
	UDDS	26.17	1.508E-04	0.3446
	US06	25.82	2.042E-04	0.3483
2	HWFET	18.54	1.593E-04	0.4866
	UDDS	14.17	2.530E-04	0.6366
	US06	14.21	3.448E-04	0.6341
3	HWFET	19.31	1.453E-04	0.4674
	UDDS	12.17	2.651E-04	0.7411
	US06	14.20	3.090E-04	0.6351
4	HWFET	14.07	1.946E-04	0.6411
	UDDS	11.42	2.904E-04	0.7902
	US06	11.16	4.032E-04	0.8081

REFERENCES

[1] Energy Information Administration, "U.S. crude oil supply and disposition," September 2008, http://tonto.eia.doe.gov/dnav/pet/pet_sum_crdsnd_adc_mbbl_m.htm.

[2] Energy Information Administration, "Weekly inputs, utilization & production," September 2008, http://tonto.eia.doe.gov/dnav/pet/pet_pnp_wiup_dcu_nus_w.htm.

[3] J. Voelcker, "Plugging away in a Prius," *IEEE Spectrum*, vol. 45, issue 5, pp. 30- 48, May 2008.

[4] Energy Information Administration, "U.S. weekly product supplied," August 2008, http://tonto.eia.doe.gov/dnav/pet/pet_cons_wpsup_k_w.htm.

[5] Energy Information Administration, Annual Energy Review 2007, tables 1.3 and 2.1b-2.1f, and 10.3.

[6] C. H. Stephan and J. Sullivan, "Environmental and energy implications of plug-in hybrid-electric vehicles," *Environ. Sci. Technol.*, vol. 42, no. 4, pp. 1185–1190, January 2008.

[7] M. Kintner-Meyer, K. Schneider, and R. Pratt, "Impacts assessment of plug-in hybrid vehicles on electric utilities and regional U.S. power grids; part 1: Technical analysis", September 2008, http://www.ferc.gov/.

[8] P. Denholm and W. Short, "An evaluation of utility system impacts and benefits of optimally dispatched plug-in hybrid electric vehicles," National Renewable Energy Laboratory, Golden, Colorado, USA, Tech. Rep. NREL/TP-620-40293, 2006.

[9] K. Parks, P. Denholm, and T. Markel, "Costs and emissions associated with plug-in hybrid electric vehicle charging in the Xcel Energy Colorado service territory," National Renewable Energy Laboratory, Golden, Colorado, USA, Tech. Rep. NREL/TP-640-41410, 2007.

[10] S. Hadley and A. Tsvetkova, "Potential impacts of plug-in hybrid electric vehicles on regional power generation," Oak Ridge National Laboratory, Oak Ridge, Tennessee, USA, ORNL/TM-2007/150, 2008.

[11] T. Markel, A. Brooker, T. Hendricks, V. Johnson, K. Kelly, B. Kramer, M. O'Keefe, S. Sprik, and K. Wipke, "ADVISOR: a systems analysis tool for advanced vehicle modeling," *Journal of Power Sources*, vol. 110, iss. 2, pp. 255-266 August 2002.

[12] Electric Power Research Institute, "Environmental assessment of plug-in hybrid electric vehicles; volume 1: Nationwide greenhouse gas emissions," EPRI, Palo Alto, Calif., 1015325, 2007.

[13] Energy Information Administration, "The National Energy Modeling System: An Overview 2003,"Washington D.C., DOE/EIA-0581, March 2003.

[14] R. Sioshansi and P. Denholm, "Emissions impacts and benefits of plug-in hybrid electric vehicles and vehicle-to-grid services," *Environ. Sci. Technol*., vol. 43, no. 4, pp. 1199–1204, January 2009.

[15] Electric Power Research Institute, "Environmental assessment of plug-in hybrid electric vehicles; volume 2: United States air quality analysis based on AEO-2006 assumptions for 2030," EPRI, Palo Alto, Calif., 1015326, 2007.

[16] C. Samaras and K. Meisterling, "Life cycle assessment of greenhouse gas emissions from plug-in hybrid vehicles: Implications for policy," *Environ. Sci. Technol*., vol. 42, no. 9, pp. 3170–3176, April 2008.

[17] S. Blumsack, S. Constantine, and P. Hines, "Long-term electric system investments to support plug-in hybrid electric vehicles" in *Power and Energy Society General Meeting – Conversion and Delivery of Electrical Energy in the 21st Century*, pp. 1-6, 2008.

[18] A. P. Meliopoulos, "Computer aided instruction of energy source utilization problems," *IEEE Transactions on Education*, vol. E-24, no. 3, pp. 204-9, August 1981.

[19] Argonne National Lab, "Powertrains system analysis toolbox (PSAT)," July 2008, http://www.anl.gov/techtransfer/pdf/PSAT.pdf.

[20] J. Meisel, G. J. Cokkinides, A. P. Meliopoulos, T. J. Overbye, and C. A. Roe, "Power System Level Impacts of Plug-In Hybrid Vehicles," *Power System Engineering Research Center (PSERC) Publication*, PENDING.

[21] MathWorks, "Technical Solutions", March 2009, http://www.mathworks.com/support/solutions/data/1-18DGY.html?solution=1-18DGY.

[22] L. Sanna, "Driving the solution the plug-in hybrid electric vehicle", *EPRI Journal*, pp. 8-17, Fall 2005.

[23] "Random variate generation" class notes for ISYE 6644 Simulation, H. Milton Stewart School of Industrial and Systems Engineering at the Georgia Institute of Technology, Summer 2008.

[24] J.E. Gentle, *Numerical Linear Algebra for Applications in Statistics.* Berlin: Springer-Verlag, 1998.

[25] A. M. Law, *Simulation Modeling & Analysis*, The McGraw-Hill Companies, Inc. 2007.

[26] Reliability Test System Task Force of the Application of Probability Methods Subcommittee, "IEEE reliability test system," *IEEE Transactions on Power Apparatus and Systems*, vol. PAS-98, no. 6, pp. 2047-54, November 1979.

[27] Tennessee Valley Authority, "TVA reservoirs and power plants," July 2008, July 2008, http://www.tva.gov/sites/sites_ie2.htm.

[28] Energy Information Administration, "Existing Capacity by Energy Source," May 2009, http://www.eia.doe.gov/cneaf/electricity/epa/epat2p2.html.

[29] Energy Information Administration, "Net Generation by Energy Source: Total (All Sectors)," May 2009, http://www.eia.doe.gov/cneaf/electricity/epm/table1_1.html.

[30] Energy Information Administration, "U.S. Electric Power Industry Estimated Emissions by State (EIA-767 and EIA-906)," May 2009, http://www.eia.doe.gov/cneaf/electricity/epa/epat5p1.html.

[31] Energy Information Administration, "Net Internal Demand, Capacity Resources, and Capacity Margins by North American Electric Reliability Council Region," May 2009, http://www.eia.doe.gov/cneaf/electricity/epa/epat3p2.html.

[32] U.S. Department of Transportation Federal Highway Administration, "State Motor-Vehicle Registration," May 2009, http://www.fhwa.dot.gov/policy/ohim/hs03/mv.htm.

[33] W. H. Kersting, *Distribution System Modeling and Analysis*. CRC Press: Taylor & Francis Group, 2007.

[34] J. F. Lindsay, "Temperature rise of an oil-filled transformer with varying load," *IEEE Transactions on Power Apparatus and Systems*, vol. PAS-103, no. 9, pp. 2530-36, September 1984.

[35] D. K. Whirlow and A. M. Lockie, "Thermal performance of distribution transformers in underground vaults: II-Mathematical model," *IEEE Transactions on Power Apparatus and Systems*, vol. PAS 87, no.9, pp. 1745-54, September 1968.

[36] A. P. Meliopoulos, "State estimation methods applied to transformer monitoring," in *Proceedings of the 2001 Power Engineering Society Summer Meeting*, vol. 1, pp. 419-23, Vancouver, BC, July 2001.

[37] A. P. Meliopoulos, G. J. Cokkinides, and T. J. Overbye, "Component monitoring and dynamic loading visualization from real time power flow model data," in *Proceedings of the 37th Annual Hawaii International Conf. System Sciences (HICSS)*, Waikoloa, Big Island, HI, USA, January, 2004.

[38] “Electric Power Quality” class notes for ECE 4833 Electric Power Quality, School of Electrical and Computer Engineering at the Georgia Institute of Technology, Fall 2007.

[39] A. P. Meliopoulos, (private communication), 2009.

[40] ANSI/IEEE C57.91-1995, Guide for Loading Mineral-Oil-Immersed Transformers.